Colorado Agricultural Experiment Station
under Grant #COL0692

STATISTICAL ANALYSIS OF WINTER OROGRAPHIC PRECIPITATION FORECASTS USING A BULK MICROPHYSICS MODEL

by Brian J. Gaudet

William R. Cotton, P.I.

Colorado State University

DEPARTMENT OF ATMOSPHERIC SCIENCE

PAPER NO. **613**

STATISTICAL ANALYSIS OF WINTER OROGRAPHIC PRECIPITATION FORECASTS USING A BULK MICROPHYSICS MODEL

by

Brian J. Gaudet

Department of Atmospheric Science

Colorado State University

Fort Collins, CO 80523

Research Supported by

Colorado Agricultural Experiment Station

under Grant #COL0692

June 12, 1996

Atmospheric Science Paper No. 613

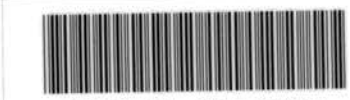

ABSTRACT

STATISTICAL ANALYSIS OF WINTER OROGRAPHIC PRECIPITATION FORECASTS USING A BULK MICROPHYSICS MODEL

The Regional Atmospheric Modeling System (RAMS) developed at CSU has been used to generate forecasts in real-time since the 1991-1992 winter season. In the past such forecasts have included a precipitation efficiency parameterization to predict winter precipitation. Such mesoscale model forecasts allow the possibility of predicting the amount of snowpack in remote mountainous regions where observational verification is difficult. However, in case studies the precipitation scheme used with the forecast model tended to greatly underestimate the total amount of precipitation when verified against SNow TELemetry (SNOTEL) automated stations.

Since the fall of 1995 the forecast model has had the capability of using the bulk microphysics scheme found in RAMS to produce real-time forecasts of precipitation. In this study one month, April 1995, is chosen for statistical analysis. Each day in the month was simulated with a bulk microphysics version of the forecast model and compared with the actual forecast produced using a 'dump-bucket' precipitation scheme. A variety of statistical analyses are performed to compare the performance of the two models with each other and with observational data, provided from a set of 32 SNOTEL stations and 167 National Weather Service and other climatological data stations. It is shown that in general the microphysics model shows enhanced skill over the other precipitation scheme at the SNOTEL sites, but not at the climatological stations. On average, both models produce similar amounts of total precipitation for the climatological data stations, but the microphysics does a significantly better job at forecasting total precipitation amounts at the higher-elevation SNOTEL stations, though total accumulations are still underestimated.

Spatial and meteorological trends in forecasting skill are discussed. Additionally, sensitivity tests, including microphysical simulations using finer grid resolution, are shown, and the results are analyzed.

ACKNOWLEDGEMENTS

I would first like to thank my adviser, Dr. William Cotton, for giving me the opportunity to work with the forecast model and for the support and guidance he has given me in my research. I also appreciate his punny funs and patience with my oft-peculiar working schedule. Additionally, I would like to thank committee members Dr. Roger Pielke and Dr. Paul Mielke of the statistics department for their suggestions and advice, both before and during the preparation of this thesis.

I would also like to thank the National Centers for Environmental Prediction (NCEP), formerly the National Meteorological Center (NMC), for the access to the gridded meteorological datasets used in this study, and to Steve Finley for maintaining the Alden corporation satellite link which became the source for the surface and rawinsonde data. I am also grateful to John Kleist and the Western Regional Climate Center for access to the SNOTEL verification data, which is maintained by the Natural Resources Conservation Service of the Department of Agriculture.

Special thanks to the elder Brian, Brian Beitler, for being the first to teach me how to use RAMS and the forecast model. In addition to his know-how, his joyful spirits and conversations on topics ranging from baseball to forgotten eighties groups are missed. I would also like to thank the original RAMS forecasting guru, Greg Thompson, for coming down from Boulder to keep me going after Brian left for active duty, and for all of his assistance over the e-mail – otherwise I would still be in a massive state of confusion.

In addition to Brian, I am indebted to my past office mates for their constant technical and emotional support. In particular, I would like to thank Sharon Nebuda for all of her wisdom (DON'T PANIC!) and generosity over the years (the beanbag and plant); Jerry Harrington for all the help in understanding the model microphysics and for making sure that I was still sane during thesis preparation; and Tara Jensen, for all the help with

forecasting-associated tasks while I was writing, not to mention those fine chocolate-chip cookies. Thanks are also due to my current office mates (Bruce Muller, Chris Golaz, and Cristian Mitrescu) for putting up with my quirky traits this past year, and for taking the time to needle me when my adviser was out of town.

Many other people in the Cotton and Pielke groups (especially Dr. Robert Walko, Dr. Lewis Grasso, Jason Nachamkin, and Cathy Finley) have been instrumental in helping me to understand a little about computer modeling and/or real-time weather forecasting. Brenda Thompson, Abby Hodges, and Connie Uliasz provided much-needed administrative assistance and exabyte tapes while Donna Chester and Hongli Jiang made sure the computers responded to my considerable demands on them – thanks! To all of the other friends I've made at the Atmospheric Science Department during my stay here I express my gratitude, and apologize to anyone whose name I left out.

Finally, I would like to thank a few outside sources of support. First, I would like to thank my family for always being there for me when I needed help and for giving me everything that I have – love you guys! I would like to thank all the friends that I've made at J23 since I've come to Fort Collins for making me feel welcome and giving me new insights. And I would like to give thanks to God, for making possible all of the above, and more.

This research was supported by the Colorado Agricultural Experiment Station under grant #COL0692.

TABLE OF CONTENTS

LIST OF FIGURES

LIST OF TABLES

Chapter 1

INTRODUCTION

Though a nuisance to the commuters near the Colorado Front Range, winter snowfall is extremely important to the state of Colorado and neighboring mountainous states, as the melting of the snowpack in the Rockies is the major source of water for the largely semiarid region. Once the amount of snowpack is known, the information can be used by a hydrological model, with which one would be able to predict the amount of meltwater, the amount of snow that simply evaporates, and the amount of snow that remains frozen, potentially allowing the forecasting of the flow of streams and even avalanche potential. While numerous communities throughout Colorado report snowfall totals and/or the amount of water contained in the snow, observations of snow at the high mountain locations where snowpack accumulates are relatively scarce. A major source of observational snowpack data now consists of a network of SNOTEL (SNOw TELemetry) pillow sensors located in such mountainous regions, but estimation of the total snowpack in a drainage basin based on these measurements requires a lot of extrapolation.

Numerical computer models offer another approach to the problem. If an accurate snowfall-predicting model existed, it would be possible to better estimate the snowfall in regions where little observational information exists. Large-scale models such as the NGM (Nested Grid Model) (Hoke et al., 1989) and the older version of the Eta model (Mesinger et al, 1988) have grid spacings on the order of 100 km and domains which range in size from slightly larger than the continental United States to an entire hemisphere. The models are extensively used by forecasters, and when the model's numerical output is combined with knowledge of the model's inherent biases and local meteorological tendencies, much useful guidance results. However, the above-mentioned models cannot be used for the task

of snowpack information because their resolution is too coarse. This is especially true for mountainous regions where large variations in elevations and slope can create extreme variability in precipitation. Accounts of winter storms exist where, for example, the Denver metropolitan region received over two feet of snow while Fort Collins received only an inch or less of snow (Reinking and Boatman, 1986).

Mesoscale models, with finer resolution than the large-scale numerical models, can be used for the purpose of snowpack prediction. (Prediction of summertime precipitation in the Rocky Mountain region, usually convective in nature, would require the use of model resolution even finer than that of most mesoscale models). They generally use the gridded analyses to the larger-scale models as input, and the actual large-scale forecasts to assist in future boundary conditions. Otherwise the mesoscale models operate completely independently. Usually a succession of finer grids is used, which allows a forecast to focus on regions the size of, for example, Colorado, while information is also kept on features which could affect the fine-scale region in the time scale of the forecast period. Mesoscale models can produce forecasts in reasonable amounts of time on relatively cost-effective workstations rather than on the supercomputers required for the large-scale numerical models. Thus it is certainly possible that in the future local forecasters desiring detailed numerical forecasts for their region of interest could each run a mesoscale model positioned according to their needs.

Two more issues regarding mesoscale forecasting accuracy need to be addressed, however. One is the initialization of the atmospheric fields. If the primary mechanism for producing fine-scale meteorological phenomena is similarly-scaled features in the initial atmospheric data, then a finer-scale model will produce no further forecast accuracy if the necessary information input is not there. However, if fine-scale meteorology is primarily determined by fine-scale physiography, vegetation, the distribution of bodies of water, soil moisture, and other relatively time-independent variables, or if for whatever reason fine-scale features can dynamically evolve from coarser features, then the necessary information is available to the mesoscale model and forecasting can be improved by the decreased grid spacing. Another issue relates specifically to precipitation prediction. The factors involved

in precipitation formation are complex and quite sensitive to small variations in temperature, wind, and moisture fields. Snow crystal generation involves a multitude of processes which occur on very small (snowflake-sized) scales. Yet, traditionally in mesoscale models which forecast precipitation, accounting for all of the processes which occur would take too much computer resources (specifically time), so relatively simple, empirically-based parameterizations must be used to create precipitation. It is not certain how accurate such schemes are when applied to a wide variety of orography. Also, these parameterizations reduce the information available in the precipitation forecasts, such as type of precipitation. An empirically-based scheme was used in the forecast version of the Regional Atmospheric Modeling System (RAMS) at Colorado State University until the fall of 1994, when increased computing speed and optimized algorithms permitted the use of full bulk microphysics in the daily forecast model.

The purpose of this study is to produce daily real-time forecasts using the forecast version of RAMS combined with the bulk microphysics option, and to see what improvement, if any, the use of bulk microphysics creates in forecasting wintertime orographic precipitation for the Colorado region. A summary of efforts to verify precipitation forecasts and of mesoscale-modeling forecast projects is presented (Chapter 2), followed by a description of similar studies completed using the forecast model of RAMS over the years (Chapter 3). Then a comparison of the two-precipitation schemes with each other, with observations, and with sensitivity studies is presented in terms of qualitative features in case studies (Chapter 4) and quantitatively in terms of various statistics as applied to a month of data (Chapter 5). Finally, findings and conclusions concerning model tendencies and future prospects in this area of research will be presented (Chapter 6).

Chapter 2

BACKGROUND

2.1 Mesoscale Modeling

Mesoscale modeling is an exciting branch of the whole field of computer modeling of the atmosphere. Relatively recently, one of the goals of mesoscale modeling has become numerical weather prediction (NWP) of features too small to be resolved by the computer models used by such organizations as the National Centers for Environmental Prediction (NCEP), formerly the National Meteorological Center (NMC). Mesoscale meteorology is the study of weather phenomena with length scales between a few kilometers to thousands of kilometers, and time scales from around 30 minutes to several days (see Cotton and Anthes, 1989; Orlanski, 1975). In this range, when the effects of diabatic heating or non-linearities are not crucial, features are frequently coarse enough so that the hydrostatic assumption can still be used, but too fine to assume that the wind field will be in gradient wind balance; these two conditions are used by Pielke (1984) as the definition of mesoscale. Scales larger or slower than this range are referred to as the macroscale and include synoptic weather patterns, while smaller and faster scales are known as the microscale and include, for example, the internal processes of clouds. Thus the mesoscale is influenced on one level by features such as height falls in advance of extra-tropical cyclones, but on another level by processes such as the evaporative cooling of ice-nucleated precipitation. Examples of mesoscale atmospheric phenomena include land and sea breezes, mountain and valley winds, rain shadows, lake-effect storms, squall lines, and mesoscale convective complexes (MCCs) (see Pielke, 1984). Accounting for both the large-scale and small-scale influences on a region is a never-ending challenge for the mesoscale modeler.

One mesoscale model is the Regional Atmospheric Modeling System (RAMS) , a model which was developed at Colorado State University as two computer modeling efforts were merged in the early 1980s. One was a hydrostatic mesoscale model developed by Mahrer and Pielke (1977); the other, a non-hydrostatic cloud model (Tripoli and Cotton, 1982). The combination allows RAMS to simulate atmospheric phenomena over a wide range of length scales, from the continental scale to the scale of turbulent eddies, in either hydrostatic or non-hydrostatic mode, though the non-hydrostatic mode is usually selected, including for this study. The model is based on the elastic, compressible primitive equations. Predicted variables include u,v, and w wind components; the Exner-function representation of pressure; dry-air density; total water mixing ratio; mixing ratio of the seven water condensate categories; and ice-liquid potential temperature (see Tripoli and Cotton, 1981). RAMS uses an Arakawa-C grid (Arakawa and Lamb, 1981), in which the u, v, and w wind components are staggered one-half grid length in the x,y, and z directions, respectively, from the thermodynamic and other scalar variables (e.g., temperature). The grid in the horizontal directions is a polar stereographic projection, whereas vertically the model uses a sigma-z (terrain-following spatial) coordinate, as described in Gal-Chen and Sommerville (1975). To enhance resolution in regions of the model domain, an arbitrary number of nested grids can be produced within a parent grid (Clark and Farley, 1984). Both grids are allowed to interact with each other at the grid interfaces. Further features of RAMS more specific to the application will be described in later sections. Numerous references to RAMS exist in the literature; good overviews can be found in Pielke et al. (1992), Nicholls et al. (1991), and Tremback (1990).

Another mesoscale model is the Mesoscale Model (MM) series developed at the Pennsylvania State University in coordination with the National Center for Atmospheric Research (NCAR). This model has developed at Penn State since the 1970s (Anthes and Warner, 1978), and in joint research with NCAR since 1983 (Warner and Seaman, 1990). A description of version 4 of this model (PSU/NCAR MM4) can be found in Anthes et al. (1987) and Warner and Seaman (1990). This version supports two-way nesting and uses a sigma-p (terrain-following, constant pressure) coordinate in the vertical. An Arakawa-B Grid is

used, similar to the Arakawa-C except that u and v wind velocities are defined at the same points, displaced in both x and y from the scalar variables (Dudhia, 1993). Version MM5 included the ability to perform non-hydrostatic model simulations, which permitted the use of reduced grid spacings (Dudhia, 1993).

Other mesoscale models developed in research environments include the Limited Area and Mesoscale Prediction System (LAMPS) described in Kalb (1985) and Perkey and Kreitzberg (1976); the University of Wisconsin Non-Hydrostatic Modeling System (UW-NMS) described in Tripoli (1992); and the Mesoscale Atmospheric Simulation System (MASS) developed as NASA-Langley (Kaplan et al., 1982; Koch, 1985). A model used at the fine end of the mesoscale range (a few kilometers) for simulating cloud-scale phenomena is the model of Clark (1979). A comparison of such models can be found in Pielke (1994).

2.2 Real-time Mesoscale Forecasting

One potential use of mesoscale models is in creating enhanced weather predictions for the local forecaster. The finer resolution of the mesoscale model compared with larger-scale forecast models offers the advantages of resolving atmospheric phenomena having smaller length scales than the resolution of the coarser model, and additionally resolving features such as valley winds which owe their existence to fine-scale variation in the landscape. This is especially true for mountainous regions such as Colorado where the orographic effects on winter storms can be complex and dominant. Such phenomena as cold-air blocking, cold-air damming (uplift of warm, moist air over blocked cold-air), windward-slope precipitation enhancement, barrier jets, and occasionally convection can be induced by the Colorado Front Range and cause sharply-delineated snowfall distributions (Reinking and Boatman, 1986; Wesley, 1991).

A few worldwide meteorology offices have used or are using mesoscale models for forecasting purposes, using output from their own larger-scale models in formulating the mesoscale model input. The United Kingdom Meteorological Office (UKMO) in the past used a non-hydrostatic, mesoscale forecasting model with a 15-km grid; it was initialized using surface observations, larger-scale models, and the model's own output from a previ-

ous cycle (see Golding, 1987; Golding, 1992), though recently the UKMO has switched to the Unified Model, which is hydrostatic and is used as both a regional and global model (Cullen, 1993). Other examples of mesoscale forecasting models used by weather-service offices include the PERIDOT (Prévision à Echéance Rapprochée Intégrant des Données Observées et Télédétectées) model of the French Meteorological Office (Imbard et al., 1987) and the Japanese Spectral Model (JSM) (Segami et al., 1987) of the Japanese Meteorological Agency. Both of these have rather simple precipitation schemes and grid spacing near 40 km. The recent addition of the meso-Eta model (referred to in Mesinger and Treadon, 1995) gives NCEP a model product of similar resolution.

Though numerous mesoscale simulations have been made of particular weather situations after the event, apparently the first use of mesoscale models to produce a real-time (i.e., useful) forecast in the university environment was that of the PSU/NCAR MM4 (Warner and Seaman, 1990). The forecast model setup included a coarse grid with 90-km grid spacing centered over the eastern U.S. and a fine grid with 30-km grid spacing. For resolvable precipitation, a scheme by Hsie et al. (1984) kept track of raindrop water content through a linear autoconversion (cloud droplet to raindrop) scheme. A Kuo-type cumulus parameterization was used to account for subgrid-scale convective precipitation. For initial and boundary conditions the model utilized the Regional Analysis and Forecasting System (RAFS), which includes the Nested Grid Model (NGM) as the forecasting component. Initialization took about 30 minutes on a VAX system and a 36-hr forecast took about 3 hours on an IBM 3090. Test forecasts were generally good although forecast precipitation amounts were over-predicted and missed several features in the observed field.

Recently, forecast models based on the PSU/NCAR MM5 have been used to produce prototype real-time forecasts at a variety of locations, including NCAR and the University of Washington. These generally include a microphysics scheme based on that of Hsie et al. (1984) which includes both ice and water phase physics, but not both in the same grid volume (Dudhia, 1989). The PSU/NCAR MM5 incorporating this scheme was tested on ceiling and visibility forecasts with plausible results (Stoelinga et al., 1994; Gayno et al., 1994).

The UW-NMS is also currently used for twice daily prototype real-time 48-hr forecasts, with the third grid achieving 27-km grid spacing over the Wisconsin region. A group in Quebec has had some forecasting success with a non-hydrostatic model using semi-implicit, semi-Lagrangian equations (similar to the nonhydrostatic UKMO model) which are stable using time steps as large as those of hydrostatic models, resulting in greatly shortened model run time for a given forecasting period (Tanguay et al., 1990).

At Colorado State University a forecast version of RAMS has been in existence since 1991. More details on forecast RAMS follow in Chapter 3 of this thesis.

2.3 Orographic Precipitation Modeling and Verification

Most published studies on the orographic influence on precipitation seem to concentrate on liquid-phase precipitation (Hill et al., 1981; Barros and Lettenmaier, 1994). In these studies even small topographic features can cause significant enhancement of observed precipitation. To explain this phenomenon, the 'seeder-feeder' mechanism is proposed, where nucleated precipitation particles in the 'seeder' cloud (or region of cloud) fall into a 'feeder' cloud of high liquid water contents; the precipitation particles collect large amounts of cloud droplets from the feeder cloud and cause a large increase in the amount of liquid water that reaches the ground (Bergeron, 1965). One observational study on solid precipitation distribution was that by Browning (1983), who studied the snowfall distribution after a 1982 Welsh snowstorm and estimated that half of the observed 3 cm h^{-1} snowfall rate was due to orographic enhancement. This enhancement was thought to be due to enhanced aggregation and deposition rather than the riming of snowflakes. Modeling studies by Choularton and Perry (1986) suggested that orographic enhancement of snowfall was even more effective than enhancement of rainfall. They found that for broad hills where the upslope merely resulted in ice supersaturation, most of the increase in snowfall was due to vapor deposition; on steeper hills, the existence of water supersaturations resulted in rimed particles forming the bulk of the enhancement. Observational studies (Rauber, 1992) and modeling studies (Meyers and Cotton, 1992; Hobbs et al., 1973) both confirm that wind drift of the lighter, relatively unrimed particles causes the peak in aggregates to occur near mountain crests

while the peak in rimed precipitation occurs tens of kilometers upwind from the mountain crest.

Verification of modeled precipitation against observations is notoriously difficult. Among the difficulties involved are the many factors which contribute to generating precipitation (temperature, dew point, vertical velocity, etc.), the sparse nature of most precipitation networks, and the large gradients in the observed fields (Tucker et al., 1989). With frozen precipitation there is the additional difficulty of measuring precipitation which is drifting in high winds. Many cases of model verification against observations in the literature involve simulations (rather than forecasts) performed on specific case studies, often using observations to help set the boundary conditions of the model at later times, instead of forecasts from other models. Simulations can eliminate poor initializations or forecasts from other models as factors in model accuracy. But the use of observations in boundary conditions gives the model an advantage which is unavailable to the real-time forecaster, as does the use of finer resolutions or sophisticated cloud physics when the time constraint of the real-time forecaster is exceeded.

One study that did quantitatively compare forecasted precipitation with observations was that of Anthes et al. (1989), who examined MM4 precipitation forecasts on an 80-km grid for the eastern U.S. and found that one type of skill score, the threat score (see Chapter 5), showed better performance at the lower precipitation thresholds (averaging 0.62 year-round at the 0.01 in. threshold for 24-hr forecasts, but 0.35 at the 1 in. threshold). The addition of a microphysics scheme which explicitly predicted cloud and rain water actually decreased the threat scores, especially at the lower thresholds (scores of about 0.45 at 0.01 in. and 0.32 at 1 in.). In general the areal coverage of precipitation was overpredicted, especially at the largest thresholds, though at large thresholds the number of stations actually receiving the amount of precipitation is small, so the statistical significance may be low at the high thresholds. However, the explicit microphysics scheme underpredicted areal coverage at all but the largest threshold, which was attributed to the absence of subgrid saturation in the model. This study did include summer precipitation events as well as winter ones; in general, forecasting skill increased during the winter. A study by Junker et al. (1989), which showed

that over a 21-month period and a 60-station network the NGM precipitation forecasts slightly overestimated areal coverage at low precipitation thresholds but underestimated by a factor of two the area of higher thresholds. In general, skill scores of the major forecasting models seem to be increasing with time, but considerable controversy still exists on how to best quantify precipitation forecast accuracy (see Glahn, 1985).

Chapter 3

RAMS REAL-TIME FORECASTING

At Colorado State University RAMS has been adapted for use in a real-time forecasting mode since November 1991 (Thompson, 1993; Cotton et al., 1994), and such forecasts have been produced on a daily basis since 1993 (Beitler, 1994; Cotton et al., 1995). During this period new model versions, increased computational speed, new initialization datasets, and modifications to the representation of physical processes have led to intermittent but unceasing change in the forecast model and the procedures used to produce a forecast.

3.1 Description

A forecast model run consists of three stages: the isentropic analysis (ISAN) stage, the atmospheric model stage, and the visualization and analysis (VAN) stage. The ISAN stage consists of converting a dataset or datasets into a gridded field of atmospheric variables suitable for use by RAMS (see Tremback, 1990). Two types of files are produced during this stage by the forecast model: an initial file, which is based on observational analyses and is used to set the initial conditions of the model; and the so-called "nudging" files, which are based on forecasts by large-domain models such as the NGM or Eta model. The latter files are used to set boundary conditions for the coarse grid of the model at later times using a Davies (1983) relaxation scheme. In this scheme a term forcing solutions towards the nudging files' field values is added to the model's own tendency terms, and is proportional to the time difference between the nudging file and the model simulation time, increasing in strength with proximity to the domain boundary. The atmospheric model stage accomplishes the actual forecast. The predicted atmospheric variables such as ice-liquid potential temperature are integrated over time, and are recorded in binary output files at two-hour

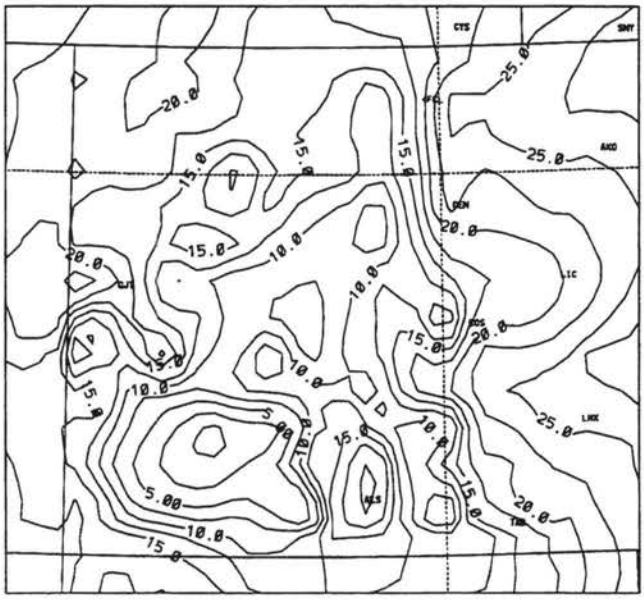

Figure 3.1: Sample fine grid plot, dew points

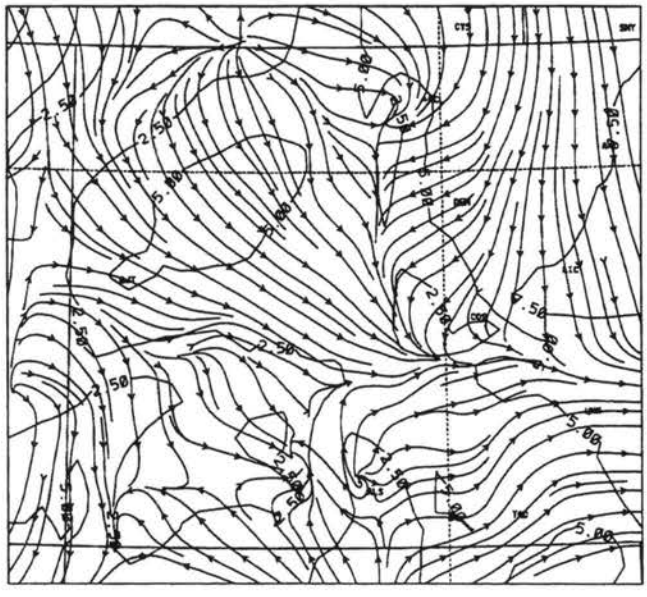

Figure 3.2: Sample fine grid plot, 700 mb streamlines

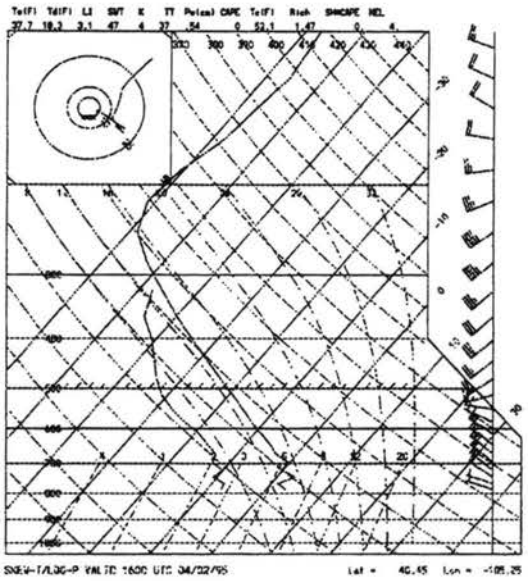

Figure 3.3: Sample skew-T plot, Fort Collins

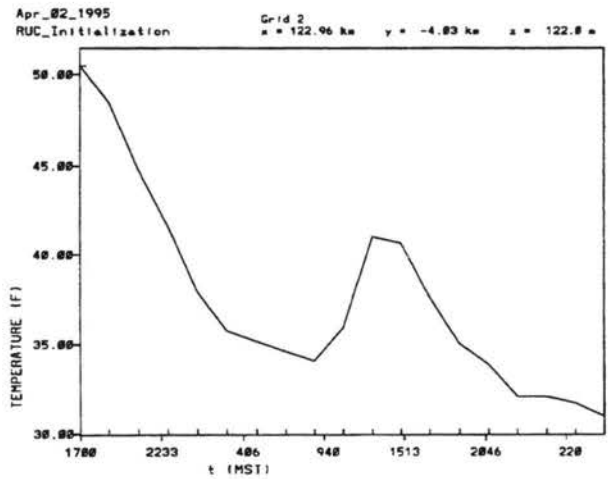

Figure 3.4: Sample time series grid plot, Fort Collins temperature

intervals. The VAN stage involves converting these output files to graphical plots. During this stage more conventional atmospheric variables such as temperature and pressure are diagnosed from the prognosed variables. Plots of meteorological variables are produced for both grids, and include map-view plots, cross-sections, and skew-T soundings. In addition, time series of variables of interest to agricultural communities such as relative humidity are produced for selected points within the model domain. (see Figures 3.1 through 3.4)

The forecast model utilizes the bulk microphysics of Version 3b of the model; more details are found in Section 3.3 of this thesis. The vegetation is allowed to vary over the model domain and is taken from a database which contains for each latitude/longitude coordinate one of the 18 vegetation types in the Biosphere-Atmosphere Transfer Scheme (BATS) (see Dickinson et al., 1986). Geographical datasets of topography (to 30 second increments), percentage of surface water, and month-dependent sea-surface temperatures are also available for use by RAMS. The radiation scheme of Mahrer and Pielke (1977) is used for the forecast model. This scheme takes into account the radiative transfer of various gases (e.g., CO_2, water vapor) but not liquid water (i.e., clouds). The Chen and Cotton (1983) radiative scheme of RAMS includes the effects of cloud water but proved too computationally expensive for use in weather prediction. To include the radiative effects of clouds in at least a simple manner, the parameterization developed by Thompson (1993) was used, which computes the longwave emission of "pseudo-clouds", or grid volumes where the relative humidity exceeds a threshold based on the horizontal model spacing. The parameterization of the shortwave cloud forcing is the one used by Thompson which uses the relationship between cloud thickness and albedo of Neiburger (1949) to remove a fraction of the surface shortwave flux based on the thickness of the highest model cloud layer.

The forecast domain consists of two nested grids. The coarse grid has 80-km grid spacing and is 39 $\times$ 31 in extent; it covers most of the western United States. The fine grid is 42 $\times$ 37 and possesses 16-km grid spacing, and covers the state of Colorado and portions of neighboring states (Figure 3.5). The vertical spacing increases from 250 m near the surface to 1 km near the top of the model domain at 17 km, encompassing 26 levels. A time step of 90 seconds is used on the coarse grid and 45 seconds on the fine grid; furthermore, a time

step shorter by a factor of three is used to update terms related to acoustic propagation (see Klemp and Wilhelmson, 1978). Hybrid time stepping is performed; that is, a leapfrog time operator is used for the velocity and pressure variables whereas other variables use simple forward time stepping. An Asselin filter and second-order advection are selected. Turbulent diffusion is accomplished horizontally by a Smagorinsky (1963)-based deformation scheme, and vertically by a one-and-a-half order Mellor and Yamada (1974) scheme. The model top set a rigid-lid boundary condition for this study, though this has recently been changed in the real-time model to a scheme which utilizes nudging towards large-scale numerical model solutions.

3.2 Data Ingest

Since 1994, the initialization dataset used by the forecast model has been the RUC (Rapid Update Cycle) analyses produced at NMC/NCEP. These analyses utilize the MAPS (Mesoscale Analysis and Prediction System) data ingest format developed at the Forecast System Laboratory (FSL) (see Benjamin et al., 1991). This dataset has the advantage of incorporating information from a diverse set of sources, including surface observations, rawinsonde observations, mesonet observations, wind profilers, and aircraft reports (Beitler, 1994). Data are analyzed to a grid with 60 km grid spacing (see Figure 3.6). The vertical coordinate used is the hybrid-b scheme version of MAPS (Bleck and Benjamin, 1993). In this scheme 25 vertical levels are used. Levels near the top of the domain follow isentropic surfaces. However, as isentropic surfaces approach the ground, the levels gradually take on the characteristics of a terrain-following coordinate (Figure 3.8). This is done because in a pure isentropic coordinate system features in the boundary layer would not be resolved.

The RUC files are obtained by anonymous ftp via the NOAA Information Center. The datasets used are the 0000 UTC analyses compressed in GRIB (GRid In Binary) format and are usually completed by 0400 UTC, at which time the data are down-loaded to the real-time forecasting computer. At the time of the start of the forecast cycle (about 0500 UTC) information from the RUC files is combined with files of surface and rawinsonde observations to produce the initialization file for the atmospheric model run. The nudging

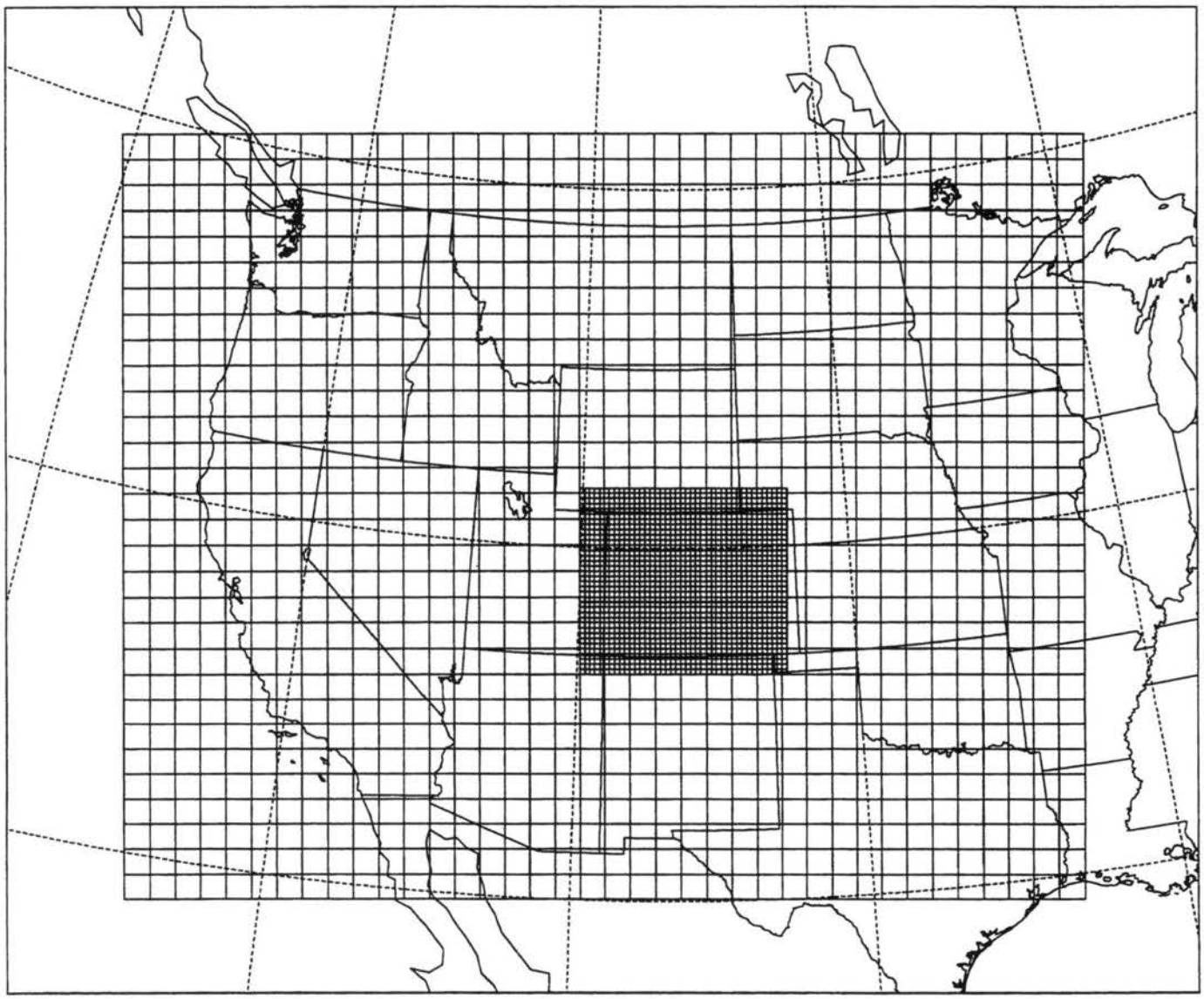

Figure 3.5: Model domain, Grids 1 and 2

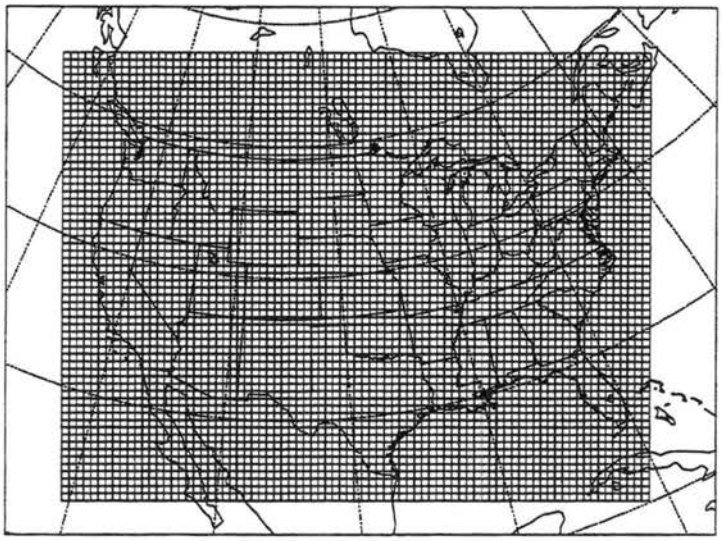

Figure 3.6: MAPS 60-km grid domain

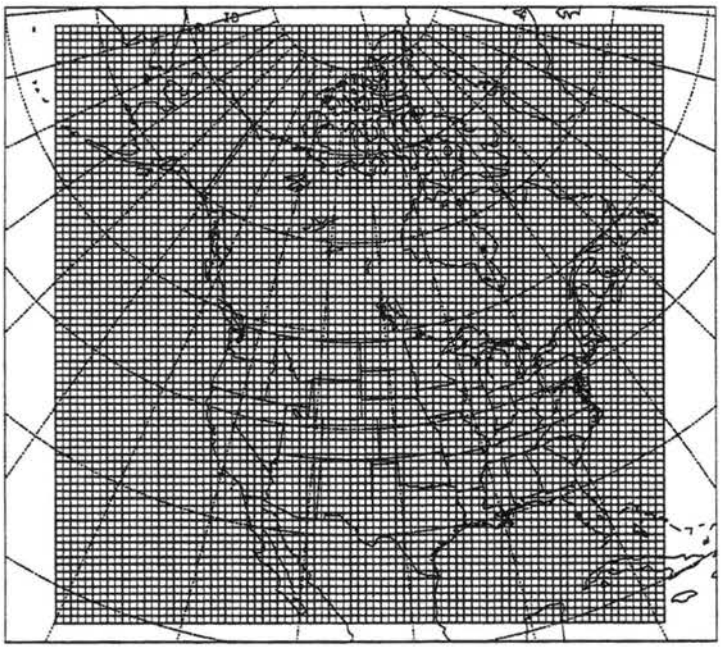

Figure 3.7: Eta 80-km grid domain

files are produced from the Eta forecasts produced at 0000 UTC because of the quality of forecasts of that particular model (see Figure 3.7). Through an arrangement with NCEP (NMC) we are also able to obtain GRIB files of the 80-km 'early-Eta' model by 0400 UTC. The 12-hr, 18-hr, 24-hr, 30-hr, and 36-hr forecasts are each used to produce a nudging file. The atmospheric model calculates a tendency to the model fields based on the fields of the two nudging files with valid times just before and after the current model run time, and then performs a weighted average of the tendency terms based on how close the model run time is to the two nudging file times. The atmospheric field variables thus resemble those of the large-scale model forecasts near the boundaries of the coarse grid.

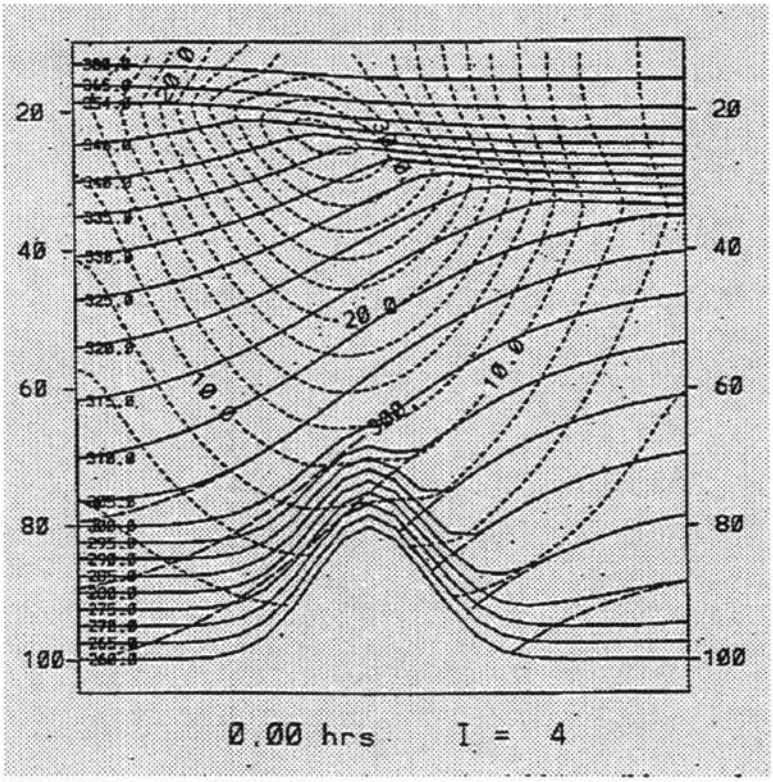

Figure 3.8: Vertical coordinates used in MAPS grid, from Bleck and Benjamin (1993). Solid lines are the coordinate surfaces while thick dashed lines are isentropes. Coordinate labels are the potential temperature for each vertical level far away from the surface. Thin dashed lines are isotachs for this particular analysis. Vertical axis labels are pressure in kilopascals.

3.3 Precipitation Prediction

Version 3b of RAMS permits the storage of the mixing ratios of seven condensed water categories at all grid points: cloud water, rain, pristine ice, snow, aggregates, graupel,

and hail (see Walko et al., 1995). The size spectra of all categories are assumed to follow generalized gamma function distributions of the form (Flatau et al., 1989; Walko et al., 1995)

$$f_{gam}(D) = \frac{1}{\Gamma(\nu)} \left(\frac{D}{D_n}\right)^{\nu-1} \frac{1}{D_n} \exp\left(-\frac{D}{D_n}\right) \tag{3.1}$$

where D is the particle diameter, ν is the shape parameter which varies the breadth of the distribution, and D_n is a characteristic diameter defined as D_{mean}/ν. This function is convenient to use because when ν is 1 the distribution reduces to the Marshall-Palmer distribution commonly used to represent hydrometeors (Marshall and Palmer, 1948). Furthermore, when properties such as particle size and fall velocity are given as power-law expressions of diameter, then quantities such as mixing ratio become moments of the function distribution, and for the generalized gamma function each moment P is simply

$$\int_0^\infty D^P f_{gam}(D) \mathrm{d}D = D_n^P \frac{\Gamma(\nu + P)}{\Gamma(\nu)}. \tag{3.2}$$

This allows mixing ratio to be easily diagnosed from the number concentration and vice-versa provided D_n and ν are specified.

In the RAMS bulk microphysics the mixing ratios for all species are predicted from microphysical equations except for the cloud water mixing ratio, which is diagnosed as the total water mixing ratio above saturation not residing in other hydrometeor species. Representations of nucleation formulas also allow the number concentration of pristine ice to be calculated by the model (Meyers, 1995; Harrington et al., 1995). The number concentration of other water species are either specified at the beginning of the run or diagnosed from specified mean diameters. Once created, all categories except cloud droplets are allowed to fall at a size-dependent terminal velocity (Walko et al., 1995) which translates into accumulated water-equivalent precipitation at the ground.

The forecast model specifies the concentration of cloud droplets and mean diameters of the other species. Mean diameters as given to RAMS are mass-weighted mean diameters: i.e., the specific diameter all the hydrometeors for a particular class would have to be in

order to possess the given mixing ratio with the same hydrometeor number concentration. If the mass of a hydrometeor is expressed as a power law expression:

$$m = \alpha D^{\beta}, \tag{3.3}$$

where D is the hydrometeor diameter and α and β are specified for each category, then the total mixing ratio of a hydrometeor species at a grid volume becomes, after integrating (Walko et al., 1995):

$$r = \frac{N_t}{\rho_a} \alpha D_n^{\beta} \frac{\Gamma(\nu + \beta)}{\Gamma(\nu)}, \tag{3.4}$$

where N_t is the total number concentration and ρ_a is the air density. Thus, the mass-mean diameter D_m can be expressed as:

$$D_m = D_n \left(\frac{\Gamma(\nu + \beta)}{\Gamma(\nu)} \right)^{1/\beta}. \tag{3.5}$$

The value of β is 3 (i.e., the mass is proportional to the cube of the length) for all categories except for pristine ice, snow, and aggregates, where it is 2, 2.4, and 2.4, respectively. The width parameter ν can be chosen by the user for each category, though for a particular water species ν stays constant throughout the duration of the model run.

The microphysical calculations are quite time-intensive, to the extent that in the past the forecast model could not be run in real-time using the microphysics of RAMS, at least if it was to be run on workstations available in the university environment. Instead, precipitation predictions were done using a parameterization based on that of Rhea (1978) which was developed for use in winter weather events in the Colorado mountains. The scheme based on the parameterization of Rhea will henceforth be referred to as the 'dump-bucket' scheme, because it operates on the bulk of available water substance without regard to microphysics or hydrometeor species, and converts it directly into ground-received precipitation. Rhea calculated a precipitation efficiency:

$$E = min(0.25, max(-kT_c, 0)), \tag{3.6}$$

where T_c is the temperature in Celsius of the highest sufficiently-saturated layer (relative humidity $> 65\%$) in the atmosphere, and k is a constant taken to be 0.01. Then during each

time step the efficiency times the amount of available condensable water is converted into precipitation. Originally 'available condensable water' would be simply the amount of total water exceeding the saturation water vapor mixing ratio over liquid. Level 2 microphysics is used in conjunction with the dump-bucket scheme, where cloud water mixing ratio is diagnosed as the amount of total water exceeding saturation, which is only performed after the dump-bucket precipitation is extracted. No other condensed water species are allowed. However, the model began to precipitate out so much water that none was left for cloud droplets. To keep this from happening, 'total condensable water' became ten percent above saturation, to ensure that the dump-bucket scheme would never be able to completely deplete a cloud.

Use of this scheme no longer became necessary in September 1995 because: 1) an IBM RISC-6000 390 workstation became available, which decreased computing time by about one-third; 2) Version 3b of RAMS, which possessed many time optimization features in the microphysics, had become available; and 3) further optimization of the microphysics was performed on the forecast model. These modifications now permitted the completion of a 36-hr forecast from initialization to graphics output in about seven hours.

3.4 Past Work With Forecast RAMS

Thompson (1993) started producing real-time forecasts using the RAMS model in the winter seasons of 1991-1992 and 1992-1993 (see also Cotton et al., 1994). He used Version 2c of RAMS along with the dump-bucket precipitation scheme, so that the forecasts could be produced in real-time on a Stardent 3000 workstation. He used a 100-km coarse grid and a 25-km fine grid extending from southern Colorado to central Wyoming, along with 300-m vertical grid spacing near the surface and 24 vertical levels. After performing statistical analysis for the whole 1991-1992 season he found that thermodynamic variables were forecast best while wind components were forecast somewhat less well and relative humidity was forecast least well. Accuracy tended to be highest in the upper troposphere but decreased near the surface. In a case study, comparisons with NGM and Eta model output showed better surface temperature and relative humidity forecasts with the RAMS model.

Then a comparison was performed to a RAMS simulation using the microphysics option. Little change was seen in the forecast variables mentioned above, but there was considerable improvement in the forecast precipitation field. Thompson also used the forecast model during the FIRE II program (First ISSCP Regional Experiment Phase II, where ISSCP is itself an acronym for International Satellite Cloud Climatology Program) in November 1991 to predict the occurrence of cirrus clouds over the test domain. This required using the microphysics option of RAMS so ice nucleation would be accounted for, so the runs had to be performed on a CRAY Y-MP supercomputer so that they would be real-time. Forecast cirrus cloud fields corresponded favorably with observations though the predicted ice-water contents of the clouds seemed to be an order of magnitude low.

Beitler (1994) started producing real-time RAMS forecasts on a year-round basis in the fall of 1993. He used a forecast model based on Version 3a of RAMS but still was required to use the dump-bucket scheme for computational speed. Initialization and nudging were both performed with the 80-km Eta datasets, as opposed to the MAPS analyses and NGM forecasts used by Thompson. In a case study of a February 1994 winter storm, Beitler found that the use of the RAMS microphysics greatly enhanced quantitative precipitation forecasting (QPF) accuracy, though such forecasts still could not be produced in real-time. A simulation of a July 1993 windstorm in the Fort Collins region using three levels of grid nesting also produced results closer to those observed when a combination of the microphysics option and addition of a third grid was used (Cotton et al., 1995).

Additionally, Snook (1993) performed a series of simulations of two Front Range case studies with a purpose of seeing how the increased resolution of the 10-km Local Analysis and Prediction System (LAPS) and a corresponding model grid spacing would improve forecasts. Performing a similar analysis to that of Thompson, he concluded that the LAPS simulations increased model performance over simulations using the coarser MAPS datasets mainly due to the finer topography in LAPS rather than the actual analysis. Precipitation validation of the model microphysics again was not statistically performed, but qualitatively forecast precipitation captured most of the observed features when convection was not present, and the precipitation amounts were accurate where observational reports existed.

For another example of the use of a RAMS forecasting model initialized from LAPS data at the Forecast Systems Laboratory (FSL), see Schultz (1995).

3.5 Current Study

The purpose of this current study, inspired by the previous work with RAMS, is to assess the quantitative performance of Version 3b of RAMS in forecasting winter precipitation events using bulk microphysics. The month of April 1995 is investigated. During that month the forecast model was still based on Version 3a of RAMS and using a dump-bucket precipitation scheme. During the fall of 1995 simulated 24-hr forecasts were performed for each of the days of that month using Version 3b of RAMS and the microphysics option. These results were then compared to the real-time forecasts actually produced during April 1995. Because of difficulties with the forecast model procedure described earlier, either due to problems with obtaining input data or to human operator error, on certain days during the month a real-time forecast was not produced. It was later decided to re-simulate these days using the dump-bucket version of the model to expand the set of days for which comparisons between the two forecast models could be performed. Both versions of the forecast model also incorporated the modified-Kuo convective parameterization described in Tremback (1990) in an attempt to account for convectively-produced precipitation, though the resolution of the forecast model is a bit finer than that recommended for optimal use of this scheme.

To provide an observational verification basis, data from SNOTEL (SNOw TELemetry) instruments for the month were utilized. These are automated pillow sensors which transmit their data by radio (see McMillan, 1981), and they are maintained by the USDA Natural Resources Conservation Service. Data include max/min temperatures, mean daily temperatures, and total water equivalent precipitation since the beginning of the Water Year, October 1. Readings are usually taken twice a day, at midnight and noon local standard time, though on some days readings are taken more frequently while on other days no readings at all are taken. The SNOTEL data for April were obtained from the Western Regional Climate Center at the Desert Research Institute in Nevada, which provided daily

reports of accumulated water-equivalent precipitation for a network of 49 stations in the Colorado Rockies. Of this set, 32 stations recorded enough data during the month to be used in this study (see Figure 3.9 and Table 3.1). A problem arose because the forecasting period extended from 0000 to 0000 UTC, whereas the SNOTEL verification period was from midnight to midnight Mountain Standard Time (MST). Additionally, the archived Rhea-scheme forecasts contained atmospheric information at 2-hour increments, which included midnight Mountain Daylight Savings Time (MDT) but not midnight MST. So, accumulated precipitation from successive microphysics model runs were spliced together to form midnight-to-midnight MDT model totals, and these were assumed to approximately correspond to midnight-to-midnight MST totals.

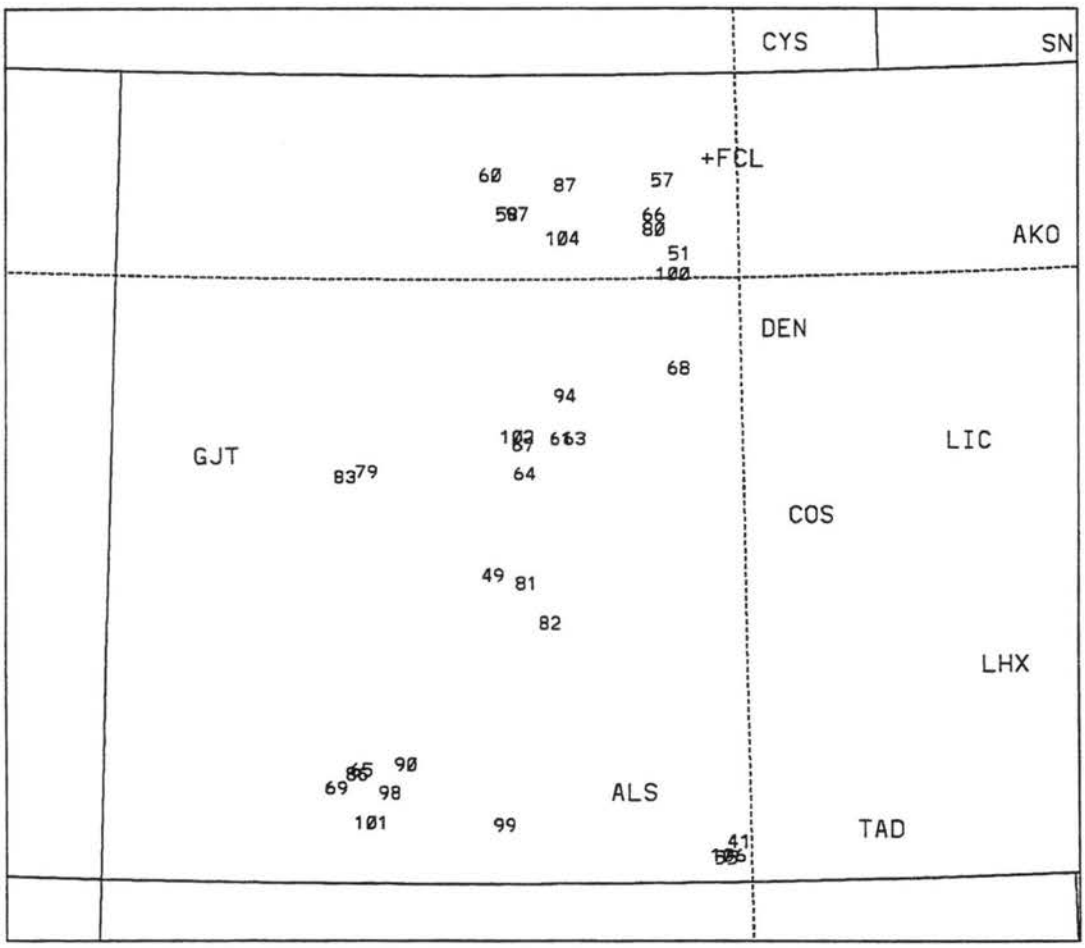

Figure 3.9: Location of SNOTEL sites, by ID number

ID	Name	Latitude	Longitude	Elevation
41	APISHAPA SNOTEL	37.20	105.04	10000
49	BUTTE SNOTEL	38.53	106.57	10150
51	COPELAND LAKE SNOTEL	40.12	105.34	8550
55	CULEBRA #2 SNOTEL	37.12	105.12	10500
57	DEADMAN SNOTEL	40.48	105.45	10220
58	DRY LAKE SNOTEL	40.32	106.47	8250
60	ELK RIVER SNOTEL	40.51	106.58	8650
61	SNOTEL	39.22	106.12	11400
63	HOOSIER PASS SNOTEL	39.22	106.03	11550
64	INDEPENDENCE PASS SNOTEL	39.04	106.36	10600
65	IDARADO SNOTEL	37.56	107.40	9800
66	JOE WRIGHT SNOTEL	40.31	105.51	10120
67	KILN SNOTEL	39.19	106.37	9600
68	LAKE ELDORA SNOTEL	39.56	105.36	9700
69	LIZARD HEAD PASS SNOTEL	37.47	107.56	10200
79	OVERLAND RSVR SNOTEL	39.05	107.38	9840
80	PHANTOM VALLEY SNOTEL	40.24	105.51	9030
81	PARK CONE SNOTEL	38.49	106.35	9650
82	PORPHYRY CREEK SNOTEL	38.29	106.20	10750
83	PARK RSVR SNOTEL	39.02	107.52	9960
86	RED MOUNTAIN PASS SNOTEL	37.54	107.43	11090
87	ROACH SNOTEL	40.46	106.08	9850
90	SLUMGULLION PASS SNOTEL	37.59	107.12	11550
94	SUMMIT RANCH SNOTEL	39.43	106.09	9300
97	TOWER SNOTEL	40.32	106.40	10560
98	UPPER RIO GRANDE SNOTEL	37.45	107.22	9350
99	UPPER SAN JUAN SNOTEL	37.29	106.50	10200
100	UNIVERSITY CAMP SNOTEL	40.02	105.35	10360
101	VALLECITO SNOTEL	37.30	107.30	10880
102	VAIL MTN SNOTEL	39.23	106.37	10300
104	WILLOW CREEK PASS SNOTEL	40.20	106.06	9550
106	WHISKEY CREEK SNOTEL	37.13	105.07	10200

Table 3.1: SNOTEL stations used for this study. Elevation is in feet.

Additionally, when it became available, the Colorado edition of the Climatological Data publication of the National Climatic Data Center was used. This bulletin contains day-by-day precipitation totals for a series of stations manned by the National Weather Service (NWS), local observationalists, or an Automated Surface Observing System (ASOS) in the case of Denver International Airport. A total of 167 stations had observational data for all days of the month and fell completely within the model fine grid, so these stations were used for verification in this thesis. This provides a more extensive database than the set of SNOTEL stations, but since most of these climatological stations are located near population centers, they are more likely to be located in lower elevations and valleys, which should produce a different climatology than the climatology of the SNOTEL stations (Doesken and Schaefer, 1987). Also, though the National Weather Service Stations report daily precipitation totals at midnight, other climatological stations report at a wide variety of times, usually early morning or early evening. For each station which reports precipitation after the model initialization time (6:00 P.M MDT), the model precipitation for Julian day x is given by:

$$P_x = (P_x^{24} - P_x^{h-18}) + P_{x+1}^{h-18}, \tag{3.7}$$

where the subscripts refer to the day of the model run, the superscripts refer to the forecast time during each 24-hr model run at which model precipitation is extracted, and h is the hour of the day at which the station reports (or the next hour, if the hour is odd, because of the 2-hr frequency of forecast analyses). For stations which report before 6:00 P.M. MDT , model precipitation is given by:

$$P_x^{tot} = (P_{x-1}^{24} - P_{x-1}^{h+6}) + P_x^{h+6}. \tag{3.8}$$

SNOTEL and NWS stations report data as if h=24. Different stations thus do not report precipitation for precisely the same period on a given date, but for a given station the model and observational periods differ by at most one hour.

Chapter 4

RESULTS – DESCRIPTION

4.1 Case Studies

4.1.1 Synoptic Overview

According to Nolan Doesken in the weather summary from the April 1995 Colorado Climatological Data NOAA publication, twelve storm systems crossed the state of Colorado during the month. While the first half was mostly dry with the exception of a storm from April 9-11, starting around April 15th storm after storm dropped precipitation on Colorado, causing rain or snow to be recorded virtually every day over most of the state. Allenspark, Leadville, and Winter Park all recorded measurable precipitation for ten consecutive days while Colorado Springs saw measurable precipitation on 13 of the last 14 days of the month. The winter had been abnormally dry up to that point, raising fears of drought conditions during the summer after the melting of the meager snowpack, but such fears were averted when stations in the Arkansas and Platte drainage basins both received about twice their normal April precipitation during the month, while the Colorado and Rio Grande basins received 50% more precipitation than average. Combined with a moist May, the state in fact saw instances of flooding when the snowpack melted in late May and early June. Thus a large set of case studies from the month is available to try to assess the performances of the two versions of the forecast model, both in general and for specific synoptic situations. What follows in this section is a discussion of some of the specific precipitation events of the month, including qualitative details of the forecasts from each model.

4.1.2 April 9-11

The first week of April was almost entirely dry in the state, with only a few scattered flurries reported in the mountains around April 2-3. Las Animas reported the highest state's

highest temperature for the month (30° C) at the relatively early date of April 8 (NOAA, 1995). The dry trend ended, though, starting late on the 8th when an upper trough and a cool surge brought snow and rain to parts of northwestern and northeastern Colorado (See Figure 4.1). On the 9th temperatures were less than 10° C at many Front Range stations, down from above 20° C the day before, and precipitation was widely recorded as a surface low passed south of the state. Arctic air surged into Colorado and by the 10th heavy snow and strong winds enveloped the state east of the Rockies, leaving 25 cm of snow near La Junta, 28 cm at Boulder, and closing all roads out of Limon during the day. Temperatures stayed below freezing for the Front Range and dropped to −21° overnight at Westcliffe. During the 11th lessening snow continued over parts of the east as the surface low moved through the Midwest.

The April 9 forecasts for both the dump-bucket and microphysics models are shown in Figures 4.2 and 4.3 respectively. Both models capture a precipitation maximum near the Wet Mountains southwest of Colorado Springs, peaking at 13-15 mm of liquid water. This is borne out by observational data of 15 mm at Westcliffe (15 cm of snow) during the same observational period as the model run (April 9, 1800 UTC to April 10, 1800 UTC). Canon City, though it isn't an official climatological station, reported 28 cm of snow out of the storm (Doesken, Climatological Data, Special Weather Summary). Other features in the east favor the dump-bucket scheme; there is no evidence of the strong maximum near Limon as in the microphysics version, but there are larger amounts to the southwest (7.6 mm at 4 miles NNE of La Junta). Also there is no evidence of quite as much snow in the mountains west of Denver as the microphysics would suggest, though a few places in this region (Coal Creek Canyon, 10.2 mm) received a little more than the dump-bucket scheme would suggest during this period. The microphysics does better capture the lack of precipitation in northeastern Colorado (only 2.3 mm total from 1300 on the 9th to 1300 on the 11th) and in most of western Colorado (Grand Junction had no measurable precipitation for the duration of the storm) except for a region near the San Juans in the southwest (Ridgway recorded 20.3 mm on the 9th; the Montrose 2 station, 5.6 mm; Mesa Verde, further southwest, recorded 0.0 mm). Though both forecasts show skill on this day,

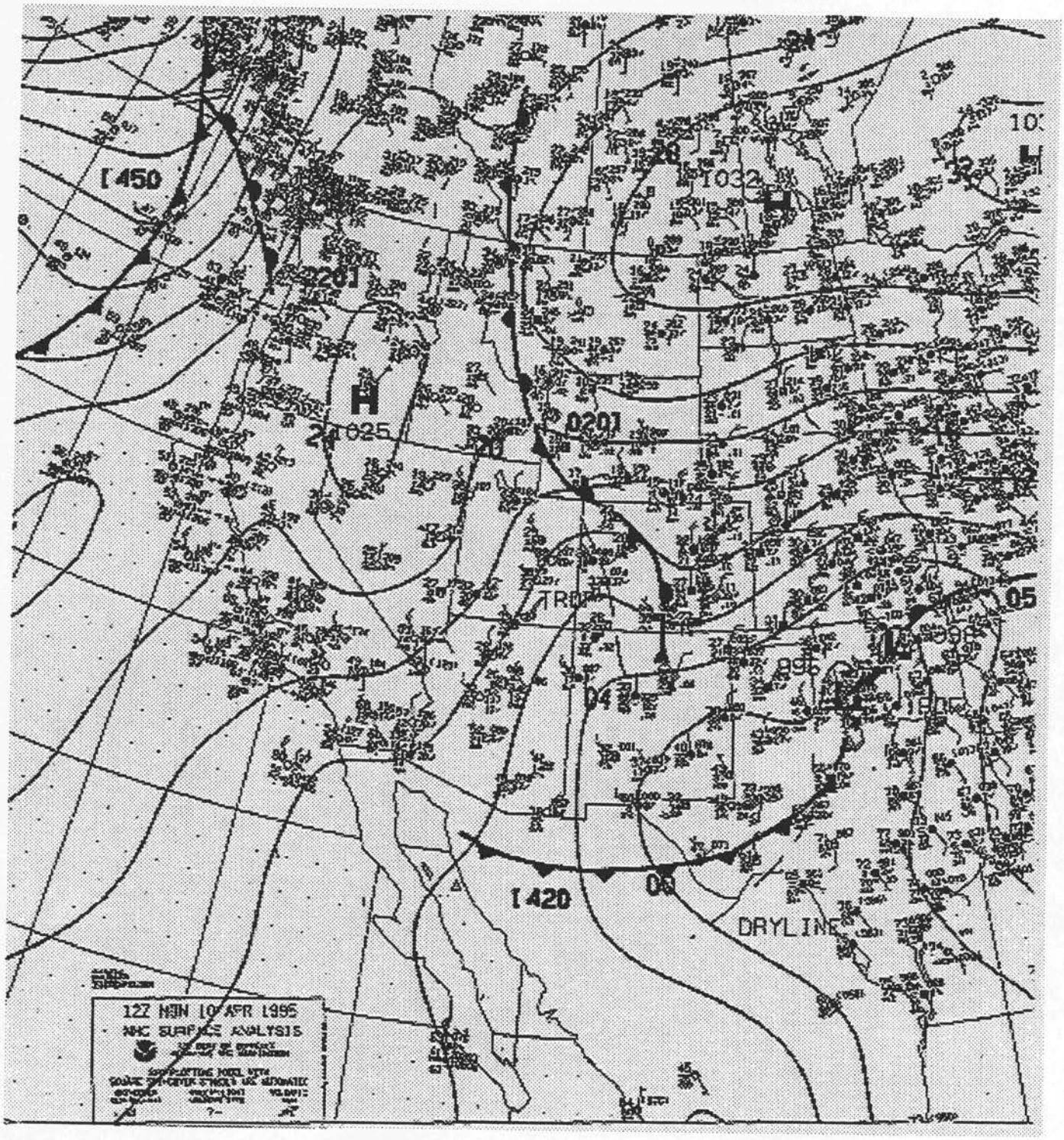

Figure 4.1: NMC surface map, 1200 GMT 10 April 1995

the dump-bucket forecast is probably better, especially on the Eastern plains. However, a characteristic of the dump-bucket scheme here which frequently occurs is over-forecasting of the smaller precipitation amounts.

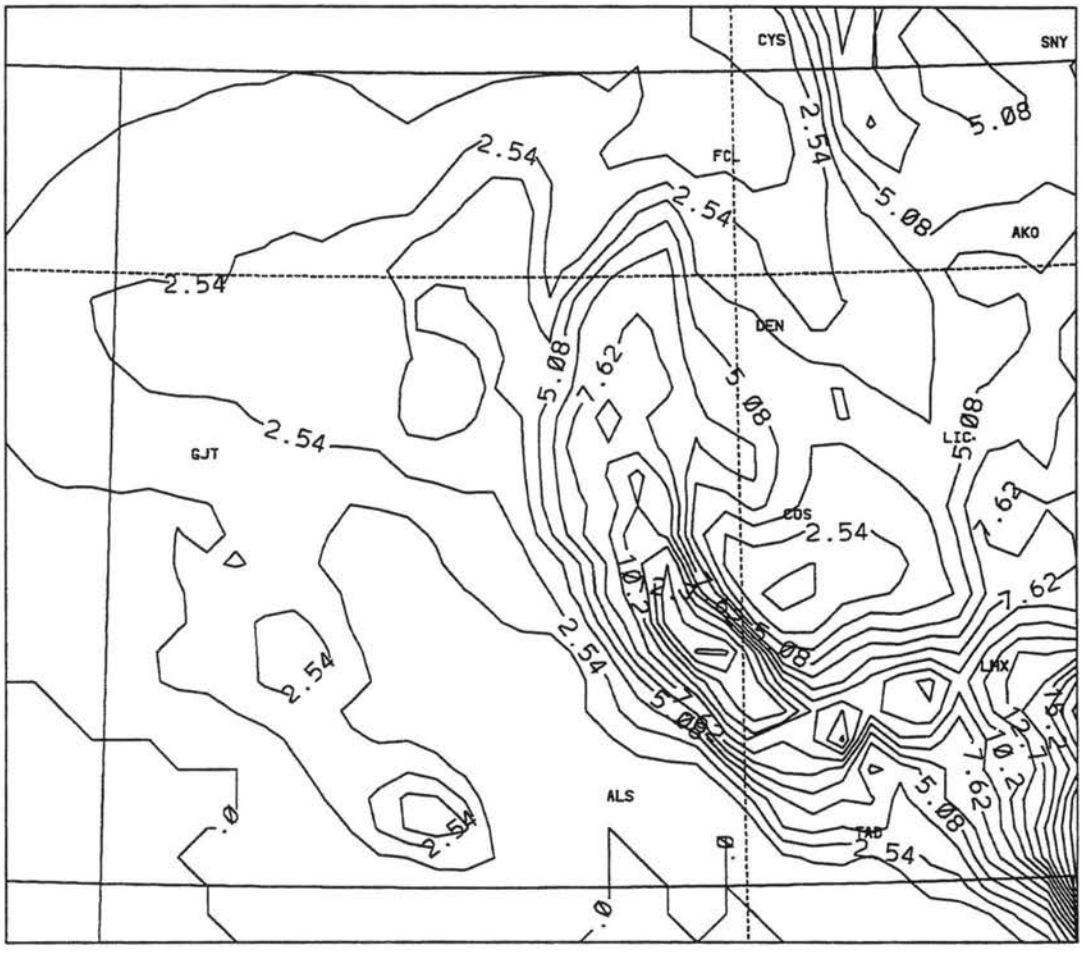

Figure 4.2: Accumulated precipitation, 0000 GMT April 9 to 0000 GMT April 10, for dump-bucket model, on fine grid. Units are millimeters of liquid water equivalent. Contour interval is 1.27 mm (0.05 inch).

Figures 4.4 and 4.5 are the model forecasts for the day of April 10. Both forecasts are very similar and accurately show the existence of the observed precipitation mostly east of the Rockies. In fact, statistics strongly suggest (see Chapter 5) that this is the most accurate significant forecast of the month for either model. The minimum on the Palmer Ridge is shown in the climatological data, though it was actually more extreme than was

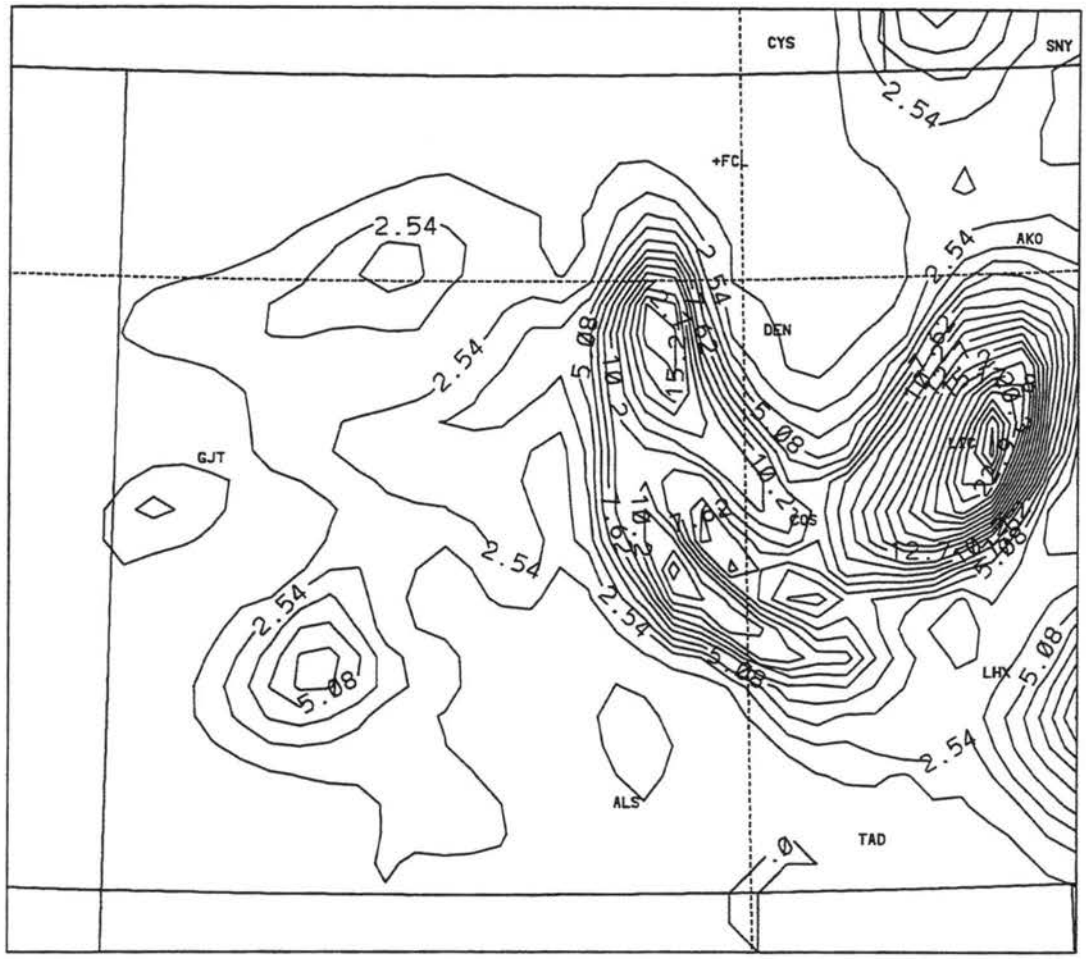

TOTAL PRECIP (mm)
24HR FCST VALID 0000 UTC 04/10/95

Figure 4.3: Same as Figure 4.2, but for microphysics model

modeled (Colorado Springs only received 1.3 mm on this day; Limon, despite the road closures, reported 4.6 mm). The maximum both west and east of Denver also appear in the observations, though again to a larger degree than in the models (32.5 mm at Strontia Springs Dam southwest of Denver; 35.3 mm at Deer Trail east of Denver). The 13 mm forecast at Denver compares to 7.9 mm reported at Stapleton. The microphysics model performs better, though, for the maximum west of Alamosa (1.3 mm at Alamosa, 16.3 mm at Monte Vista to the west, but only 7.9 even further west at perennially snowy Wolf Creek Pass!) and the far southeast (the site 15 miles NNE of Kim reported 22.1 mm). Also better

captured is the lack of precipitation near Fort Collins (1.0 mm) at this or any other time during the storm.

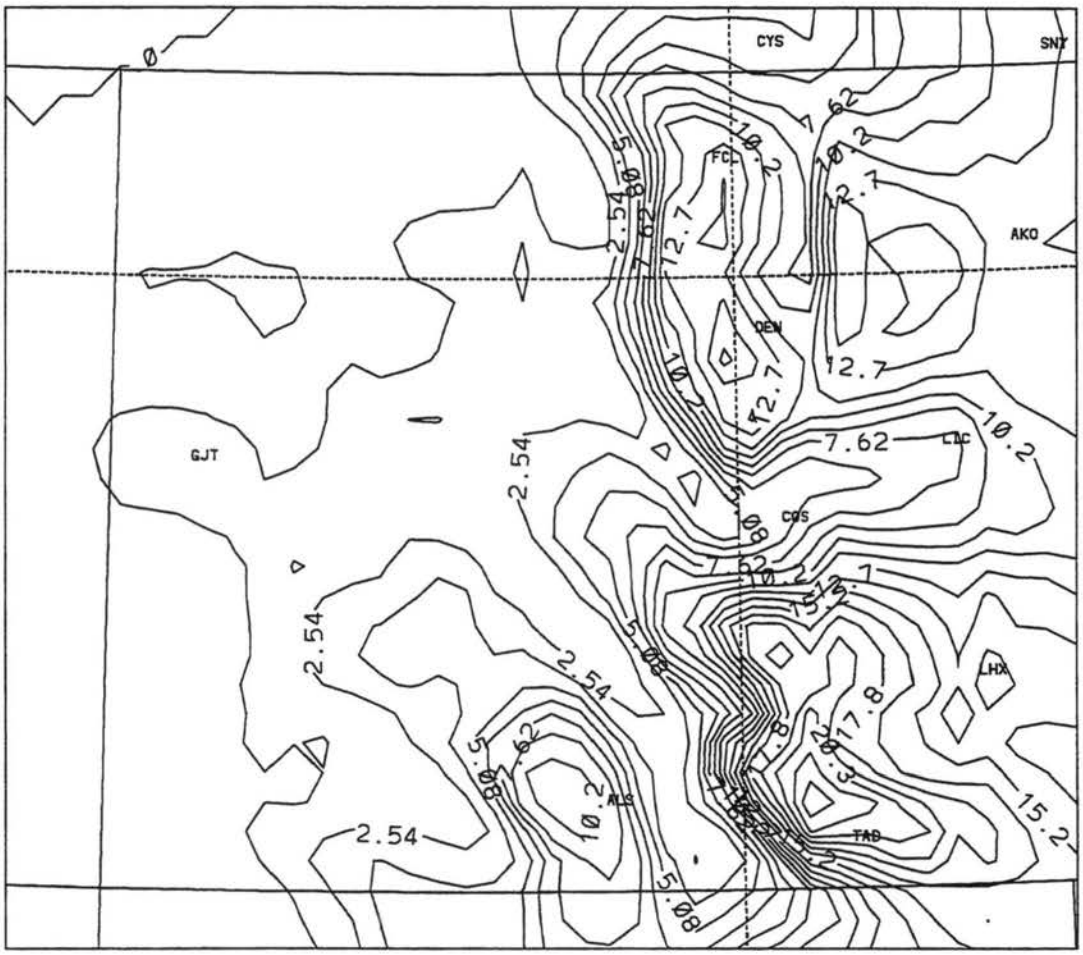

Figure 4.4: Accumulated precipitation, April 10 forecast, dump-bucket model

On the day of April 11, when only lingering 'wrap-around' snowfall remained, both models (Figures 4.6 and 4.7) had the right idea in concentrating precipitation in the northeast, but the modeled amounts were way too low for most of the area (Fleming in the lower Platte valley reported 10.2 mm this day, though Sterling only reported 2.0 mm). The larger snow region in the mountains did not occur as far west in the data (14.0 mm at Mt. Evans) as in the models. Greeley did report 8.1 mm on this day, which is vaguely suggested by a local maximum in the dump-bucket model forecast. Interestingly, when model precipitation

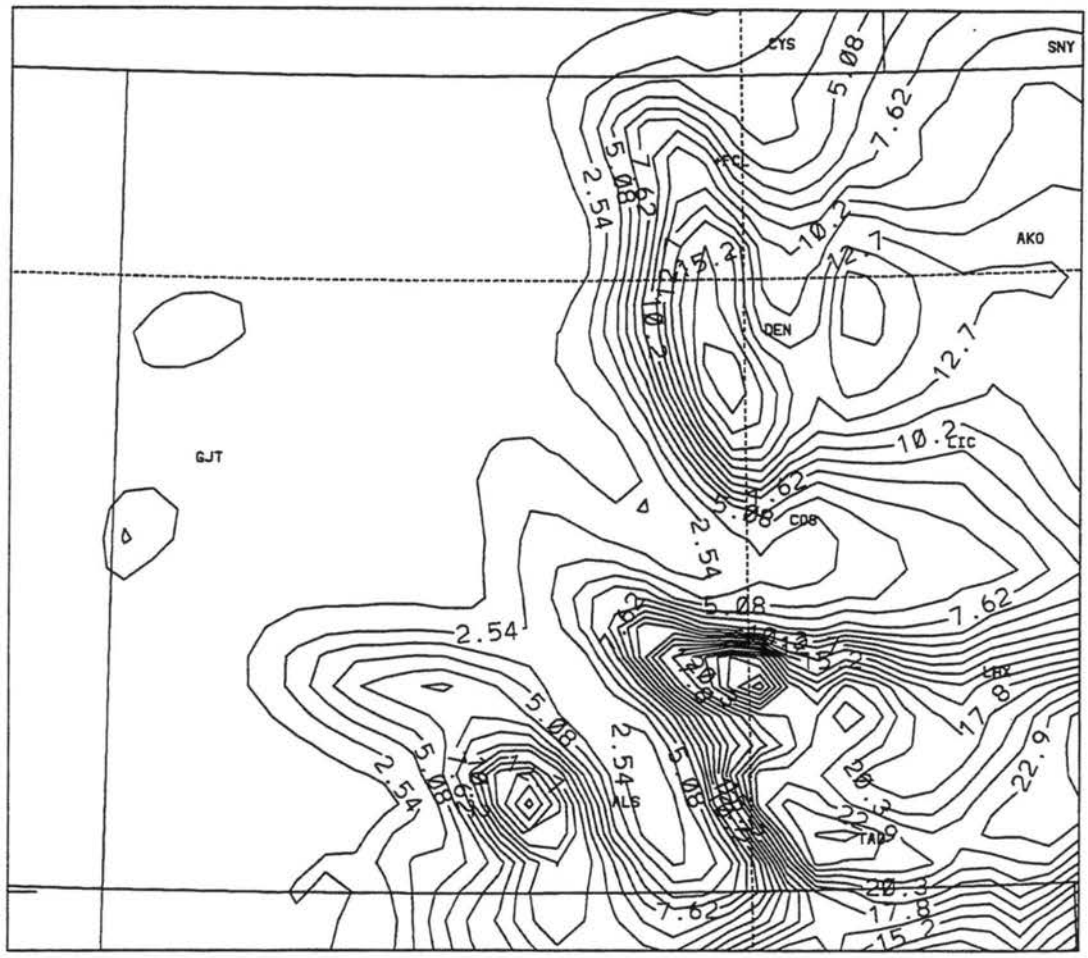

Figure 4.5: Same as Figure 4.4, but for microphysics model

for this day is averaged over all the sites, it is found that for April 11 model snow amounts were actually greater than the observed amounts (see Chapter 5). The explanation seems to be two-fold; one is that there were many stations reporting little or no precipitation interspersed with those mentioned above, which lowered the observational total precipitation below that of the smoothly-contoured model values. The other explanation seems to be that the day of April 11 included the final six hours of the April 10 simulation, which in the case of some stations exceeded the observed precipitation for the following 18 hours.

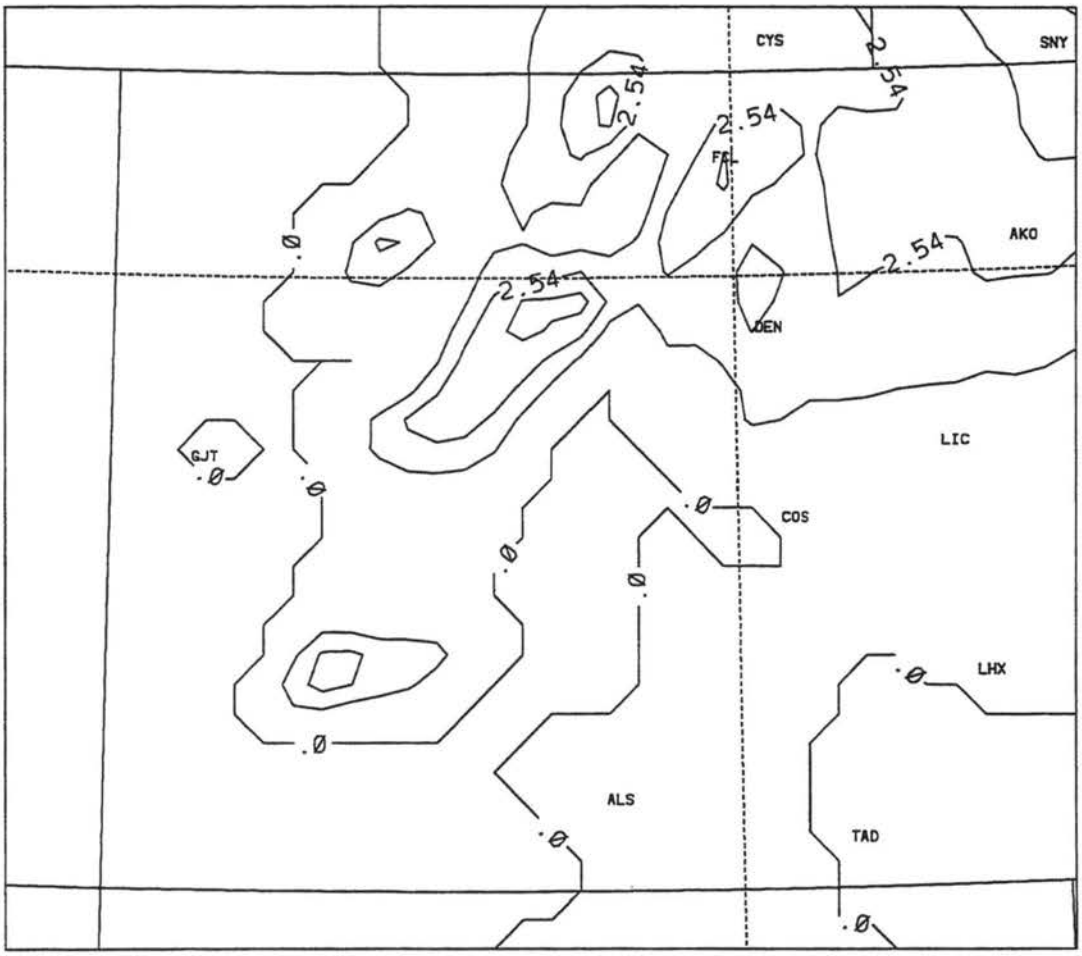

Figure 4.6: Accumulated precipitation, April 11 forecast, dump-bucket model

4.1.3 April 19-20

On April 19 a broad low-pressure system tracked through the state from the southwest (Figure 4.8). The Mt. Evans station recorded the greatest single day precipitation total (39.4 mm) of any climate station in the state for the month. Overall metro Denver was hardest hit (Lakewood got 21.1 mm) but also getting hard hit were the upper Arkansas River Valley (28.4 at Buena Vista) and parts of the southwest (12.7 mm at Durango Water Resources).

Figures 4.9 and 4.10 are the model forecasts for this time. The microphysics differs in that it virtually lacks precipitation on the plains. This was pretty accurate in many

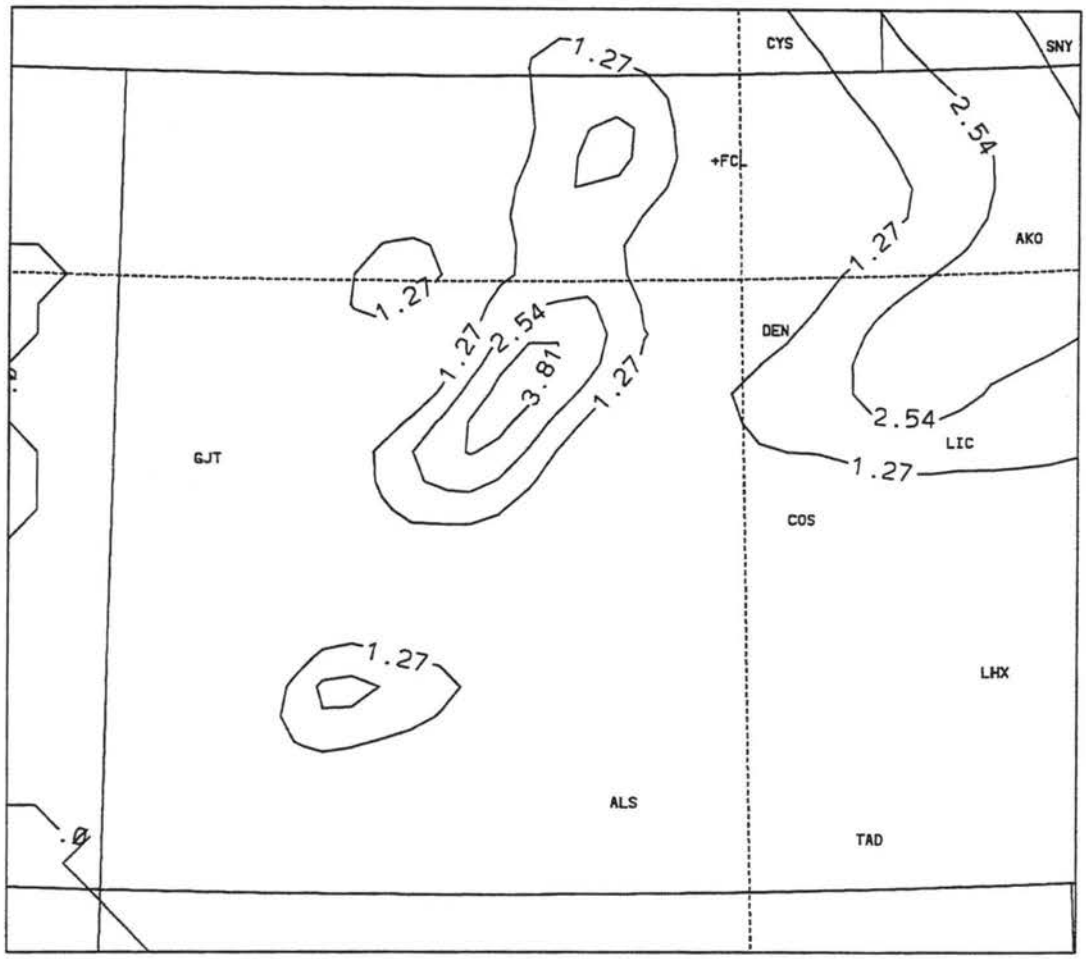

Figure 4.7: Same as Figure 4.6, but for microphysics model

areas (Byers, Limon) but not in others (La Junta). Trinidad saw about 3.6 mm, in between the two model values. The dump-bucket model location of the precipitation in southern Colorado is closer to the truth, with the 12.7 mm recorded at Durango Water Resources in the far southwest, but further to the north Telluride only received 1.0 mm. The precipitation maxima in the northern mountains is displaced from its actual position due west of Denver. In addition to Mt. Evans, nearby Inter Canyon saw 24.1 mm, close to the maximum value of 20.2 mm in the microphysics run, but no place near the precipitation maximum west of Fort Collins in the microphysics run received near that amount in the observations. This helps illustrate the strengths and weaknesses of each model – the dump-bucket scheme tends

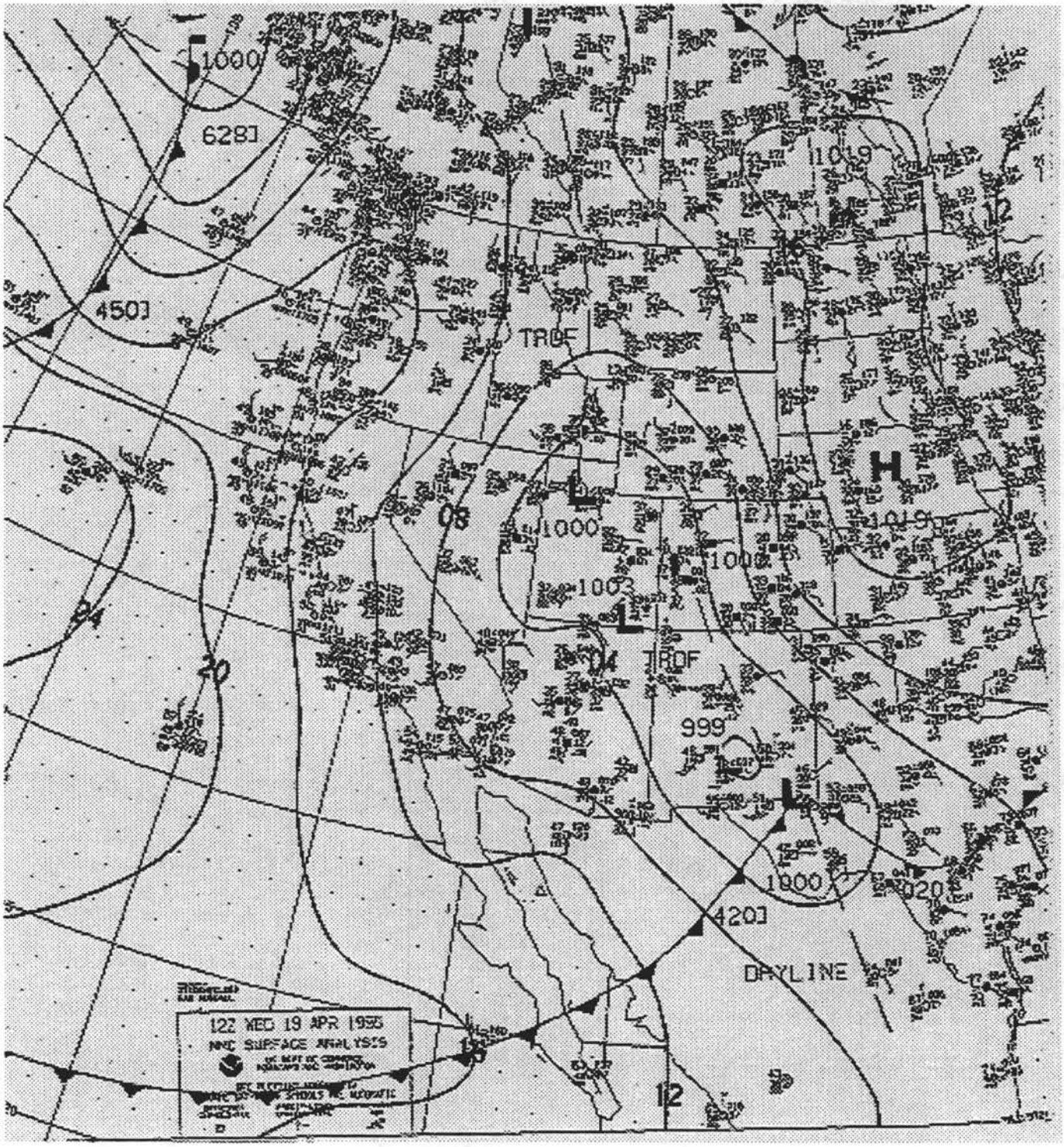

Figure 4.8: NMC surface map, 1200 GMT 19 April 1995

to reduce the maximum values in the precipitation fields by spreading them out, but the microphysics tends to produce localized centers of large precipitation amounts which can produce large forecast errors for particular regions.

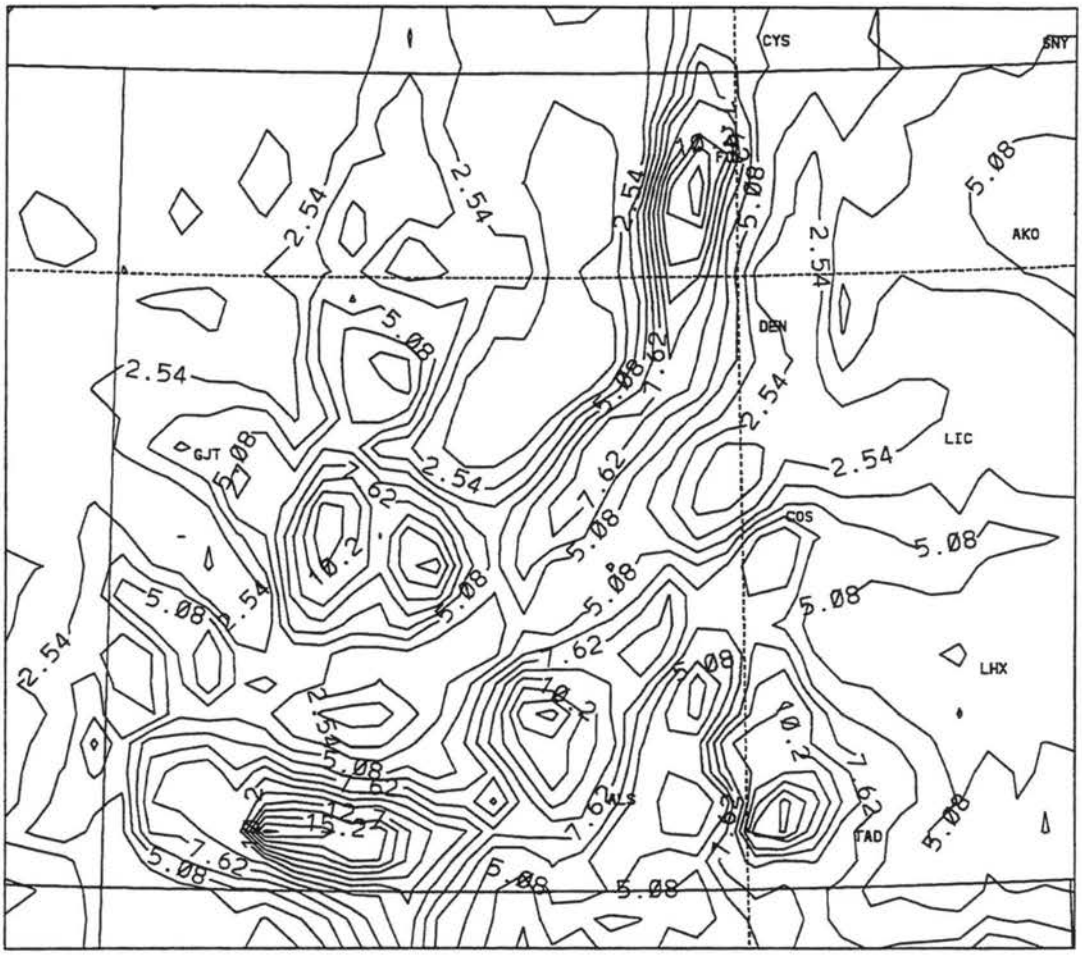

Figure 4.9: Accumulated precipitation, April 19 forecast, for dump-bucket model

4.1.4 April 26

A late-season blizzard struck the higher regions of the eastern plains as a cold surge from the north phased with an eastward-moving trough (Figure 4.11). Thunderstorms were observed on the eastern plains as the front approached on the 25th, while tempera-

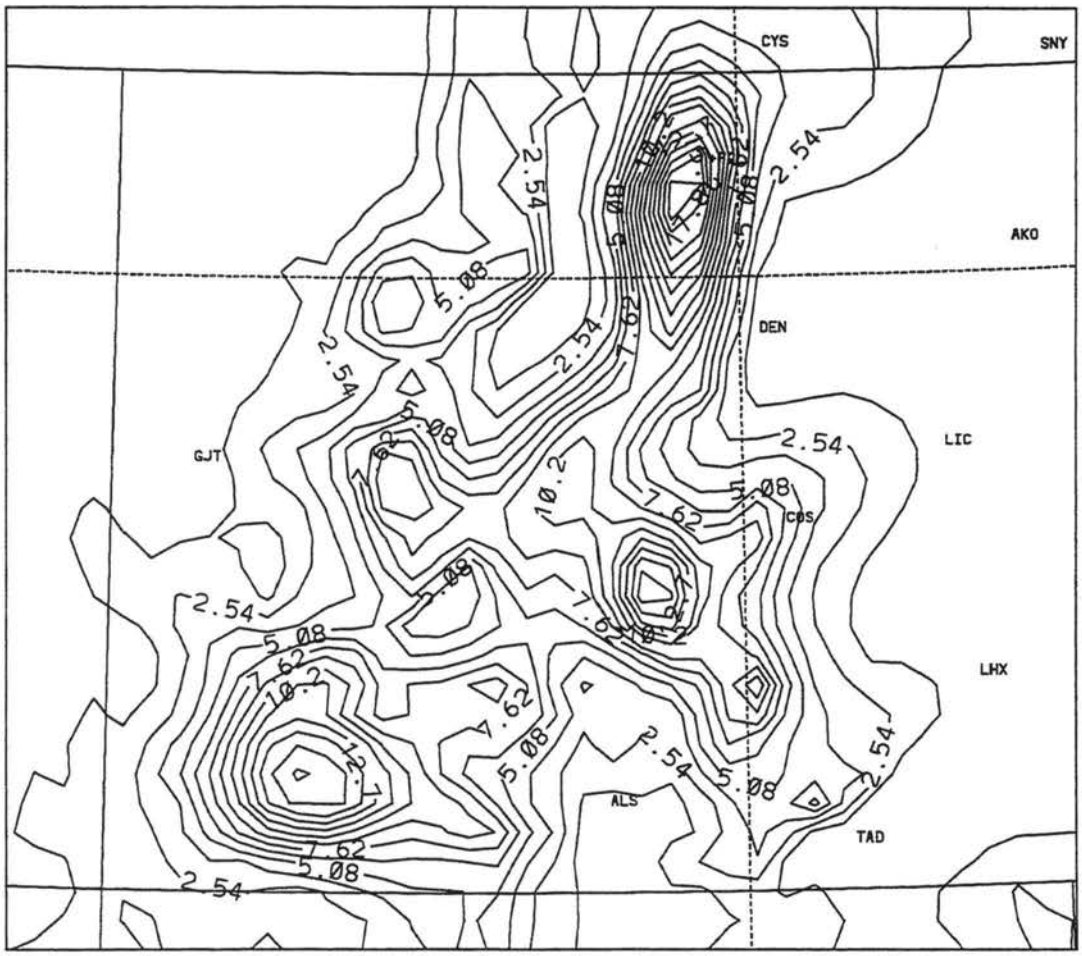

Figure 4.10: Same as Figure 4.9, but for microphysics model

tures dropped from near 20° C on the 25th to near freezing on the 26th, accompanied by widespread snow.

When comparing Figures 4.12 and 4.13 one should note that both model forecasts missed most of the advancing cold air. Figure 4.14 shows the forecast microphysics model temperature at 1200 GMT, and this is clearly warmer than what is indicated on the synoptic map of 4.11. When the synoptic features are not forecast well by the model, the precipitation forecasts cannot be expected to be accurate no matter what scheme is used.

In this forecast the microphysics model actually produces more precipitation on the eastern plains than the dump-bucket model. In actuality, the eastern plains received more

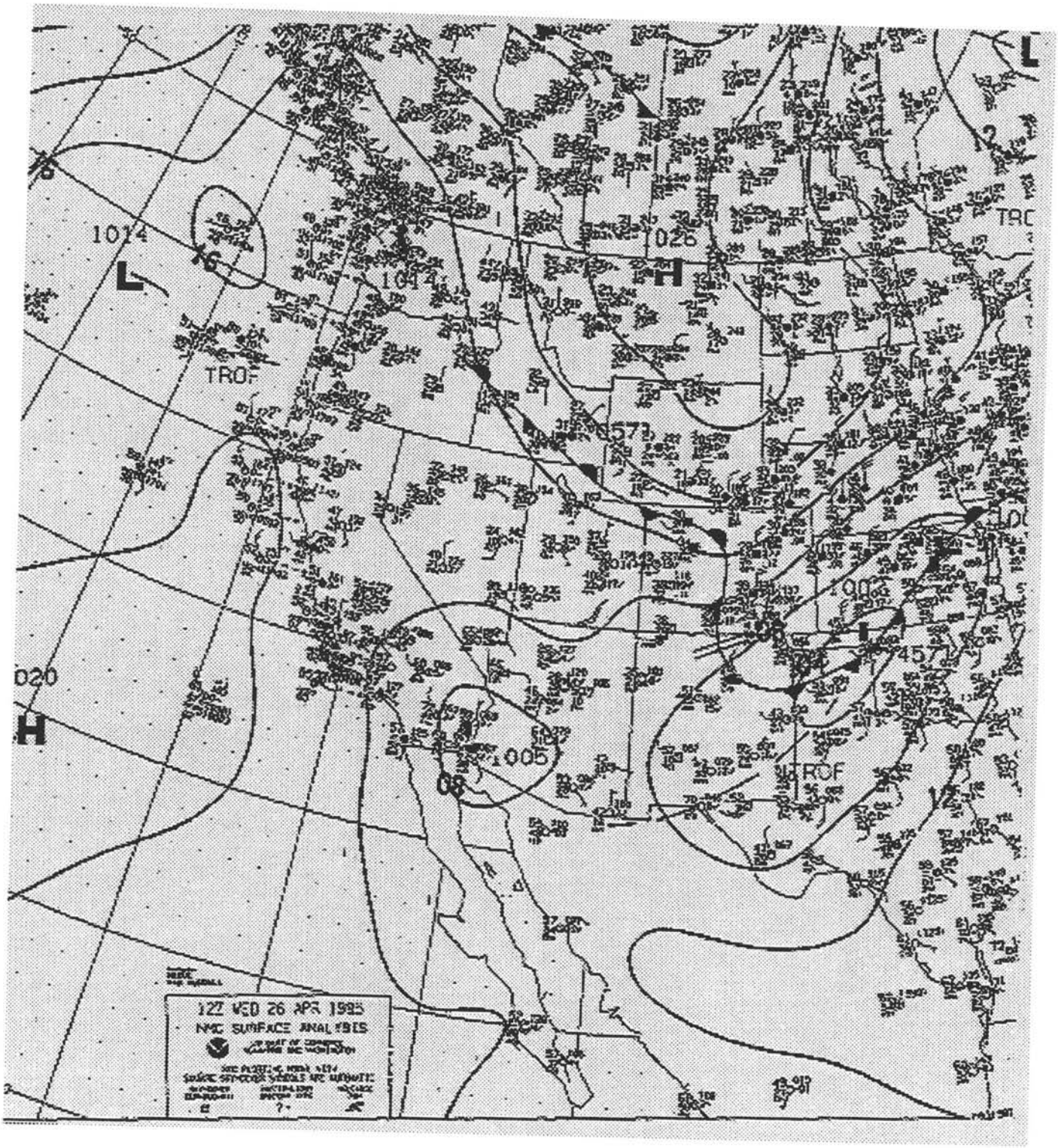

Figure 4.11: NMC surface map, 1200 GMT 26 April 1995

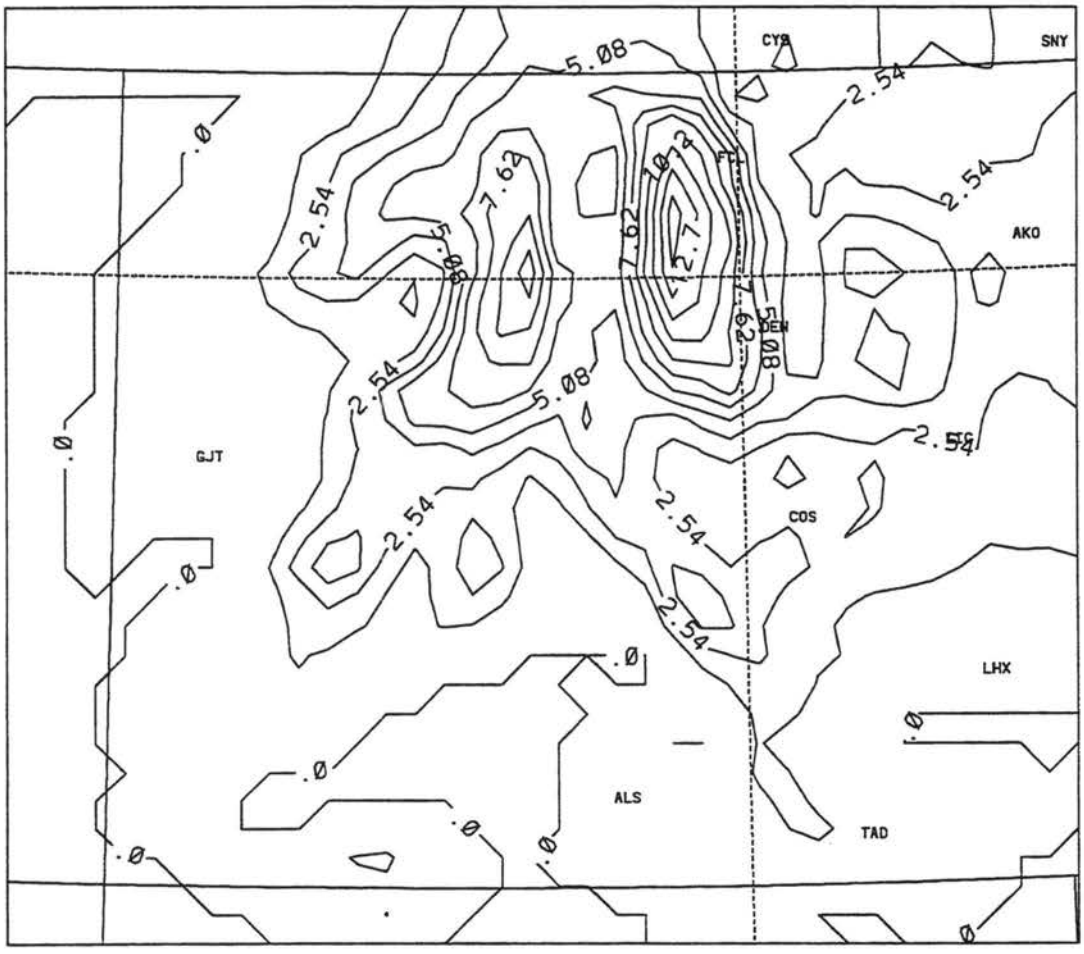

TOTAL PRECIP (mm)
24HR FCST VALID 0000 UTC 04/27/95

Figure 4.12: Accumulated precipitation, April 26 forecast, for dump-bucket model

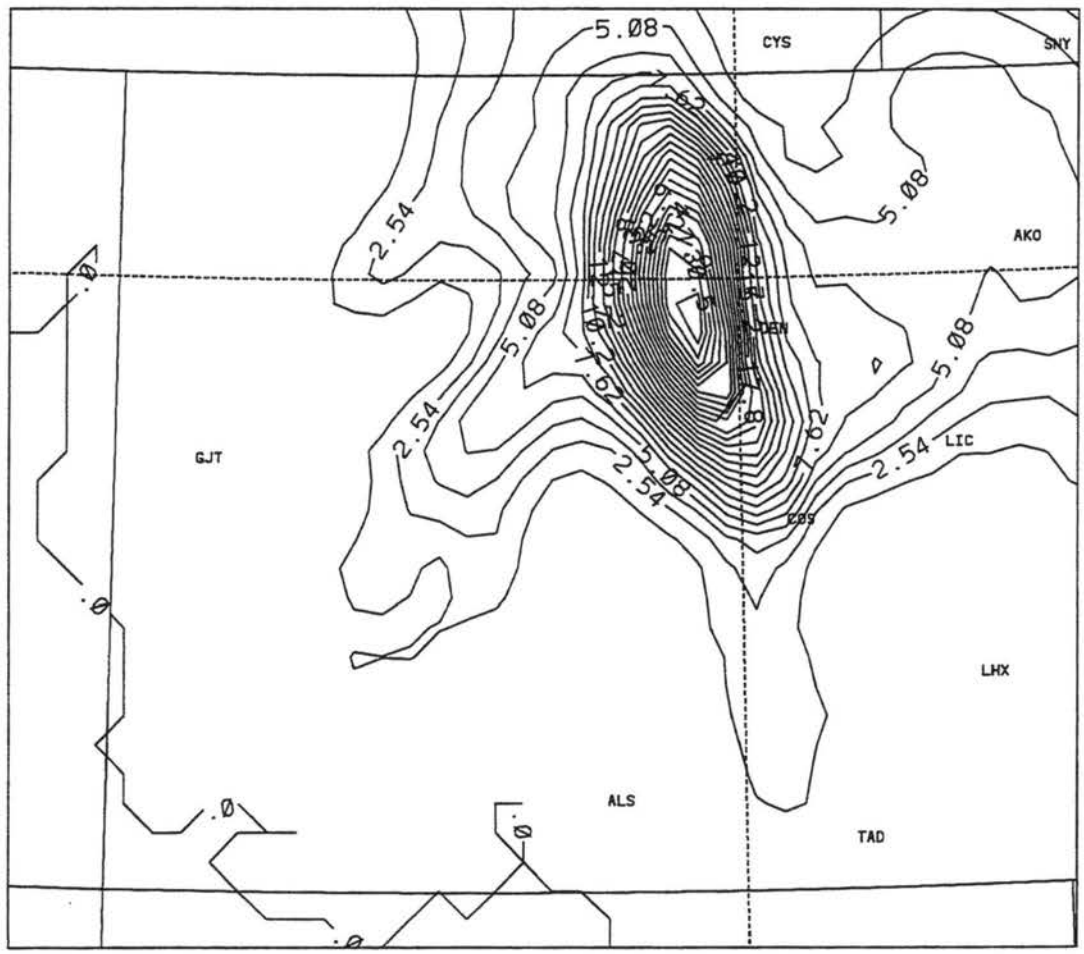

Figure 4.13: Same as Figure 4.12, but for microphysics model

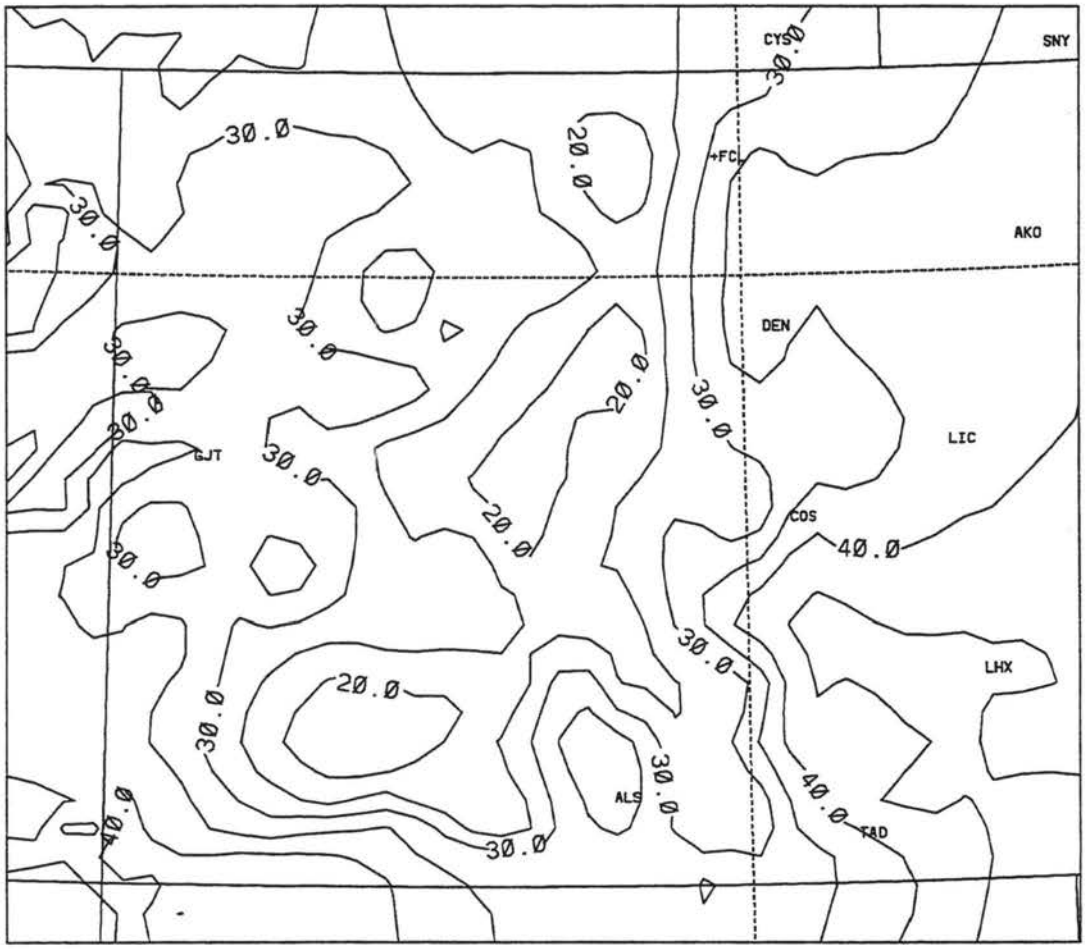

Figure 4.14: Screen height temperature in degrees Fahrenheit, 1200 GMT April 26 forecast, microphysics model

precipitation than indicated by either model (9.1 mm at Rocky Ford, 7.4 mm at Limon) as did the far west (20.1 mm near Meeker). Gross Reservoir near Boulder received the most precipitation at 25.4 mm, which is actually pretty close to the maximum in the models, and closer to the microphysics-produced value for the verification period (27.2 mm) than the dump-bucket value (14.7 mm).

What is interesting is that this is one of the few days in which the model predicted on average more precipitation at the SNOTEL stations than was observed. No SNOTEL station received more than 10 mm (recorded at University Park SNOTEL west of Boulder, among other sites) on April 26, though more SNOTEL sites in the southwest mountains received measurable snow than the models would lead one to believe. Most of the SNOTEL stations actually reported the most precipitation on April 25; that is, from midnight April 25 to midnight April 26, which covers the first six hours of the displayed model plots. The Joe Wright SNOTEL south of Estes Park, for instance, received 28 mm of precipitation for April 25. This could be due to the model being slow to advance the front for the April 25 forecast. Additionally, there is some evidence that much of the snow on the 25th was convective in nature (see Chapter 5), and mountain convective activity cannot be well resolved by the current forecast model grids.

4.2 Variations in Setup

4.2.1 Fine Grid vs. Coarse Grid Microphysics

At the beginning of this study it was believed that it might be beneficial to only use bulk microphysics on the fine grid domain in order to save computational time (cloud water would still be diagnosed on the coarse grid), since in practice the coarse grid precipitation fields are not likely to be used by the forecaster. Such a forecast might not be expected to be very accurate on the boundary of the fine grid but one might expect comparable forecasts near the interior of the fine grid. However, the absence of hydrometeors in the coarse grid can produce numerical reflection into the fine grid. Figure 4.15 shows an example of a forecast performed using one-grid microphysics. When this is compared to the two-grid microphysics run in Figure 4.7, the boundary condition is seen to have a substantial

effect a quarter of the way into the domain. It can be shown statistically (see Chapter 5) that using microphysics on only the fine grid substantially lowered model performance for the climatological stations. And on days, such as this one, with a large ratio of fine-grid hydrometeor amounts to coarse-rid hydrometeor amounts, the time savings gained by the one-grid microphysics is rather negligible (on other days up to a third of the computational time is saved). So a decision was made to use two-grid microphysics on all days where substantial precipitation was observed.

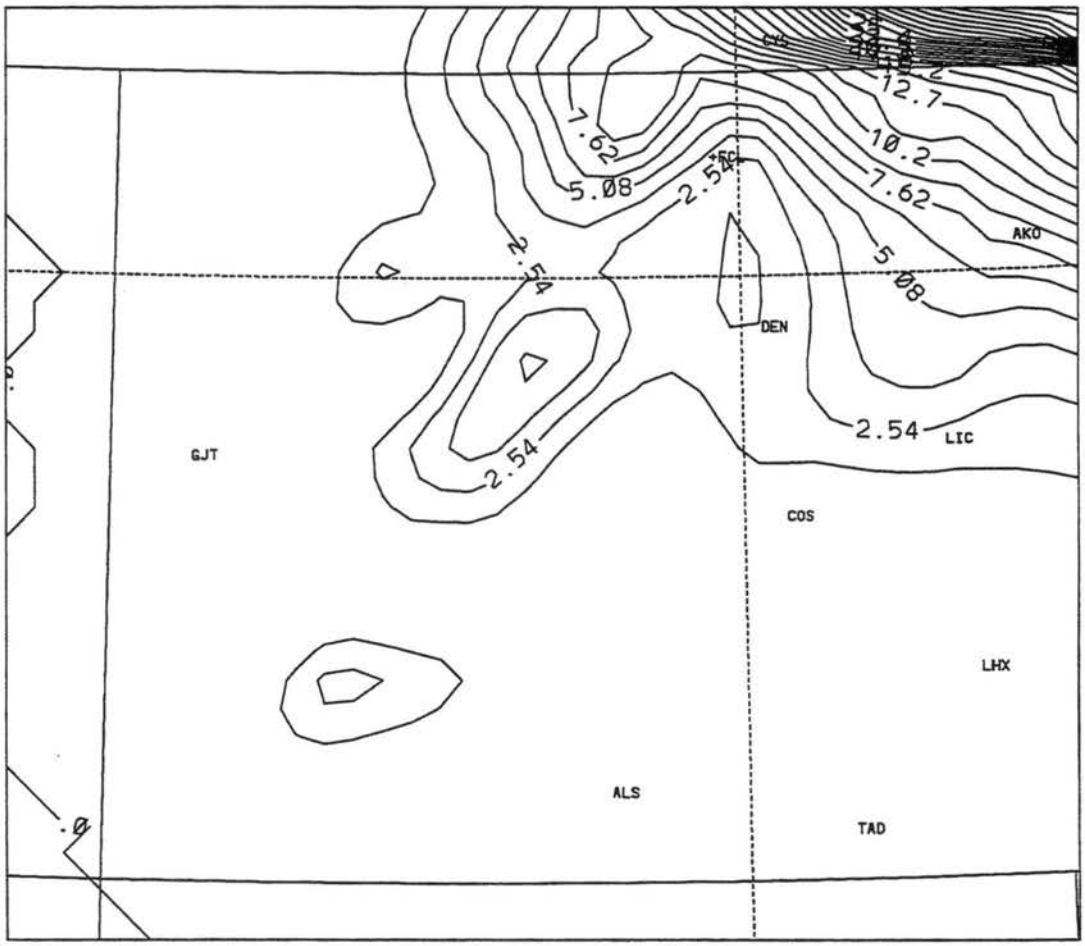

Figure 4.15: Same as Figure 4.7, but using microphysics on the fine grid only

4.2.2 Variation in Hydrometeor Mean Diameters

RAMS allows the freedom for the user to select mean diameters for each water species. With freedom, however, comes the responsibility for the forecast modeler of choosing mean diameters which are representative for a wide variety of cases. Of course, there may very well be no such mean diameter appropriate for all cases nor even throughout the duration of one particular case. Keeping this in mind, a test was performed by varying the mean sizes of various hydrometeors.

Figure 4.16 shows a precipitation plot using input parameters given in the left column of Table 4.1, while Figure 4.17 was made using the parameters in the right column. The values in the left column are standard ones commonly used with the RAMS model; the values in the right column were used after referring to sources in the literature on characteristic mean sizes of observed precipitation (Pruppacher and Klett, 1978) and functions of some of the categories (Harrington, personal communication). It was found that the two different model runs differed in the amounts of precipitation of each type but the two figures show that the total amount of precipitation was not greatly changed (from 27 mm to 24 mm at the peak, but an increase in measurable precipitation on the eastern plains). This would be consistent with the studies of Meyers and Cotton (1992) and Rauber (1992) since increasing the mean particle size of graupel tends to increase the amount of graupel precipitation at the expense of aggregates; the mass of graupel tends to create maximum accumulation tens of kilometers upwind from the mountain crest, while maximum aggregate accumulation tends to occur closer to the maximum elevation.

In the observational network, the highest mountain precipitation amounts in this region was about 28 mm at a SNOTEL site. However, there certainly was considerable precipitation on the eastern plains (and the western slope for that matter) on this day; as previously discussed, the model did not handle the timing of this event well, so it is difficult to say which version of the model is superior based on this run. But because of the observational basis, the mean diameters used in the second run were those used for the major part of this

study. Note that both of these runs were performed using microphysics on only the fine grid, so they differ from Figure 4.13, which contains microphysics on both model grids.

Another sensitivity test was performed in which just the mean diameter of the snow and snow aggregate categories was increased. This was completed after statistical analysis showed that, in particular, aggregate precipitation seemed to be not reaching the ground as much as it should. It was also found that the relationship between mass-mean and number-mean diameter had not been handled properly; specifically, the factor on the right side of Equation 3.5 had been left out. For aggregates ($\nu = 1, \beta = 2.4$) and snow ($\nu = 2, \beta = 2.4$) this factor turned out to be 1.58 and 2.98 respectively. So the sizes of the input mean diameters for these categories was increased to 630 microns and 650 microns, and the case of April 25 was re-simulated, a day when the mountains received well over the model forecasted amount of precipitation. However, a comparison of Figures 4.18 and 4.19 reveals that the change in hydrometeor size had little effect on the model output, only producing a slight increase of the hail category precipitation south of the Cheyenne ridge.

category	run 1	run 2
cloud	300	300
rain	1000	1000
pristine ice	*	*
snow	1000	400
aggregate	1000	400
graupel	1000	2000
hail	3000	2000

Table 4.1: Values of input parameters to microphysics forecast model. All values are mean diameters in microns except for cloud, which is droplet concentration in number per cubic centimeter. Asterisk denotes that both number concentration and mixing ratio are predicted by model so an input parameter is not necessary.

4.2.3 Variation in Width Parameter

For the majority of runs, the value of the width parameter ν of the gamma distributions was 1 for all water species, except for snow and cloud droplets, which had $\nu = 2$. A value of 1 for the width parameter gives an exponential distribution, which is consistent with the

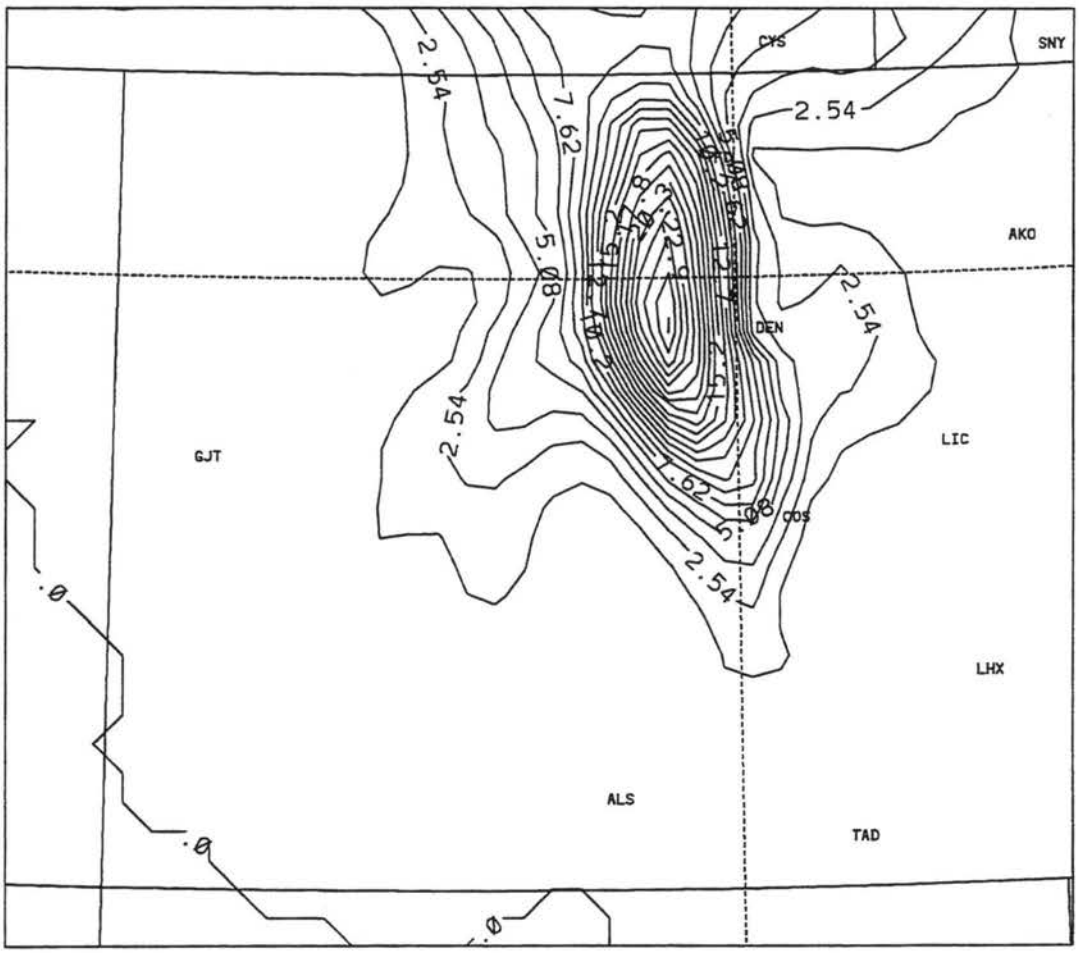

TOTAL PRECIP (mm)
24HR FCST VALID 0000 UTC 04/27/95

Figure 4.16: Total precipitation, April 26 forecast, using old mean diameters and one-grid microphysics.

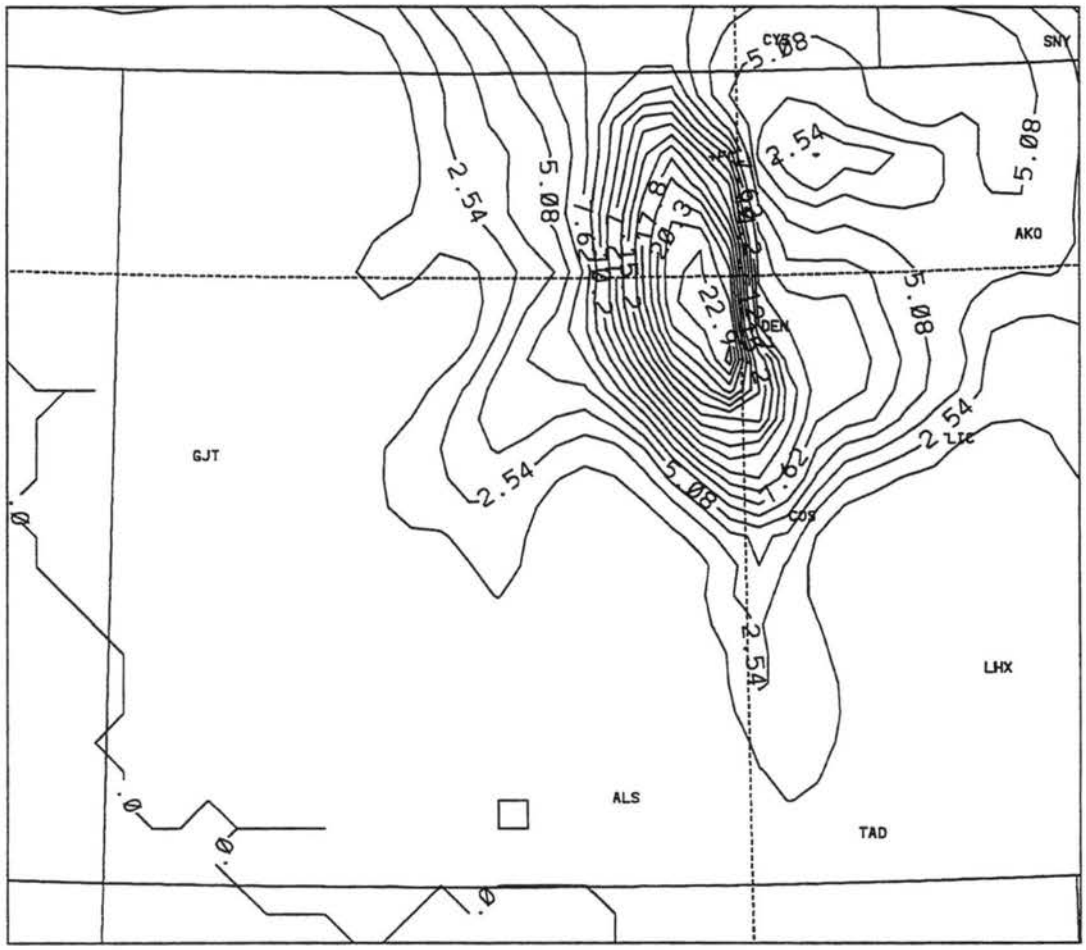

Figure 4.17: Total precipitation, April 26 forecast, using new mean diameters and one-grid microphysics.

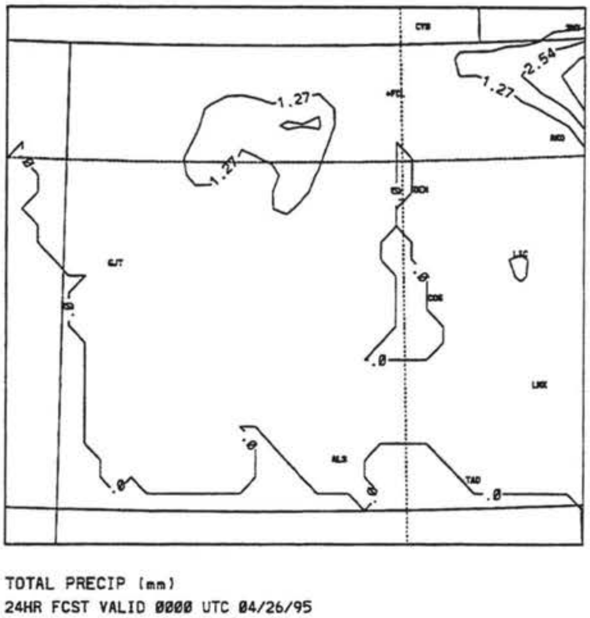

Figure 4.18: Total precipitation, April 25 forecast, microphysics model, without convective scheme.

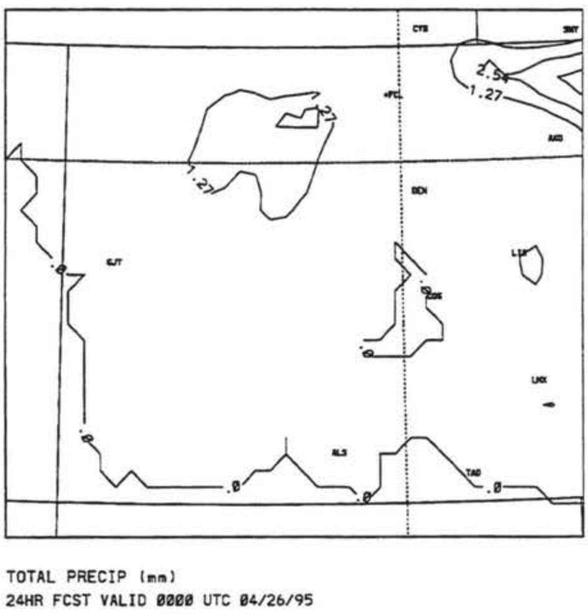

Figure 4.19: Same as 4.18, but using larger ice species.

Marshall-Palmer distribution, and corresponds to the experimentally-found hydrometeor size distributions in many studies (Pruppacher and Klett, 1978). With greater values of ν, the gamma distribution contains a peak and is positively-skewed, with a broad tail at larger sizes (see Figure 4.20). Cloud droplets typically show at least one peak in the size distribution, and often more. The width parameter was set to 2 for snow because this category consists of particles in the pristine ice category which grow enough by deposition to exceed a threshold size, so at the small end snow particles simply remain in the pristine ice category.

To see how large an effect varying ν has on the forecasts, a run was done in which cloud droplets were given a width parameter of 1. Figure 4.21 is from a run identical to that of Figure 4.16 except $\nu = 1$ for cloud water. Again, the regions of precipitation are quite similar, but when the width parameter is 1 the precipitation amounts are higher both near the maximum (the peak is 34 mm, up from 27 mm), and on the eastern plains, where the precipitation is now noticeable. For exponential distributions the same mixing ratio of liquid water gives more droplets at smaller sizes than when $\nu = 2$, so this may reflect the importance of the smaller cloud drops to the riming process and in increasing the precipitated water.

Figure 4.22 shows the effect of changing ν to 5. As can be seen in Figure 4.20, when the mixing ratio (which is proportional to the third moment of the distribution for spherical particles such as cloud droplets) is fixed, increasing ν has the effect of increasing the modal diameter and narrowing the droplet spectrum. This time the precipitation maximum is decreased over the mountains, compared to the control run (peak precipitation is 24 mm) though amounts seem relatively unchanged on the plains.

4.3 Finer-Grid Runs

A few case studies were simulated using the same input data but with smaller grid spacings. Such simulations were well too slow to be usable as a real-time forecast (at least on a single-processor IBM RISC-6000/390 workstation), but were performed to see what

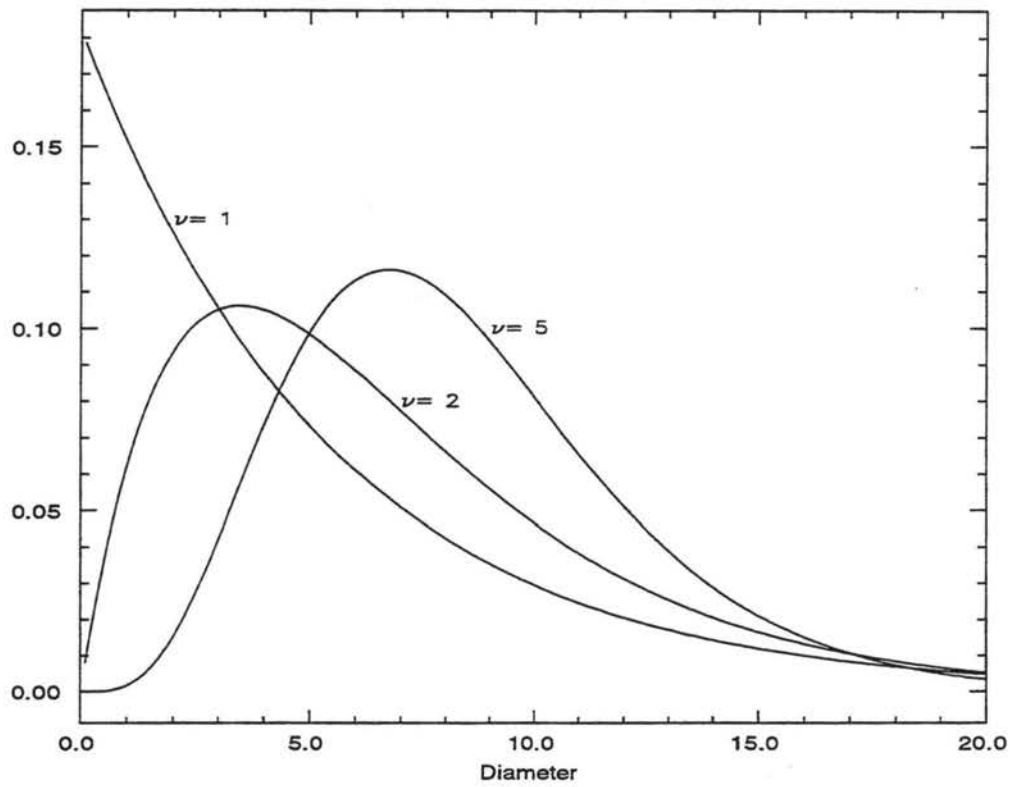

Figure 4.20: Plot of normalized gamma functions for ν values of 1,2, and 5. Third moment of the distribution is kept fixed at $(10.0)^3$. Units are arbitrary.

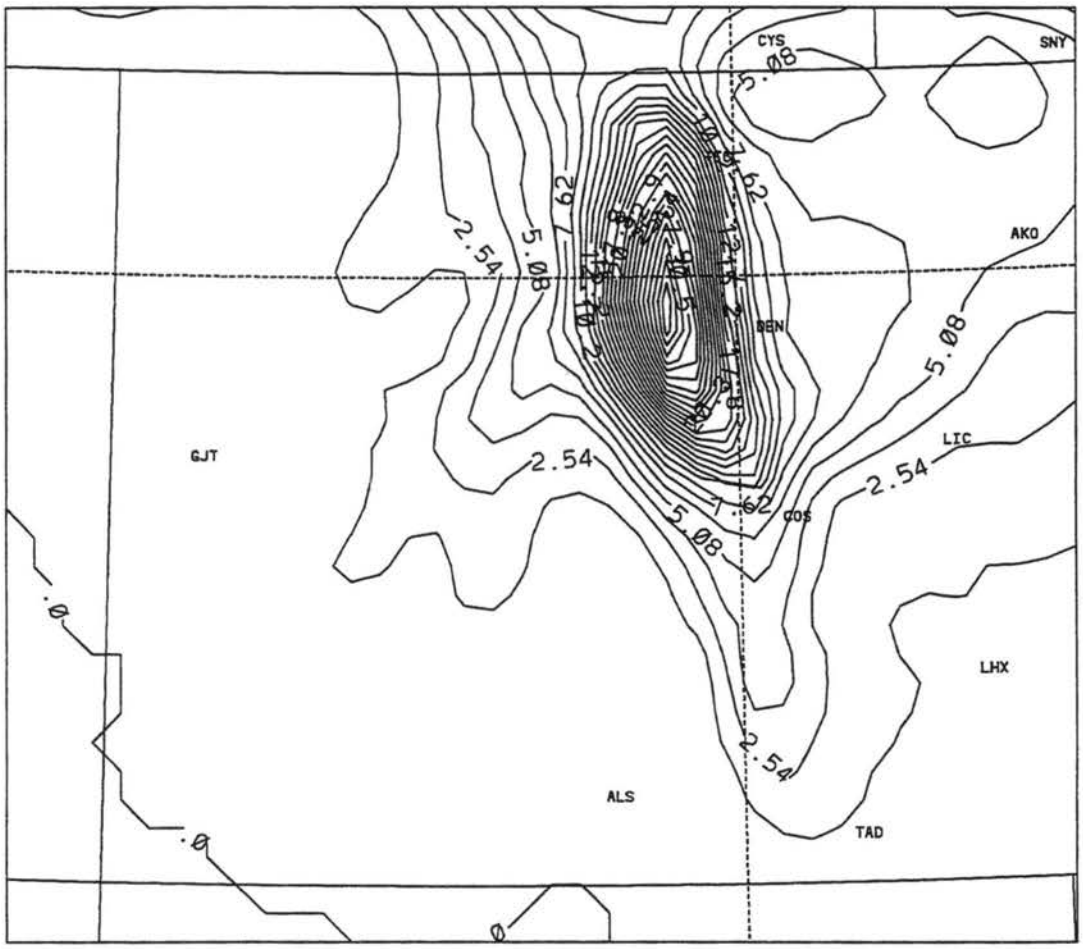

Figure 4.21: Same as 4.16, only with $\nu = 1$ for cloud water

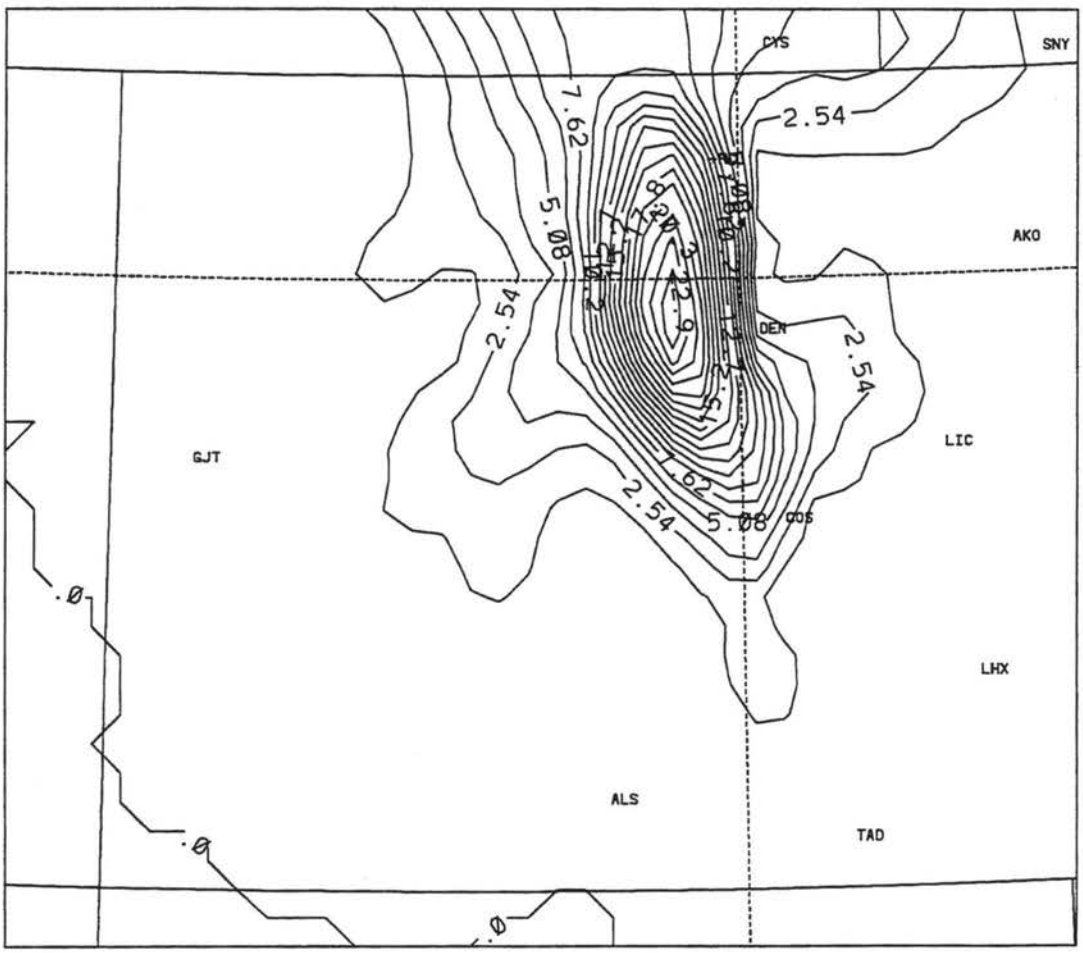

Figure 4.22: Same as 4.16, only with $\nu = 5$ for cloud water

improvements, if any, could be obtained by using smaller grid spacings and correspondingly fine-scale physiography.

One such run was performed using the same grid domain as before, but with 8-km grid spacing on the fine grid instead of 16-km (see Figure 4.23). The day simulated was April 19. Microphysics was called on both grids. The resulting simulation took a little less than three days to complete. The resulting precipitation 24-hour forecast is shown in Figure 4.24. The main qualitative features are relatively unchanged from those in the 16-km fine grid run (Figure 4.10), except that there is more detail, and the highest amounts of precipitation, mostly graupel and aggregates, have increased. The inclusion of measurable precipitation on the far Western slope may be an improvement in the forecasts; perhaps in this region topography on scales smaller than 16-km is important because of the absence of major mountain ranges. However, the 8-km run is over-predicting the amount of precipitation along the Front Range by a considerable amount.

A second run was performed, using a 2-km fine grid. Because of the large size difference between the 80-km and 2-km grid, three grids were required for this simulation. The second grid possessed 10-km grid spacing and covered the same domain as the fine grids for the other simulations; the third grid was 77×52 and was positioned in northern Colorado between the urban corridor and the Northern Park Range (see Figure 4.25). The fine grid was positioned so that ten SNOTEL stations could be included, and a day was chosen (April 23) which included significant precipitation within the finest grid but little precipitation elsewhere. Still, the simulation took about a week to perform, plus additional time simulating the first six hours of April 24, which is included in the April 23 SNOTEL report.

One complicating factor, though, is the fact that a 2-km grid is well below the applicable length scale for the convective parameterization, so the simulation was performed with the scheme turned off. In order to provide a way to isolate the effect of the finer grids, a run was performed using the conventional two-grid setup, but without the convective scheme. Figures 4.26 and 4.27 show the microphysics runs of April 23 with and without the convective scheme. It can be seen that the convective parameterization has a definite effect on the simulations, even when (as in this case) the parameterization is producing essentially no

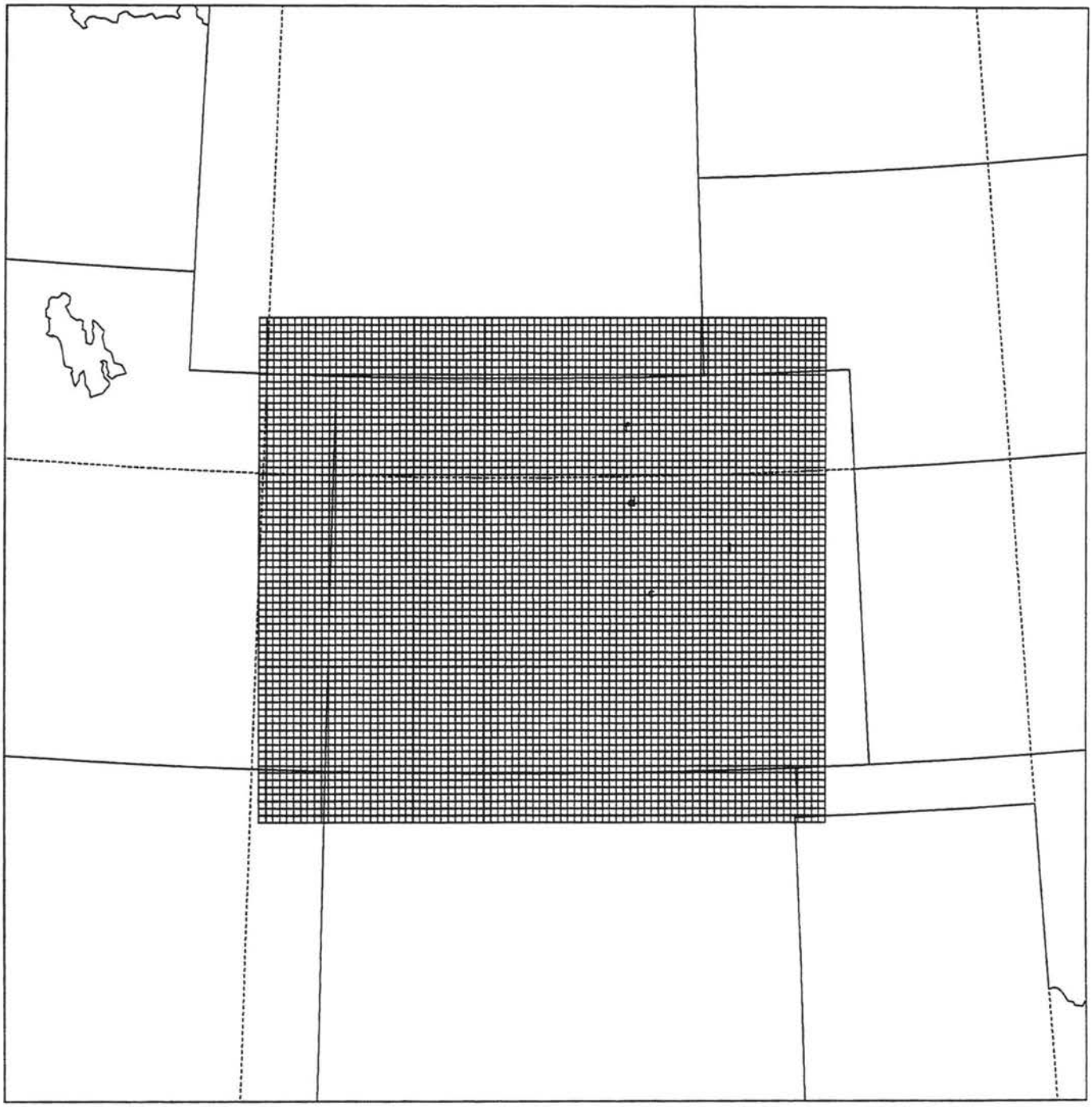

Figure 4.23: Grid 2, 8-km run. Grid 1 is identical to the coarse grid of the standard model runs.

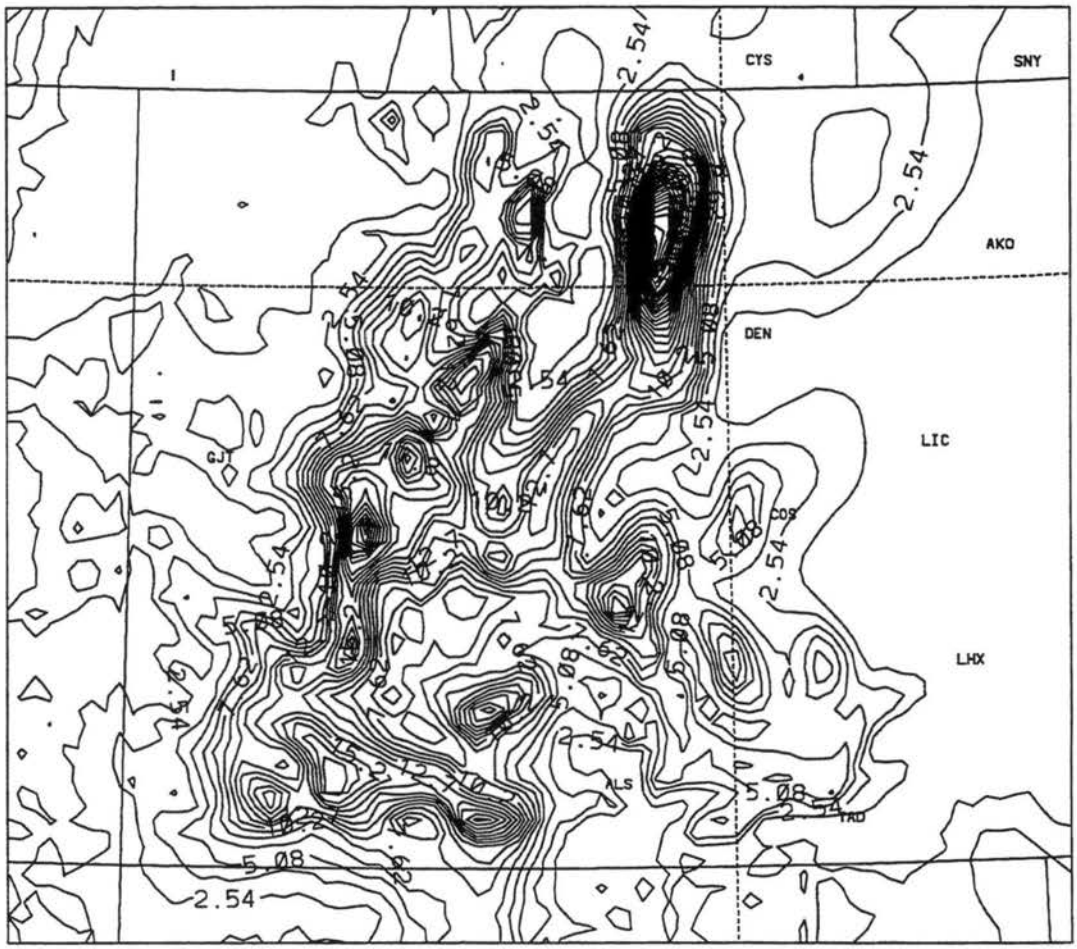

TOTAL PRECIP (mm)
24HR FCST VALID 0000 UTC 04/20/95

Figure 4.24: Total precipitation, April 19 forecast, using microphysics and 8-km fine grid. Maximum amount is 44.5 mm

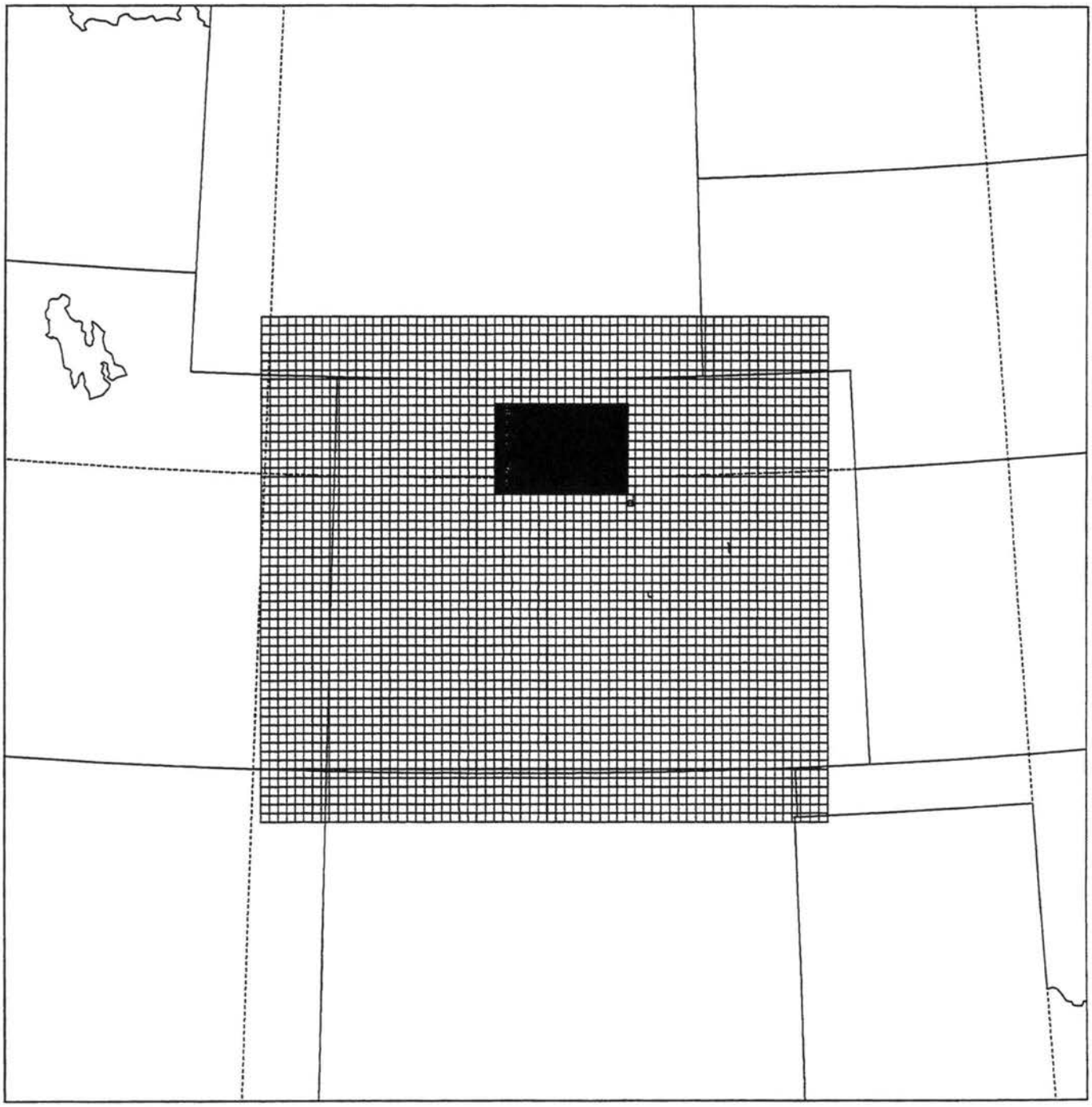

Figure 4.25: Grids 2 and 3, for 2-km run. Grid 1 is identical to the coarse grid of the standard model runs.

precipitation. The reason is evidently due to the convective scheme's adjustment of the environmental wind and moisture fields – more discussion on this topic is given in Chapter 5. Here the major effect of the convective scheme is reducing the maximum precipitation amounts, from 18 to 10 mm. With the scheme the model does not predict precipitation in the Sangre de Cristos south of Colorado Springs, but does predict some precipitation in the mountains west of the Front Range. In actuality both of these locations received precipitation on this day. For the 24 hours ending 2000 UTC April 24 (virtually all the model precipitation fell after 1800 UTC) Inter Canyon west of Denver reported 9.7 mm, closer to the convective run value, but at a higher altitude Mt. Evans station reported 19.1 mm as of 1400 UTC April 24, closer to the values in the non-convective run. The SNOTEL stations also received closer to the higher precipitation amount – 20 mm at University Camp (ID 100), 18 mm at Lake Eldora (ID 68) and Copeland Lake (ID 51).

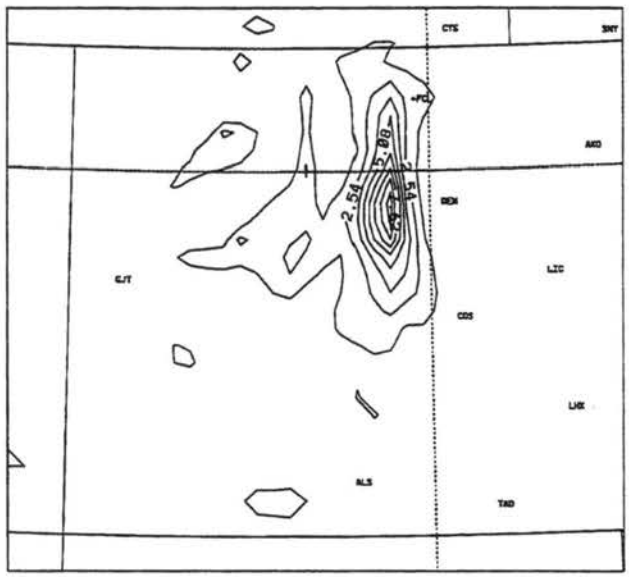

Figure 4.26: Total precipitation, April 23 forecast, using microphysics, convective scheme, and 16-km fine grid. Maximum amount shown is 10.2 mm.

Figure 4.28 shows the accumulated precipitation for the three-grid microphysics run on April 23. The second grid, with 10-km spacing, is the grid displayed in this figure. The finer-scale run increases the maximum precipitation amount to 22 mm, but this is in one localized

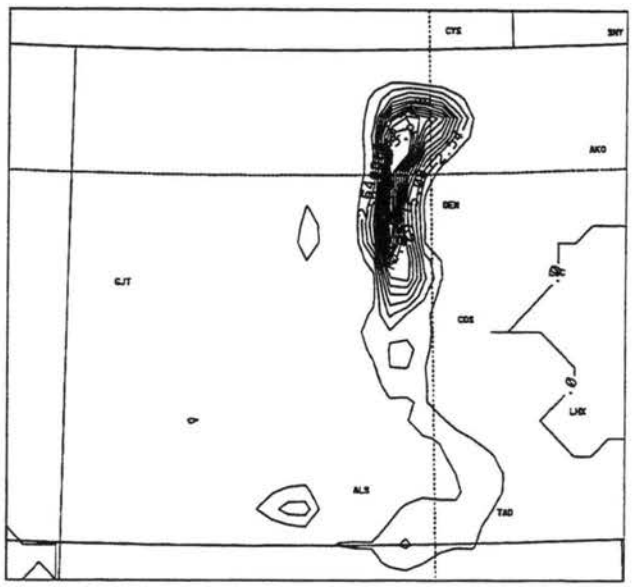

Figure 4.27: Total precipitation, April 23 forecast, using microphysics, no convective scheme, and 16-km fine grid. Maximum amount shown is 17.8 mm.

region; overall, the amounts of precipitation are relatively unchanged by the finer-scale run, at least when averaged to the second grid. The areas of precipitation, though, are decreased, which can cause problems in statistical verification of relatively sparse datasets such as the SNOTEL stations. The three-grid run does improve some features with respect to the two-grid run. The model now captures the fact that there is a minimum of precipitation at the Joe Wright (ID 66) and Phantom Valley (ID 80) SNOTELs compared to the University Camp and Copeland Lake sites; the former recorded 8 and 3 mm, respectively. There is no evidence of the second precipitation maximum just west of Fort Collins because there are no SNOTEL stations there; Fort Collins itself recorded 3.0 mm from this event. The three-grid simulation also underestimates the precipitation at Lake Eldora and the climatological stations west of Denver, though it should be pointed out that these lie outside the 2-km grid. Better captured by the three-grid run are the precipitation maximum near ID 99, Upper San Juan SNOTEL (10 mm), and absence at this station's westerly neighbors (0 mm at ID 101, Vallecito); and the feature near ID 97, Tower, although Tower SNOTEL reported 46 mm during this period which is well above any model prediction! The three-grid model

does not help in predicting snow for the SNOTELs near the central mountains, when in fact Hoosier Pass (ID 61) recorded a half an inch of precipitated water. Since the convective scheme did forecast some precipitation at these sites, this may be an indication that the central mountains did in fact receive mainly convective precipitation on this day.

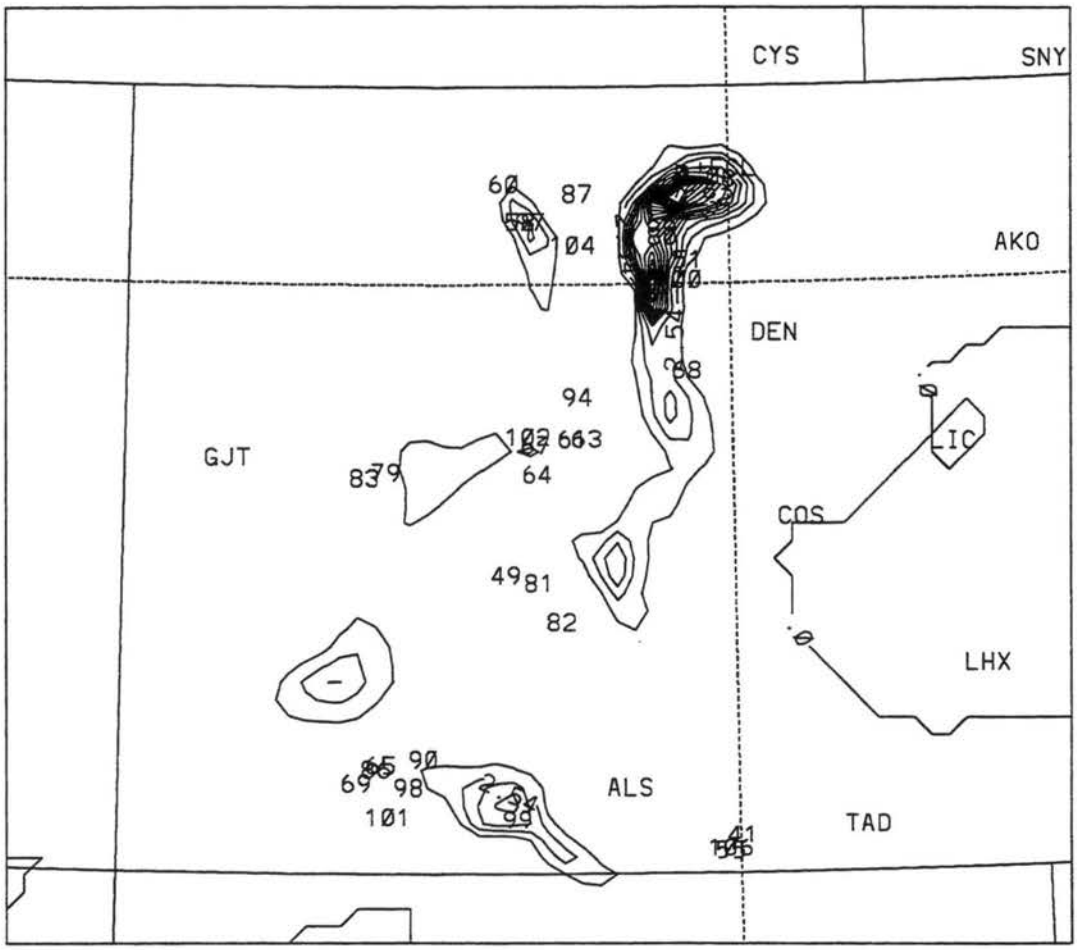

TOTAL PRECIP (mm)
24HR FCST VALID 0000 UTC 04/24/95

Figure 4.28: Total precipitation, April 23 forecast, using microphysics and three grids, on second grid. Maximum amount is 21.6 mm. Contour interval is 2.54 mm (0.10 in.)

The precipitation field for Grid 3 is shown in Figure 4.29. The features described for Grid 2 are seen here in more detail. The total precipitation amount is increased to over 30 mm in parts of the northeast; unfortunately, the lack of SNOTEL stations in this region make it difficult to verify this. The band of precipitation near University Camp and

Copeland Lake on Grid 2 is now several model points away on Grid 3, so that in terms of quantitative statistics the three-grid run actually performs worse than the two-grid run (see Chapter 5). This is frustrating to the numerical modeler desiring better-quality forecasts, but not unprecedented: Tucker et al. (1989) reported that QPF skill was in fact maximized when precipitation forecasts from a 24-km model run were averaged to a 96-km grid.

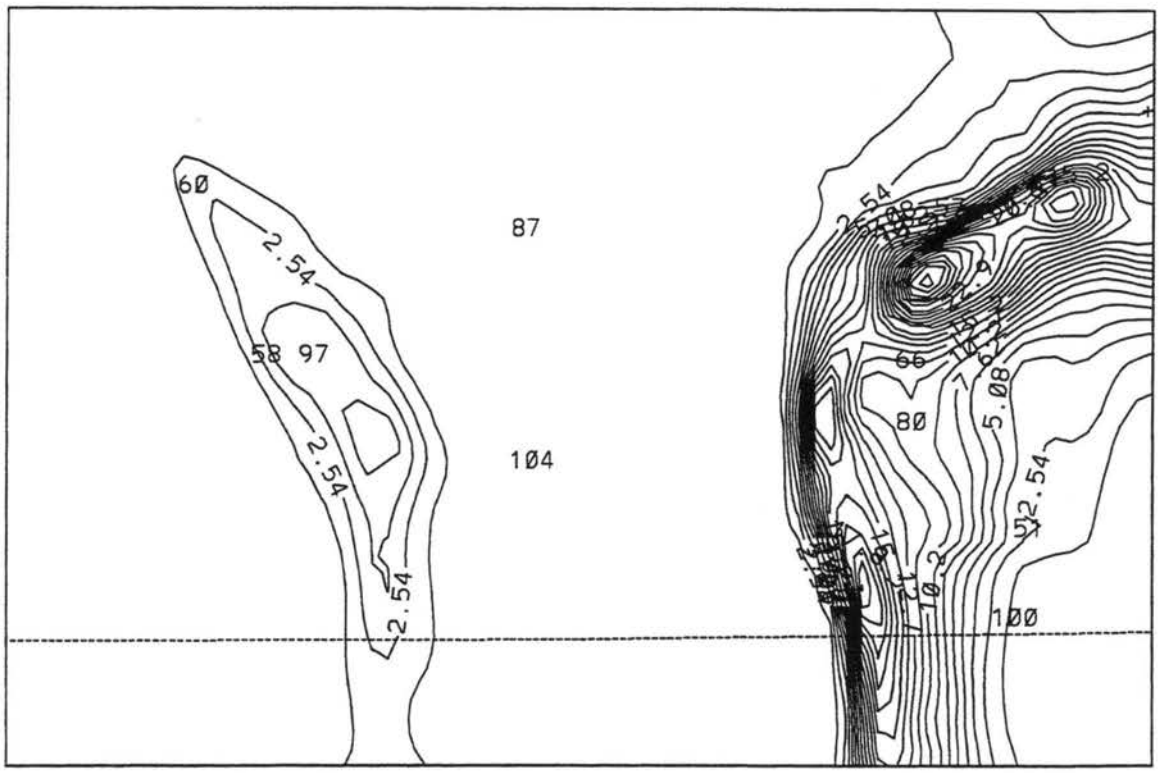

Figure 4.29: Total precipitation, April 23 forecast, using microphysics and three grids, on third grid. Maximum amount is 31.8 mm

In short, switching to a finer-scale model is similar to switching from a dump-bucket scheme to a microphysics scheme; extreme amounts of precipitation are usually better forecast, as are areal extents of precipitation; however, often these features are not precisely where they are supposed to be. In particular, the more sophisticated model forecasts often have problems in forecasting a lack of precipitation where precipitation does in fact occur.

4.4 Summary

The various case studies seem to indicate:

1) Both microphysics and dump-bucket models show considerable skill at identifying features in the precipitation field, but neither has exhibited a clear advantage over the other.

2) The dump-bucket has more of a tendency to spread out regions of low- to-moderate precipitation and to reduce the intensities of precipitation maxima.

3) The microphysics model tends to localize regions of moderate-to-heavy precipitation next to mountainous topographic barriers. Sometimes this enhances forecasting accuracy but sometimes it causes large errors at particular locations for a case study.

4) Changes in many microphysical parameters slightly change forecast precipitation amounts but do not cause significant qualitative variation in the model results.

5) Finer grid resolution produces features with more fine-scale features which often correspond better to observed features, but not always. Comparisons between models of different resolution might only have meaning when averaged to the scale of the coarser of the two grids, or perhaps over longer time periods than those used in this study, which would allow the random errors a chance to cancel each other in the mean.

Chapter 5

STATISTICAL ANALYSIS

Though much can be learned from a simple analysis of the qualitative features of model forecast features, it is difficult to draw conclusions of any certainty without the use of quantitative statistical procedures. In this application these mainly consist of finding some 'average error' between model output and observations, and determining characteristics of this error. Unfortunately, quantitative statistics are sometimes not as objective as they may appear at first glance. Often the choice of procedure has a large influence on the reported 'accuracy' of a given model. Therefore, it is important to carefully examine ways of verifying model accuracy.

5.1 Point by Point Validation – Single Case Studies

In point by point validation, each observational data point is compared to the corresponding model data point to determine how large the difference is between the two (henceforth known as 'errors', though in theory poor resolution in the observational database or the non-representativeness of a data point within the model grid volume could be responsible for the deviations). The set of errors for all the stations is then combined in some manner to represent overall model conformity with the observations. Perhaps the most common of these is the root-mean-square (rms) error:

$$\text{rms} = \left[\sum_{i=1}^{N}(\phi_i - \phi_{i_{obs}})^2/N\right]^{1/2} \tag{5.1}$$

(see Keyser and Anthes, 1977; Pielke, 1984) where N represents the number of observations. In this way both positive and negative deviations from the observations are weighted equally, and a model which contains equally large positive and negative deviations from

the observations does not give a false impression of little overall error, which may occur in a simple arithmetic average of all the point errors. Problems with this technique, though, include: 1) since all the errors are squared before being summed, a single large error value will have a disproportionately large effect (Mielke, 1985), and 2) if model fields show close resemblance to observational fields but are displaced somewhat from them, the rms error will erroneously show poor agreement between the two (Anthes, 1983; Pielke, 1984). Also, to gain a true appreciation of a model's skill, the rms error must be compared to the observational standard deviation,

$$\sigma_{obs} = \left[\sum_{i=1}^{N}(\phi_{i_{obs}} - \phi_{0_{obs}})^2/N\right]^{1/2}, \tag{5.2}$$

where $\phi_{0_{obs}}$ is the average of the observation fields, since even if the rms is large there can be forecasting skill if σ_{obs} is larger (Pielke, 1984).

An additional problem occurs when using point-by-point verification techniques specifically applied to predicting precipitation, and that is the fact that the model output is actually a grid-volume average whereas observational data are measurements at a point. This creates severe errors in rain and snow forecasting because of the fine-scale spatial variability of these fields; unlike pressure, for instance, there are no direct physical processes which act to minimize large gradients in precipitation. This has caused such agencies as NMC to use two special ways to evaluate precipitation forecasting ability: bias scores and threat scores (Anthes, 1983; Junker et al., 1989; Schultz, 1995). The bias score B is given by:

$$B = \frac{F}{O}, \tag{5.3}$$

where F is the number of stations in which the model predicts precipitation will reach or exceed a certain threshold, and O is the number of stations where precipitation was observed to exceed the same threshold. So the bias score is a way to determine if areal coverage is overforecast or underforecast, while the matching of features' location is not considered. The threat score T is defined to be:

$$T = \frac{CF}{F + O - CF}, \tag{5.4}$$

where CF is the number of correctly forecast stations (both model and observations produce precipitation at or above a given threshold), and F and O are as defined above. Stated in terms of sets, CF is the intersection of sets F and O, and the threat score is the ratio of the intersection of F and O to their union. The largest possible threat score then is 1.0, when F and O are exactly the same set of stations. The least possible threat score is 0.0, which occurs when no stations are correctly forecast and either F or O is non-empty. A good bias score (near 1) but a low threat score imply that areal extent is well represented by the model, but geographical location is not. When the bias score or its reciprocal is equal to the threat score, then one of either the forecast precipitation or observed precipitation is completely contained within the other.

A feature of the threat score is that it does not take into account correct forecasts of no precipitation, which becomes a problem in model verification when the number of such cases is large. Doswell et al. (1990) propose use of the Heidke skill score, HSS, for such situations, defined as

$$HSS = \frac{C - E}{N - E}, \tag{5.5}$$

where N is the total number of stations, and C is the number of correct forecasts both of precipitation and of non-precipitation (so $C = CF + (N - F - O + CF)$) . E is the number of correct forecasts expected due purely to chance, given by

$$E = \frac{O \times F + (N - O) \times (N - F)}{N}. \tag{5.6}$$

One problem with skill scores occurs when stations are not evenly distributed. When many stations are located in a particular region (such as metropolitan Denver), predictability in that region could have an inordinate influence on such statistics as the bias score.

5.2 MRBP Statistics – An Overview

One form of non-parametric statistical analysis well-suited for meteorological verification is Multivariate Randomized Block Permutation statistics (MRBP). Descriptions of this procedure can be found in Mielke (1984), Mielke (1991), and Cotton et al. (1994), and applications of these statistics to meteorological data can be found in Tucker et al. (1989), Lee (1992), Thompson (1993), and Snook (1993). MRBP is an extension of MRPP (Multiresponse Permutation Procedures) which can be applied when the data can be divided into blocks (here, observations and particular model setups) to be compared with each other.

In MRBP, a set of g independent treatments of a phenomenon for each of the b blocks are used to represent the range of values in analysis space; for this study, the treatments consist of 24-hour precipitation forecasts for each of the g days on which a given analysis can be performed. Then a function, δ, is formed using the equation (see Mielke, 1991):

$$\delta = \left[g \begin{pmatrix} b \\ 2 \end{pmatrix} \right]^{-1} \sum_{i=1}^{g} \sum_{j<k} \Delta(x_{ij}, x_{ik}), \tag{5.7}$$

where g is the number of treatments, b is the number of blocks, $\Delta(x_{ij}, x_{ik})$ is a symmetrical distance function to be defined later, and the summation is to be performed on all j and k such that $1 \leq j < k \leq b$. In the case where the comparison is to be between observations and a single model, $b = 2$ and the equation for δ reduces to:

$$\delta = g^{-1} \sum_{i=1}^{g} \Delta(x_{i1}, x_{i2}), \tag{5.8}$$

where the first subscript on x refers to the treatment and the second denotes the block.

Note that this method differs from the root-mean-square method of combining the treatments, given by:

$$\text{rms} = \left[g^{-1} \sum_{i=1}^{g} \Delta(x_{i1}, x_{i2})^2 \right]^{1/2}. \tag{5.9}$$

The fact that MRBP is based on the combination of Euclidian distances rather than their squares has the effect of minimizing the influence of isolated extreme values (Cotton et al., 1994), which frequently occur in meteorological fields. Furthermore MRBP has the

advantage of using an analysis space which corresponds to the space in which the data exists (Mielke 1985).

The symmetric distance function is given by (Mielke, 1991):

$$\Delta(x,y) = \left[\sum_{i=1}^{r}(x_i - y_i)^2\right]^{\nu/2}, \tag{5.10}$$

where r denotes the number of responses allowed for each treatment. For this thesis, r is the number of stations with data for each of the g days used in a study. Here ν is chosen to be 1, for which the distance function gives conventional Euclidian distance.

The value of δ in Equation (5.8) can be referred to as δ_0 when the index i is the same for x_{ij} as x_{ik}, i.e. corresponding treatments in each block are compared. It is also possible to get values of δ for each of the $(g!)^b$ possible ways to group g treatments in one block with those of the other blocks. If corresponding treatments are very well correlated between the blocks, then none of the other possible values of δ would be as small as δ_0, and it would be clear that the block correlation would not be due to chance. However, the existence of many other values of δ less than δ_0 would suggest that the correlation between blocks could be due to chance agreement between treatments (the null hypothesis). So a correlation coefficient ρ can be defined as (Tucker et al., 1989):

$$\rho = (\mu_\delta - \delta_0)/\mu_\delta, \tag{5.11}$$

where μ_δ is the mean of all possible δ values. When $\rho = 1.0$ then δ_0 is 0.0, which means that the blocks perfectly agree with each other. However, when $\rho = 0.0$ then the observed correlation between the blocks, which could be observational data and model output, would be as likely as not due to chance, whereas if ρ were negative, random chance would probably show better agreement with observations than the model.

In practice, if g becomes much larger than 10, then it becomes impossible to calculate all $(g!)^b$ values of δ in a reasonable amount of time (see Mielke, 1991). Since for a month g is about 30, another method must be found. What can be done is assume that the statistic

$$T = (\delta - \mu_\delta)/\sigma_\delta \tag{5.12}$$

follows a Pearson-type III distribution with the same mean μ_δ, standard deviation σ_δ, and skewness γ_δ as that of the exact δ distribution (see Tucker et al., 1989). Algorithms exist to find these three characteristics using on the order of g^3 calculations, which is much more manageable than $g!$. Then ρ directly follows from μ_δ while the null-hypothesis probability can be determined from the distribution of T.

5.3 Results: Errors and Averages – Day by Day

If all 167 climate stations are used, then for the middle 28 days of the month of April model and observational precipitation fields can be compared. Table 5.1 shows for the dump-bucket model average observed precipitation, average model precipitation, the ratio of observed to model precipitation, rms errors, and the standard deviations of model and observed precipitation totals, where the summations are performed over all climate stations for a given date. For each station the model value was found by using the precipitation produced at the geographically nearest model grid point.

First, it is apparent that on the days, mostly at the beginning of the month, where little or no precipitation was observed, the model tends to slightly overforecast precipitation. However, most model precipitation on these days was due to the convective parameterization, which tended to be over-generous with rainfall for this period, so this problem cannot be blamed on the microphysics. For meaningful comparisons, one can limit comparisons to days on which site-average precipitation was at least 1.0 mm, as in Table 5.2

Unfortunately, what also becomes apparent is that when one of the skill criteria of Pielke (1984) is used (that for a forecast to show skill the rms should be less than σ_{obs}), only one forecast (April 10) shows definite skill, though the rms is slightly less than σ_{obs} on the additional days of April 19, April 22, April 24, and April 26. Probably not coincidentally, April 10 is also the day that had the most observed precipitation throughout the state, with April 26 second. Another criterion mentioned by Pielke (1984) for forecast skill is that σ_{obs} and σ_{model} be approximately equal; here, while this criterion is met on some days, there is a

DATE	$\bar{p}_{obs}$	$\bar{p}_{model}$	$\bar{p}_{obs}/\bar{p}_{model}$	rms	σ_{obs}	σ_{model}
2	.03	.02	1.43	.19	.18	.10
3	.06	.11	.52	.48	.40	.25
4	.00	.01	.00	.06	.00	.06
5	.00	.19	.00	.58	.00	.55
6	.00	.50	.00	.95	.00	.81
7	.00	.52	.00	.96	.00	.81
8	.24	.55	.43	1.68	1.30	.99
9	3.40	2.53	1.34	4.99	4.48	2.73
10	7.58	7.76	.98	6.52	8.36	5.56
11	1.71	2.27	.75	2.98	3.10	2.59
12	.26	.06	4.07	.90	.91	.19
13	.06	.15	.42	.95	.80	.48
14	.01	.20	.07	.44	.08	.43
15	.18	.43	.41	.94	.69	.75
16	1.23	1.35	.91	2.35	2.31	1.69
17	3.07	4.91	.62	4.88	4.68	4.10
18	4.87	4.42	1.10	5.06	5.19	3.94
19	5.39	3.86	1.40	6.68	6.94	3.41
20	3.14	3.92	.80	5.22	5.12	2.89
21	3.53	2.74	1.29	5.71	5.71	2.92
22	4.52	3.55	1.28	5.92	6.31	3.16
23	1.72	1.17	1.47	3.19	3.06	1.54
24	2.89	2.53	1.14	3.95	4.24	2.32
25	.84	.63	1.33	2.42	2.83	1.78
26	7.26	3.65	1.99	6.54	6.75	3.89
27	.46	.52	.89	1.89	1.84	.82
28	.47	.61	.76	1.70	1.68	.96
29	2.48	1.17	2.12	3.80	3.46	1.57

Table 5.1: Statistics for dump-bucket vs. observational precipitation, at climatological stations. Units are mm of water- equivalent precipitation.

DATE	$\bar{p}_{obs}$	$\bar{p}_{model}$	$\bar{p}_{obs}/\bar{p}_{model}$	rms	σ_{obs}	σ_{model}
9	3.40	2.53	1.34	4.99	4.48	2.73
10	7.58	7.76	.98	6.52	8.36	5.56
11	1.71	2.27	.75	2.98	3.10	2.59
16	1.23	1.35	.91	2.35	2.31	1.69
17	3.07	4.91	.62	4.88	4.68	4.10
18	4.87	4.42	1.10	5.06	5.19	3.94
19	5.39	3.86	1.40	6.68	6.94	3.41
20	3.14	3.92	.80	5.22	5.12	2.89
21	3.53	2.74	1.29	5.71	5.71	2.92
22	4.52	3.55	1.28	5.92	6.31	3.16
23	1.72	1.17	1.47	3.19	3.06	1.54
24	2.89	2.53	1.14	3.95	4.24	2.32
26	7.26	3.65	1.99	6.54	6.75	3.89
29	2.48	1.17	2.12	3.80	3.46	1.57
avg.	3.77	3.27	1.15	4.84	4.98	3.02

Table 5.2: Statistics for dump-bucket model vs. observational precipitation, climatological stations, for major events. Units are mm of water-equivalent precipitation.

tendency for $\sigma_{model} < \sigma_{obs}$, normally by about a factor of two late in the month, suggesting that the dump-bucket model is not capturing all of the spatial variability of the observations. It should be expected that $\sigma_{model} < \sigma_{obs}$ because not all of the fine-scale terrain influences on observed precipitation can be resolved on a 16-km grid. The large variability in the observed field, when in some cases the standard deviation exceeds the average, would make it very difficult for any forecast model to achieve a low rms score with these case studies and station set.

What other conclusions can be drawn from Table 5.2? If the second column is averaged over all the dates shown and divided by the average of the first column, it is found that the dump-bucket model produces about 87% of the total observed precipitation. Two of the days on which precipitation was overpredicted (April 11 and April 20) were post-cold frontal. However, when Pacific lows passed over the mountains almost continually late in the month, total precipitation was underforecast. This suggests that the dump-bucket model overpredicts precipitation in upslope flows on the Eastern plains of Colorado but tends to underestimate synoptic shortwave-induced orographic precipitation.

DATE	$\bar{p}_{obs}$	$\bar{p}_{model}$	$\bar{p}_{obs}/\bar{p}_{model}$	rms	σ_{obs}	σ_{model}
9	3.40	2.05	1.66	5.14	4.48	3.03
10	7.58	8.26	.92	6.49	8.36	6.94
11	1.71	2.20	.77	2.60	3.10	2.47
16	1.23	.93	1.33	1.82	2.31	1.78
17	3.07	3.71	.83	4.66	4.68	5.03
18	4.87	3.72	1.31	5.97	5.19	4.20
19	5.39	2.89	1.86	6.67	6.94	3.34
20	3.14	3.59	.88	5.62	5.12	2.87
21	3.53	2.31	1.53	6.05	5.71	2.56
22	4.52	4.00	1.13	6.15	6.31	4.56
23	1.72	1.24	1.39	2.94	3.06	1.79
24	2.89	3.13	.92	4.89	4.24	3.58
26	7.26	5.87	1.24	6.71	6.75	7.84
29	2.48	.73	3.42	3.75	3.46	.75
avg.	3.77	3.19	1.18	4.96	4.98	3.62

Table 5.3: Statistics for microphysics model vs. observational precipitation, at climatological stations, for major events. Units are mm of water-equivalent precipitation.

How did the microphysics version of the model do on these cases? Table 5.3 corresponds to Table 5.2, only applying to the microphysics version of forecast RAMS. It is seen that output from both precipitation schemes is very similar; the differences in rms errors between the two models is normally much less than the natural variability of this error from case to case. Or, more specifically, and unfortunately for the forecaster, for both models the rms error tends to approach the standard deviation of the observations. Neither model shows a clear advantage in rms forecasting; the largest rms error differences are for the April 18 and 24 cases, where the dump-bucket model is about 0.9 mm better; and the April 16 case, where the microphysics is about 0.5 mm better. However, the microphysics model has standard deviations closer to the standard deviations of the observed fields for most of the larger precipitation events. In particular, for April 10, 22, and 26 the microphysics model achieves approximately the same rms error as the dump-bucket model with σ_{obs} much closer to the observed value.

Overall, for the dates given in Table 5.3, the microphysics scheme predicts about 85% of the observed precipitation, just slightly less than that of the dump-bucket scheme, though

there is a lot of scatter about this value for any particular case. In general, it seems the dump-bucket model was better at predicting the total precipitation when winter events were reaching their peak on the eastern plains of Colorado; it shows a tendency to underforecast as systems cross the mountains and to overforecast as systems leave the state, perhaps because the cold air masses that often prevail in these situations are not being properly represented.

Next, statistical analysis for the 32 SNOTEL stations was performed. Radio reports of seasonal accumulated precipitation are produced by the SNOTEL sites. Twice during April 1995 reports were not received from these instruments, which meant that the next day's report contained the total precipitation from the previous two days but no information on how much precipitation fell on which day. Thus April 12-13 and 19-20 to be excluded from the analysis leaving a set of 24 days to use for the SNOTEL comparisons. Tables 5.4 and 5.5 are for the dump-bucket and microphysics schemes, respectively.

Clearly both models underestimate SNOTEL precipitation more than the climate station data. The SNOTEL sites generally receive more precipitation during the month than the climate stations. So this implies that the models underestimate orographic enhancement effects. The dump-bucket model overall predicts 38% of the observed SNOTEL precipitation while the microphysics model predicts about 50% of the observed total.

To summarize:

1) Both models are very similar in terms of rms scores for a given case.

2) Neither model possesses an rms score which differs significantly from the standard deviation of the observations; in only one case (April 10) is skill clearly indicated.

3) Performance of models seems to be positively correlated to the amount of precipitation associated with an event.

4) The models have smaller standard deviations in their precipitation outputs than the observations. For the larger precipitation events the standard deviation of the microphysics model normally comes closer to that of the observations.

5) The models predict from 80-90% of the total precipitation at the climate stations but do less well for the SNOTEL stations, which receive on average more precipitation.

DATE	$\bar{p}_{obs}$	$\bar{p}_{model}$	$\bar{p}_{obs}/\bar{p}_{model}$	rms	σ_{obs}	σ_{model}
2	.24	.20	1.20	.76	.74	.24
3	.48	.01	60.00	1.10	.99	.04
4	1.03	.03	32.50	2.57	2.36	.08
5	.48	.09	5.45	1.12	.99	.26
6	.16	.82	.19	1.51	.61	1.15
7	.16	.21	.74	1.07	.61	.83
8	3.65	.30	12.11	5.48	4.35	.51
9	8.26	4.43	1.86	8.49	6.54	2.65
10	5.40	2.90	1.86	5.72	4.52	3.15
11	4.60	.35	13.18	5.98	4.33	.57
14	1.03	.29	3.51	2.47	2.36	.59
15	4.84	1.51	3.21	4.92	3.78	1.72
16	5.24	3.23	1.62	6.36	6.25	3.13
17	10.48	5.56	1.88	8.28	7.37	3.63
18	7.78	2.07	3.75	7.61	5.46	1.38
21	6.27	3.98	1.57	6.52	7.04	5.57
22	5.56	2.00	2.78	5.86	5.10	1.46
23	9.21	3.04	3.03	10.75	8.68	3.53
24	3.57	.33	10.98	4.88	3.58	.71
25	10.08	2.40	4.21	10.38	8.34	2.81
26	4.60	2.78	1.66	4.90	4.14	3.24
27	1.27	.37	3.40	2.08	1.91	.57
28	1.91	.83	2.29	3.64	3.24	1.25
29	6.19	1.29	4.79	6.27	4.44	1.48

Table 5.4: Statistics for dump-bucket vs. observational precipitation, at SNOTEL stations. Units are mm of water-equivalent precipitation.

DATE	$\bar{p}_{obs}$	$\bar{p}_{model}$	$\bar{p}_{obs}/\bar{p}_{model}$	rms	σ_{obs}	σ_{model}
2	.24	.92	.26	1.29	.74	.90
3	.48	.02	30.00	1.10	.99	.06
4	1.03	.31	3.33	2.59	2.36	.47
5	.48	.50	.95	1.41	.99	.86
6	.16	1.40	.11	2.02	.61	1.39
7	.16	.28	.57	1.25	.61	1.05
8	3.65	.35	10.45	5.47	4.35	.46
9	8.26	3.81	2.17	8.96	6.54	3.66
10	5.40	3.39	1.59	5.45	4.52	3.74
11	4.60	.48	9.67	5.98	4.33	.55
14	1.03	.29	3.51	2.47	2.36	.39
15	4.84	1.54	3.14	5.17	3.78	2.00
16	5.24	3.41	1.54	6.55	6.25	4.40
17	10.48	9.72	1.08	9.91	7.37	8.97
18	7.78	1.94	4.00	7.96	5.46	1.20
21	6.27	6.17	1.02	8.02	7.04	6.70
22	5.56	3.73	1.49	5.76	5.10	3.88
23	9.21	2.52	3.66	10.85	8.68	2.28
24	3.57	.40	9.00	4.76	3.58	.55
25	10.08	2.47	4.08	9.92	8.34	2.74
26	4.60	4.96	.93	8.26	4.14	8.21
27	1.27	.32	4.00	2.13	1.91	.37
28	1.91	.21	8.89	3.65	3.24	.24
29	6.19	1.55	4.00	5.79	4.44	1.56

Table 5.5: Statistics for microphysics model vs. observational precipitation, at SNOTEL stations. Units are mm of water-equivalent precipitation.

The microphysics predicts more of the recorded SNOTEL accumulations (50%) than the dump-bucket scheme (38%).

5.4 Skill Scores – Day by Day

Tables 5.6 and 5.7 show a list of the previously discussed skill scores (bias, threat, Heidke) for the dump-bucket and microphysics runs, respectively, for the set of climatological stations. What the bias scores seem to indicate is that, while the models tend to underpredict the total amount of precipitation, they overpredict the areal coverage of the smaller precipitation thresholds, whereas there is underprediction of the area of the larger precipitation thresholds.

In general, the microphysics scheme does better at bias scores than the dump-bucket schemes. Normally the bias scores of the microphysics are lower than for the dump-bucket scheme, which produces scores closer to unity for the smaller thresholds. For larger thresholds the bias scores become less than one which causes the dump-bucket model to perform better, though at the largest threshold for major precipitation events there are signs that the microphysics again possesses more realistic bias scores.

The threat scores are pretty similar between the two models, but the Heidke skill score is usually better (closer to unity) for the microphysics model. This suggests that some of the success of the dump-bucket scheme in threat scores is due to overpredicting (see Doswell et al., 1990). Since the threat score is proportional to the number of correctly forecast stations above a threshold, one could, to take an extreme example, forecast that the threshold will be exceeded for the entire domain. This ensures that every station that exceeds the threshold in the domain will be counted as a correctly forecast station, which tends to maximize the threat score in the case of infrequent events. The Heidke score protects against this possibility by counting both correct event and non-event prediction, and by subtracting out from the correctly forecast stations the number of stations one would expect to correctly predict from chance, based on a random distribution of the model forecast stations among the total station network.

So, to summarize:

1) Both models, while tending to underpredict the total amount of precipitation, overpredict the areal coverage of the lower precipitation thresholds.

2) At larger precipitation thresholds, the models underpredict the areal coverage.

3) The microphysics performs better than the dump-bucket scheme in bias scores at the higher and lower thresholds.

4) The microphysics performs better in the Heidke skill score, probably due to a lesser tendency to overpredict areas of precipitation.

5.5 MRBP Statistics – Whole Datasets

Using MRBP the set of daily forecasts for each station can be combined in an appropriate data space to give some indication as to which model corresponds most closely to the observations. When this is done, the correlation coefficient ρ for the models and station sets is given in Table 5.8. Both models perform much better at the climatological stations than the SNOTEL stations. The numbers for the climatological stations compare favorably to those obtained by Tucker et al. (1989). They used the model described in Tucker and Reiter (1988) with 24-km grid spacing, and obtained a value of 0.194 for ρ, although this actually improved to 0.266 when the model output was averaged to a 96-km grid. The dump-bucket scheme shows better performance at the climate stations while the microphysics model is the better performer at the SNOTEL stations, consistent with some of the discussion above. Using the bulk microphysics on just the fine grid points (see Section 4.2.1) is seen to have not much effect on the SNOTEL stations but has a noticeable negative effect on forecasting skill for the climatological stations. This is probably due to the fact that some climatological stations are located near the boundaries of the fine grid, while virtually all the SNOTEL sites are well within the fine grid. The lack of microphysical species on the coarse grid can produce numerical noise in the precipitation field which propagates from the boundaries (particularly on the plains of northeastern Colorado).

As previously stated, the model values of precipitation were found by using the nearest grid point to the station. It is possible that this procedure may not give the most accurate representation of the model precipitation at a station without using some interpolation

	bias score				threat score				Heidke skill score			
DATE	0.254	2.54	6.35	12.7	0.254	2.54	6.35	12.7	0.254	2.54	6.35	12.7
2	1.25	*	*	*	.20	*	*	*	.30	*	*	*
3	4.56	.00	*	*	.04	.00	*	*	-.01	.00	*	*
4	*	*	*	*	.00	*	*	*	.00	*	*	*
5	*	*	*	*	.00	.00	*	*	.00	.00	*	*
6	*	*	*	*	.00	.00	*	*	.00	.00	*	*
7	*	*	*	*	.00	.00	*	*	.00	.00	*	*
8	7.00	3.00	.00	.00	.07	.00	.00	.00	.05	-.05	.00	.00
9	1.43	.84	.36	.11	.55	.26	.20	.00	.00	.00	.22	-.01
10	1.30	1.22	1.34	.88	.77	.71	.55	.39	.00	.42	.44	.43
11	1.54	1.47	1.36	.00	.57	.36	.13	.00	.37	.32	.17	.00
12	.80	.00	.00	*	.38	.00	.00	*	.47	.00	.00	*
13	32.00	3.00	.00	*	.00	.00	.00	*	-.01	-.01	.00	*
14	8.67	*	*	*	.07	.00	*	*	.08	.00	*	*
15	3.19	1.17	*	*	.24	.08	*	*	.24	.12	*	*
16	2.12	.74	.86	.00	.44	.17	.18	.00	.19	.14	.28	.00
17	1.65	1.74	1.77	1.00	.57	.45	.32	.11	.07	.30	.33	.15
18	1.16	1.09	.84	.39	.80	.55	.29	.14	.15	.29	.23	.19
19	1.29	1.07	.80	.09	.77	.58	.29	.00	.14	.42	.26	-.02
20	1.49	1.42	1.58	.00	.65	.50	.17	.00	-.02	.36	.14	.00
21	1.49	1.09	.42	.27	.66	.45	.15	.08	.03	.36	.16	.12
22	1.51	1.26	.43	.35	.66	.45	.18	.15	.16	.22	.16	.22
23	1.65	.47	.43	.00	.55	.17	.05	.00	.22	.15	.05	.00
24	1.57	1.16	.43	.25	.61	.44	.18	.00	.19	.35	.22	-.01
25	2.00	.75	.83	.00	.31	.33	.22	.00	.32	.46	.34	.00
26	1.15	.77	.38	.20	.83	.59	.33	.11	.53	.43	.29	.13
27	3.87	.60	.00	.00	.13	.14	.00	.00	.02	.21	.00	.00
28	6.65	1.09	.00	*	.13	.10	.00	*	.07	.11	.00	*
29	1.35	.47	.13	.00	.55	.18	.08	.00	.17	.09	.13	.00

Table 5.6: Skill scores for dump-bucket model, at climatological stations. Labels on heading denote thresholds used to evaluate each score, in mm of precipitation. Values of * represent cases where the given score is undefined.

	bias score				threat score				Heidke skill score			
DATE	0.254	2.54	6.35	12.7	0.254	2.54	6.35	12.7	0.254	2.54	6.35	12.7
2	4.75	*	*	*	.18	*	*	*	.24	*	*	*
3	9.89	6.00	*	*	.09	.00	*	*	.07	-.01	*	*
4	*	*	*	*	.00	*	*	*	.00	*	*	*
5	*	*	*	*	.00	.00	*	*	.00	.00	*	*
6	*	*	*	*	.00	.00	.00	*	.00	.00	.00	*
7	*	*	*	*	.00	.00	*	*	.00	.00	*	*
8	8.33	1.80	.00	.00	.08	.00	.00	.00	.05	-.04	.00	.00
9	1.44	.51	.30	.33	.54	.26	.16	.00	-.05	.16	.18	-.03
10	1.24	1.09	1.27	1.10	.78	.75	.61	.47	.19	.56	.54	.52
11	1.56	1.35	1.55	.00	.59	.51	.33	.00	.40	.54	.46	.00
12	1.60	.00	.00	*	.47	.00	.00	*	.54	.00	.00	*
13	22.00	.00	.00	*	.00	.00	.00	*	-.01	.00	.00	*
14	9.00	*	*	*	.05	*	*	*	.04	*	*	*
15	1.76	.00	*	*	.29	.00	*	*	.34	.00	*	*
16	1.61	.74	.14	1.00	.58	.30	.14	1.00	.49	.34	.24	1.00
17	1.26	1.03	1.19	1.50	.60	.36	.33	.39	.32	.26	.37	.53
18	1.04	.97	.59	.33	.76	.56	.16	.04	.24	.36	.06	.03
19	1.06	.81	.57	.04	.82	.47	.28	.04	.57	.32	.29	.07
20	1.46	1.42	1.12	.12	.67	.46	.11	.00	.08	.29	.05	-.01
21	1.38	.82	.33	.09	.62	.29	.05	.01	.00	.15	-.01	.16
22	1.49	1.08	.77	.47	.63	.44	.43	.14	.09	.26	.47	.19
23	1.36	.65	.57	.00	.56	.34	.16	.00	.33	.38	.23	.00
24	1.48	1.27	.86	1.25	.65	.50	.21	.00	.34	.43	.23	-.03
25	1.52	.50	.67	.00	.36	.33	.25	.00	.42	.47	.38	.00
26	1.10	.76	.55	.73	.81	.63	.43	.34	.51	.52	.37	.38
27	4.65	1.80	1.00	.00	.16	.08	.00	.00	.06	.07	-.02	.00
28	5.18	.00	.00	*	.13	.00	.00	*	.07	.00	.00	*
29	1.35	.12	.00	.00	.56	.10	.00	.00	.19	.12	.00	.00

Table 5.7: Same as Table 5.6, but for microphysics model.

	climate	SNOTEL
dump-bucket	0.311	0.154
microphysics	0.290	0.173
one-grid microphysics	0.267	0.174

Table 5.8: Values of ρ coefficient from MRBP statistics.

	climate	SNOTEL
dump-bucket	0.315	0.156
microphysics	0.292	0.175

Table 5.9: Values of ρ coefficient from MRBP statistics, using linear interpolation

procedure. So a simple interpolation scheme was utilized to see if this is a major effect. The distances between each station and the four nearest grid points were found. Then the model precipitation at each of those four grid points were weighted according to:

$$p_{interp} = w_{11} \times p_{11} + w_{21} \times p_{21} + w_{12} \times p_{12} + w_{22} \times p_{22}, \tag{5.13}$$

where p is the amount of precipitation at a grid point and the subscripts 11, 21, 12, and 22 refer to the southwest, southeast, northwest, and northeast corners, respectively, of the model grid area surrounding the station. The weighting factors w_{ij} are given by:

$$w_{ij} = \frac{(\Delta x_{total} - \Delta x_i) \times (\Delta y_{total} - \Delta y_j)}{\Delta x_{total} \times \Delta y_{total}}, \tag{5.14}$$

with Δx_1, Δx_2, Δy_1, and Δy_2 referring to distances from the station to the western, eastern, southern, and northern boundaries, respectively, of the surrounding model grid area. Δx_{total} and Δy_{total} are the total west-east and south-north distances across the grid area. When this procedure is used, values for the MRBP ρ coefficient are given in Table 5.9. It can be seen that this procedure improves all the scores, but only by a very slight amount, suggesting that simply using the nearest model grid point values does not significantly change the forecasting skill, and that producing better resolution of the observed precipitation fields would require the use of reduced model grid spacing.

5.6 MRBP Statistics – Individual Climatological Stations

With MRBP it is also possible to treat just a single response (station) at a time. In this manner it is possible to determine exactly which stations are handled well by a given model for the set of case studies. For the climatological stations, Figures 5.1 and 5.2 show

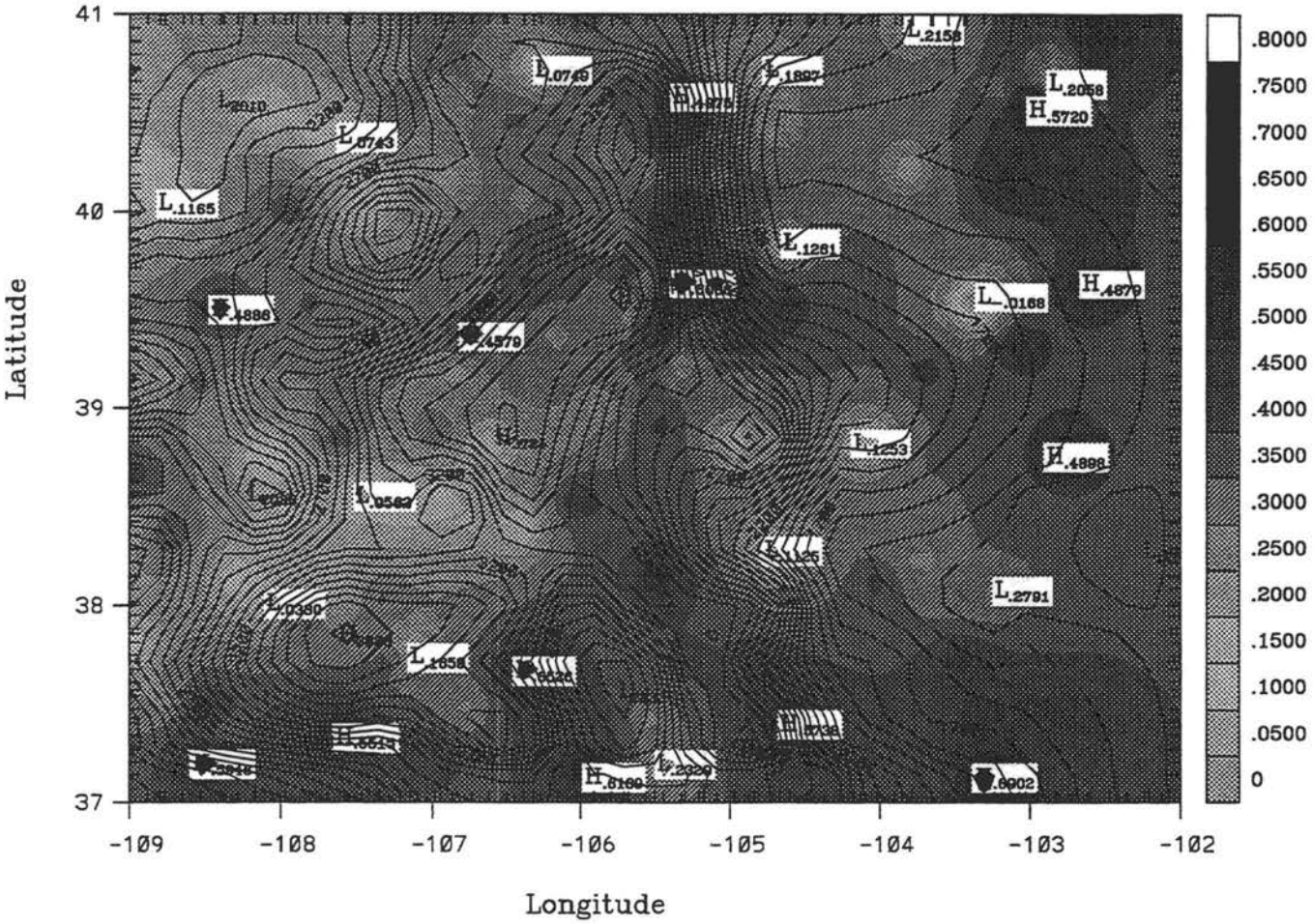

Figure 5.1: Values of ρ at climatological stations, for dump-bucket model. Contour lines are elevation in meters. Values of ρ have been smoothed to a regular grid.

geographic plots of ρ for the dump-bucket and microphysics schemes, respectively, at the climatological stations. Figures 5.3 and 5.4 show those stations where each respective model outperforms the other.

Overall, both models perform best in the Denver region, Front Range, southeastern Colorado, and parts of the southwest, while both models have their most difficult time in the west, northwestern plateau, high mountain parks, and certain regions near the Palmer Divide. A comparison between the two models shows:

1) The dump-bucket scheme is superior over most of the state west of the Continental Divide, except for a band in the central and southern Rockies. The microphysics scheme performs better over the southeast and parts of the Platte River Valley.

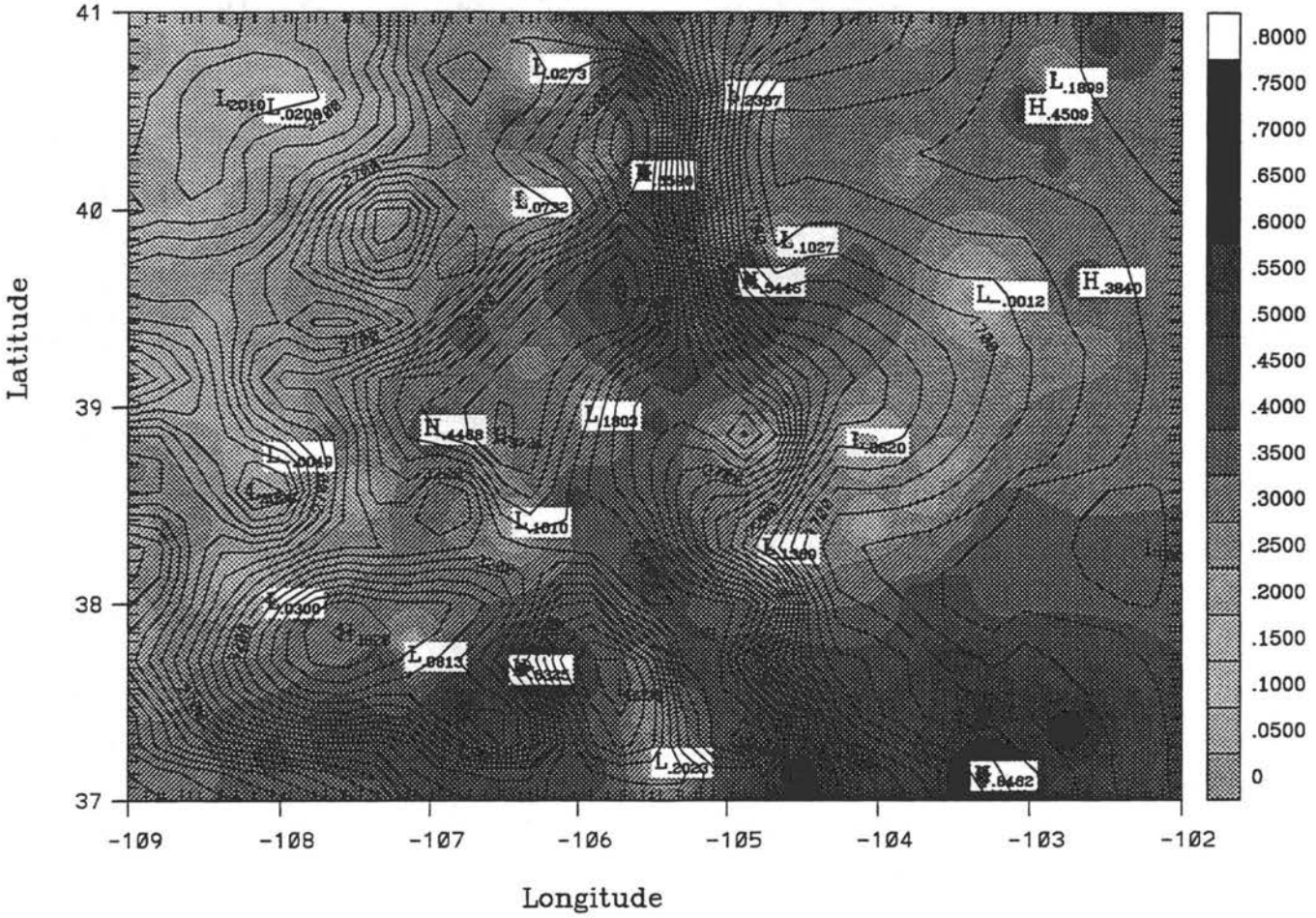

Figure 5.2: Values of ρ at climatological stations, for microphysics model.

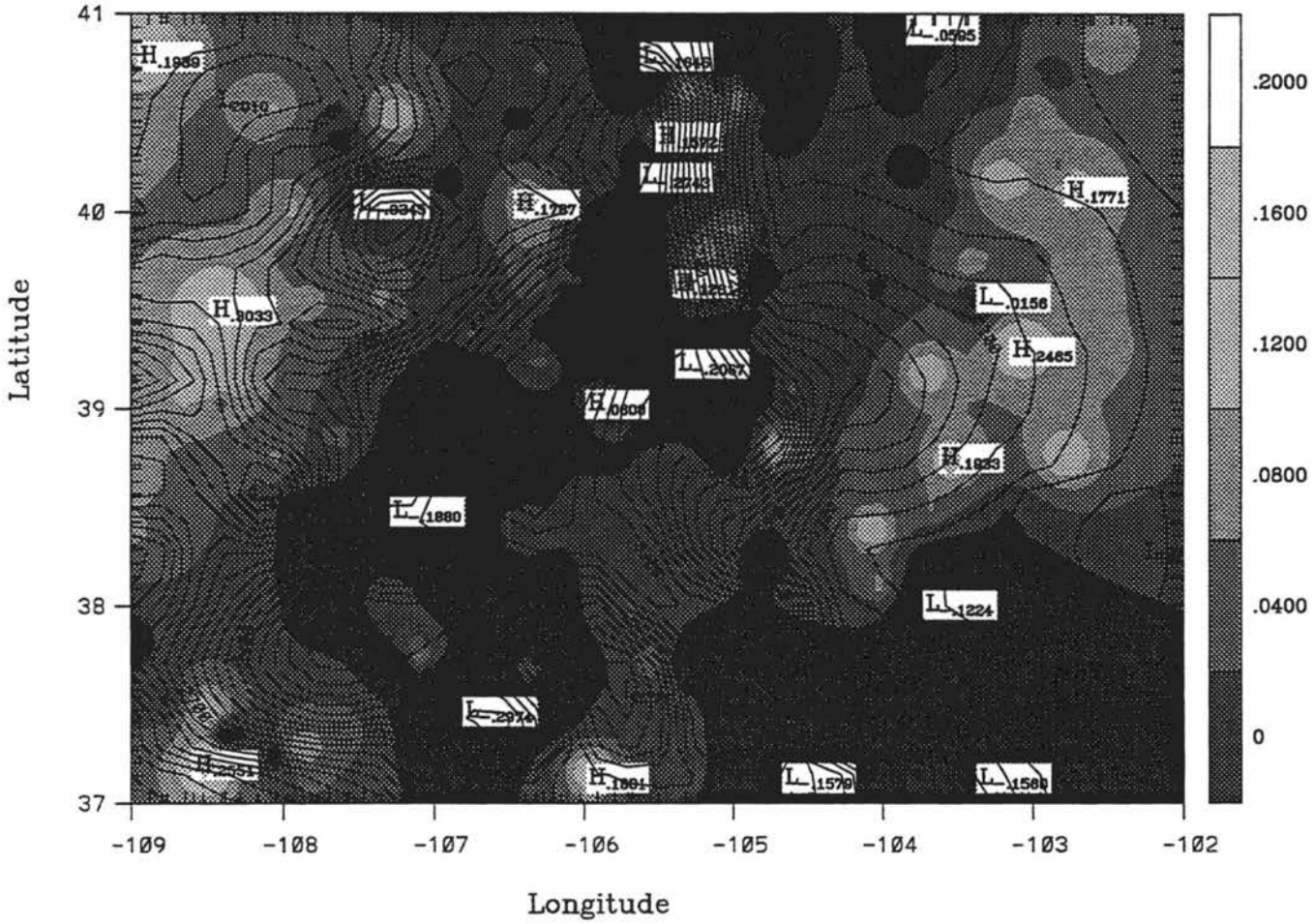

Figure 5.3: Difference of ρ values – dump-bucket minus microphysics. Darkest contour indicates region where the microphysics model possesses a greater value of ρ.

2) The microphysics shows better performance at most high elevation locations, especially right along the Continental Divide (Figure 5.4), but not high elevation valleys, such as North Park, Middle Park, South Park and the San Luis Valley.

3) The Palmer Ridge and other drainage divides in the east are regions of poor microphysics performance.

Plots of the ratio of total observed precipitation to total model precipitation for each climatological station are shown in Figures 5.5 and 5.6. As noted previously, both the microphysics and dump-bucket models underpredict total precipitation by about 15%. Comparing these figures to Figures 5.1 and 5.2, it is seen that underprediction of total precipitation is more common than overprediction in the regions of poor model performance, but this

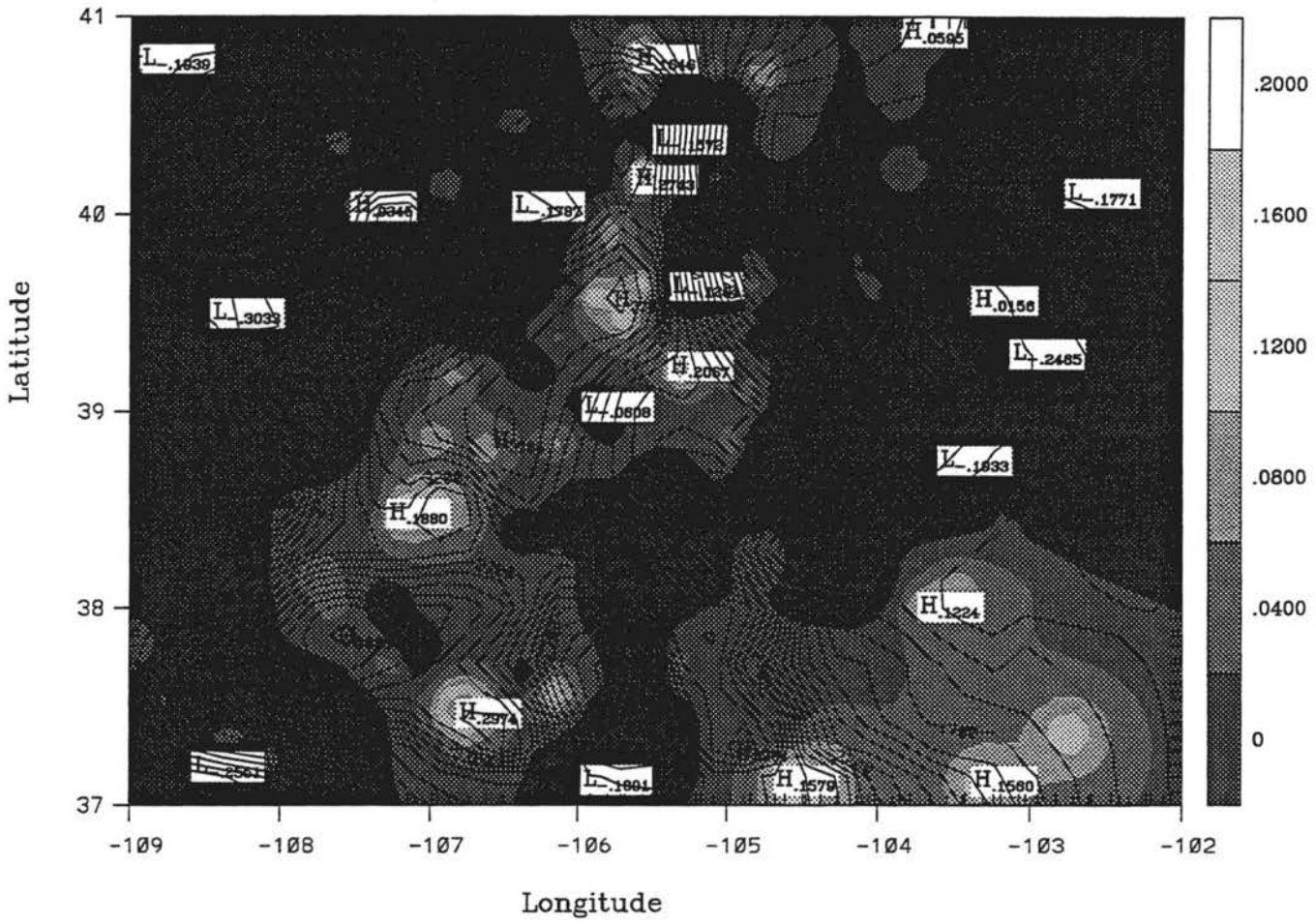

Figure 5.4: Difference of ρ values – microphysics minus dump-bucket. Darkest contour indicates region where the dump-bucket model possesses a greater value of ρ.

pattern is not absolute for the climate stations. For example, the microphysics generally underpredicts precipitation on the western slope and near Colorado Springs, but overpredicts precipitation in the high mountain valleys and north of Limon; all are regions of poor microphysics forecasting skill. Conversely, there are regions in which the microphysics model either significantly underpredicts (La Junta) or overpredicts (far southwest) precipitation but still has a high ρ value. Some regions of poor forecasting performance, such as near Walden, received little precipitation during the time period, so the lack of numerous samples of precipitation may make it difficult for any model to perform well statistically in such regions.

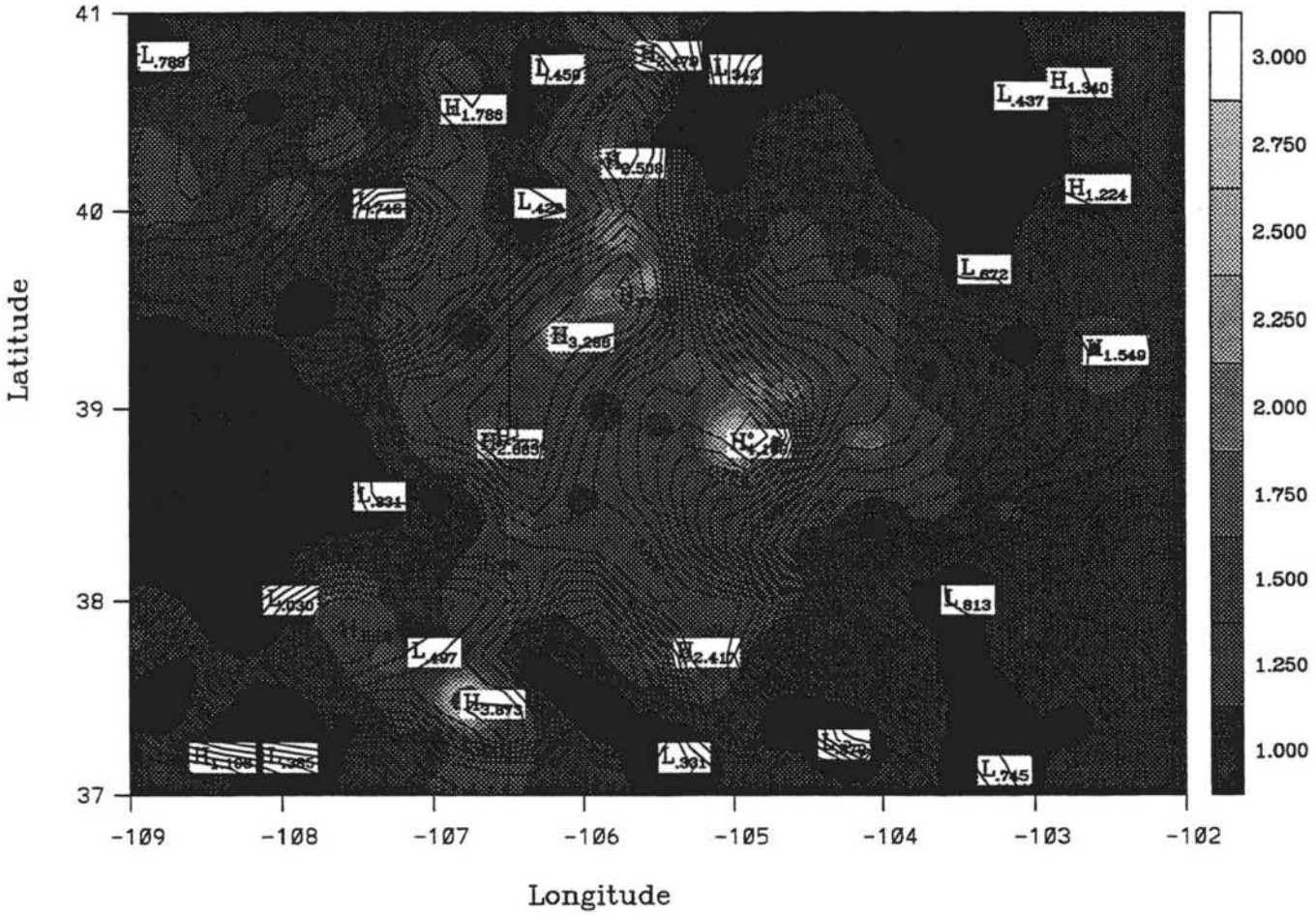

Figure 5.5: Ratio of total observed precipitation to total model precipitation at climatological stations, for dump-bucket model.

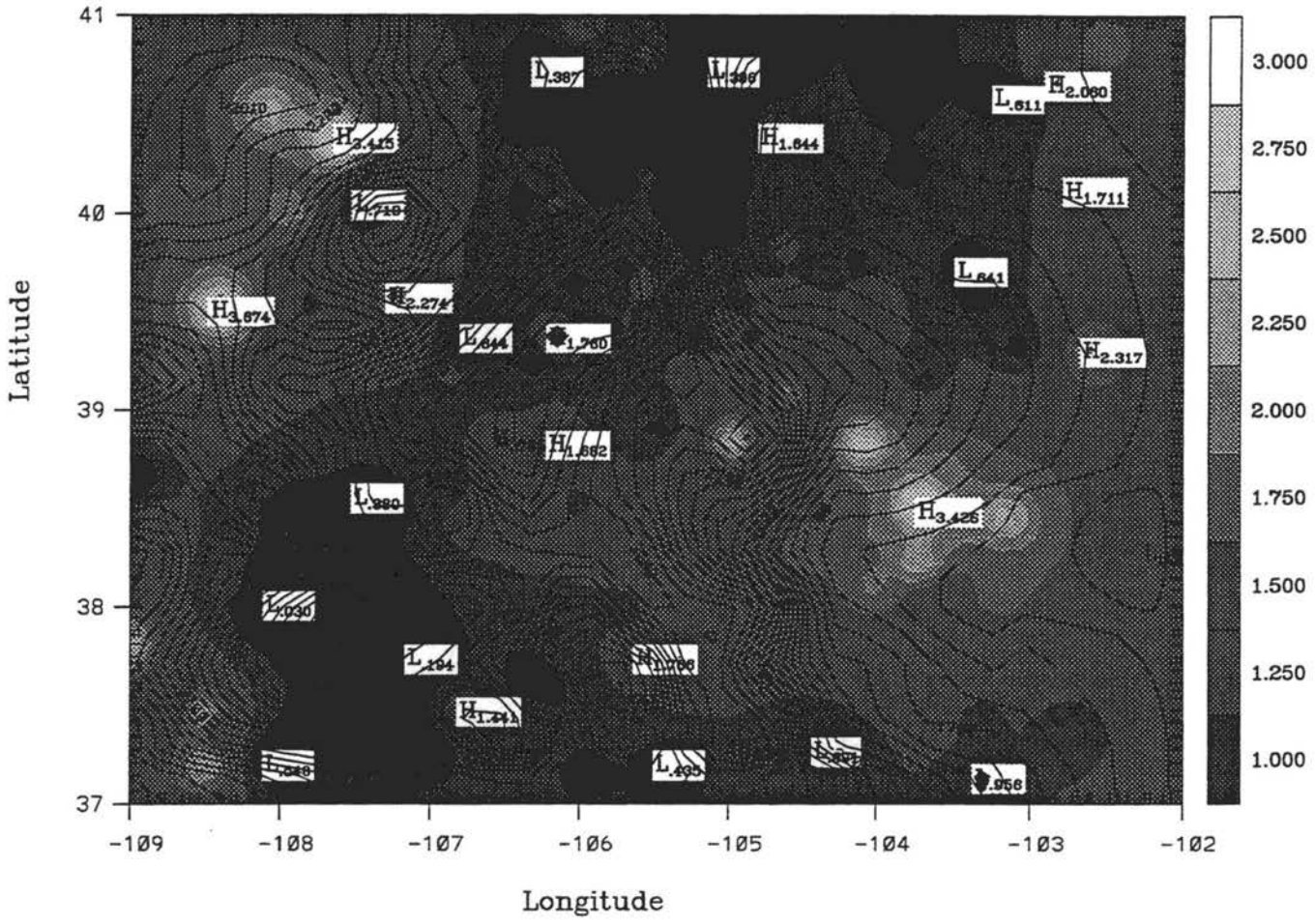

Figure 5.6: Ratio of total observed precipitation to total model precipitation at climatological stations, for microphysics model.

5.7 MRBP Statistics – Individual SNOTEL Stations

If a similar geographical analysis is performed on the SNOTEL stations, the results are shown in Figures 5.7 and 5.8 for the dump-bucket and microphysics models, respectively. Comparing the skill scores, a trend similar to that found in the climatological stations is found. There is a strong correlation between proximity to the Continental Divide and performance of the microphysics model, the only real exceptions being in those stations (Dry Lake, Elk River, and Tower SNOTELs) to the northeast of Rabbit Ears' Pass in North Park; and the stations east of Gunnison, for which both models show about equal performance.

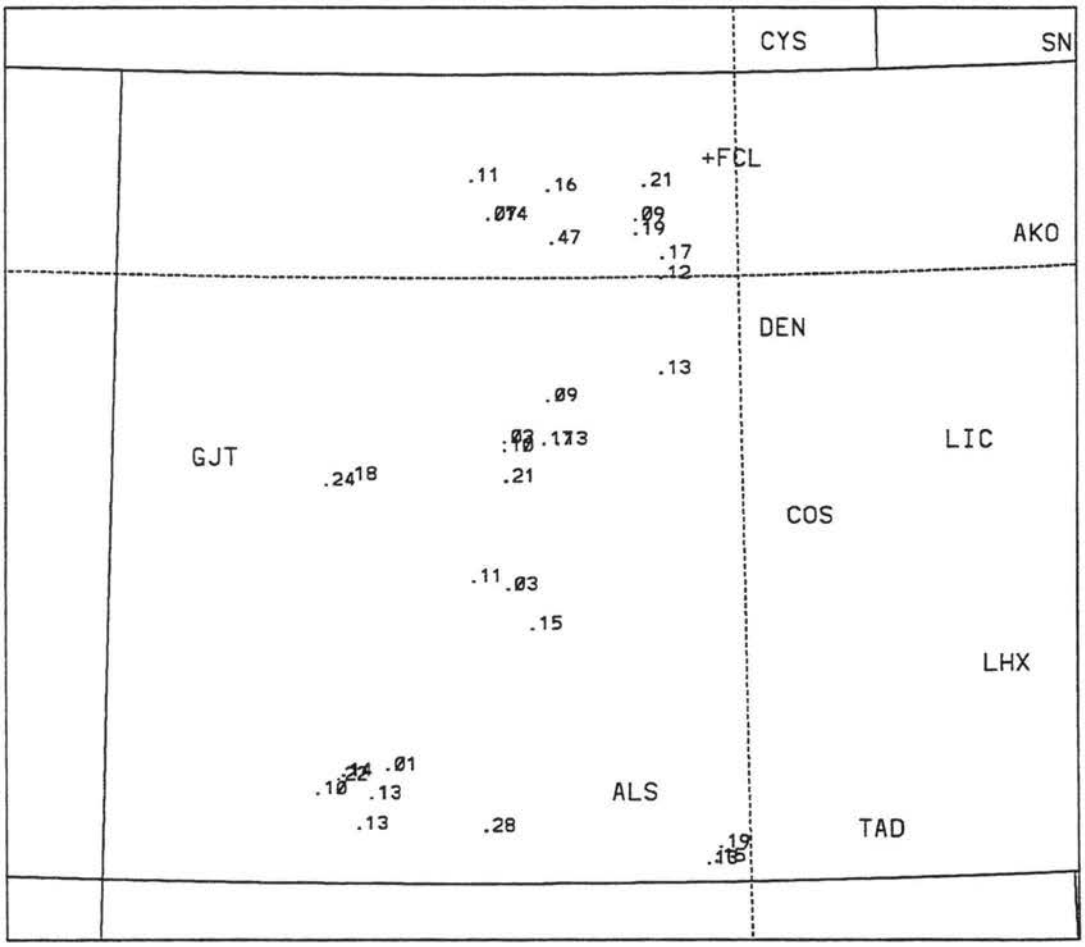

Figure 5.7: Values of ρ at SNOTEL stations, for dump-bucket model.

Looking at the ratios of observed precipitation to model precipitation in Table 5.10, it is seen, as suggested in Section 3, that almost always the models underestimate SNOTEL

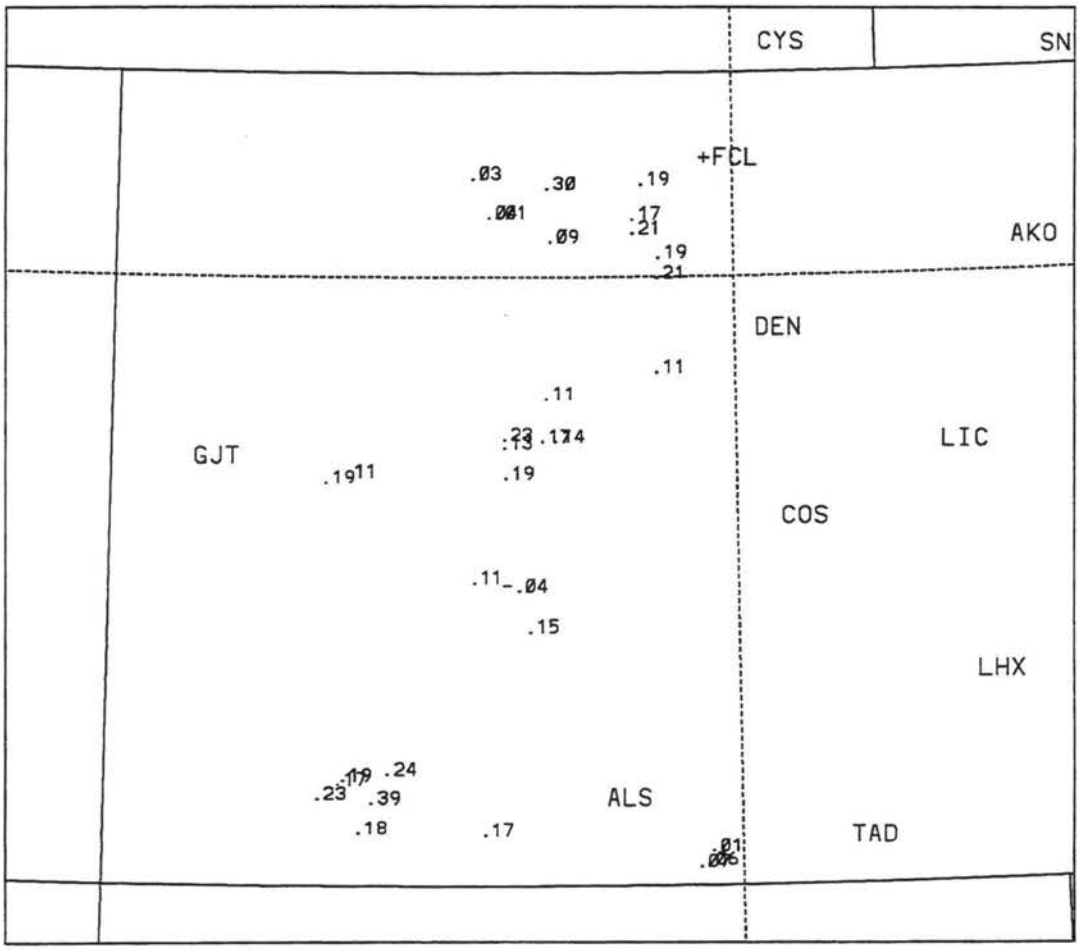

Figure 5.8: Values of ρ at SNOTEL stations, for microphysics model.

precipitation (true for 31 of the 32 stations with the dump-bucket model and 30 of the 32 stations with the microphysics model). For 22 of the 32 stations the microphysics predicts the greater amount of total precipitation, which is an improvement for 21 of those 22 stations. For 21 of the 32 SNOTEL stations, the model which predicted more overall precipitation at a station also had the better ρ parameter.

Of the stations in which the microphysics predicts less precipitation than the dump-bucket scheme, six of these are located near the rims of large intermontane valleys: the west end of North Park (Dry Lake, Elk River, and Tower) or the east end of the San Luis Valley (Apishapa, Culebra #2, and Whiskey Creek). Both of these locations might be considered in the lee of major mountain ranges with respect to moisture-bearing winds. This suggests that the microphysics model is creating too large of a rain-shadow effect in these regions. However, at towns even further away from the mountains in North Park (Walden) and the San Luis Valley (San Luis), where the observed precipitation for the month was meager compared to the above SNOTEL sites, the model actually overpredicts the precipitation. So it appears that what the model is doing is starting a rain-shadow too close to the mountain crest, whereas in reality some precipitation is advected over the crest to the nearby lee side.

5.8 Discussion

So why do both models seem to have more trouble with predicting observed snowfall totals at the SNOTEL stations than at the climatological stations? Doesken and Schaffer (1987) note that climatological stations are usually lower in elevation than the SNOTEL sites, and that the increase of precipitation with elevation is most extreme during the winter months. So, for whatever reason, the model output seems more typical of the climatological station environment than the SNOTEL environment. Part of the answer may lie with the observations and modeling studies suggesting that most of the winter orographic precipitation at the ridge crest consists of aggregates while the rimed particles become more significant further upwind (Meyers and Cotton, 1992; Rauber, 1992; Hobbs et al., 1973). This pattern is also found in this study, as can be seen in Figures 5.9 and 5.10. The SNOTEL sites are mostly in the aggregate regime. Note, however, that on the

ID	Name	Microphysics	Dump-bucket
41	APISHAPA SNOTEL	6.50	5.42
49	BUTTE SNOTEL	2.13	2.23
51	COPELAND LAKE SNOTEL	1.34	1.55
55	CULEBRA #2 SNOTEL	5.67	4.72
57	DEADMAN SNOTEL	.95	1.35
58	DRY LAKE SNOTEL	3.20	2.51
60	ELK RIVER SNOTEL	3.85	3.09
61	SNOTEL	3.57	4.00
63	HOOSIER PASS SNOTEL	5.46	3.88
64	INDEPENDENCE PASS SNOTEL	3.58	5.64
65	IDARADO SNOTEL	2.16	5.14
66	JOE WRIGHT SNOTEL	1.02	1.37
67	KILN SNOTEL	2.73	4.94
68	LAKE ELDORA SNOTEL	1.67	2.39
69	LIZARD HEAD PASS SNOTEL	1.27	2.04
79	OVERLAND RSVR SNOTEL	1.43	1.32
80	PHANTOM VALLEY SNOTEL	.47	.69
81	PARK CONE SNOTEL	3.38	3.51
82	PORPHYRY CREEK SNOTEL	6.17	8.60
83	PARK RSVR SNOTEL	3.02	2.13
86	RED MOUNTAIN PASS SNOTEL	1.93	4.58
87	ROACH SNOTEL	2.43	4.56
90	SLUMGULLION PASS SNOTEL	1.74	4.43
94	SUMMIT RANCH SNOTEL	2.04	3.44
97	TOWER SNOTEL	4.76	3.74
98	UPPER RIO GRANDE SNOTEL	1.08	1.79
99	UPPER SAN JUAN SNOTEL	1.54	5.83
100	UNIVERSITY CAMP SNOTEL	1.60	2.12
101	VALLECITO SNOTEL	1.89	1.42
102	VAIL MTN SNOTEL	3.29	5.95
104	WILLOW CREEK PASS SNOTEL	3.01	4.71
106	WHISKEY CREEK SNOTEL	6.83	5.69

Table 5.10: Ratio of total observed precipitation to total model precipitation at SNOTEL sites

day of these figures (April 26) there is a large area of overlap for the two hydrometeor categories. This is also one of the days when the SNOTEL stations were not underforecast by the microphysics model. The underprediction problem seems to be associated with the aggregate category, at least when it is not in the process of conversion to the graupel or hail categories, which can occur either through riming or melting of the aggregates. Generally a certain fraction of aggregates is converted to graupel upon riming or melting; further riming or melting converts the graupel category to the hail category (Walko et al., 1995).

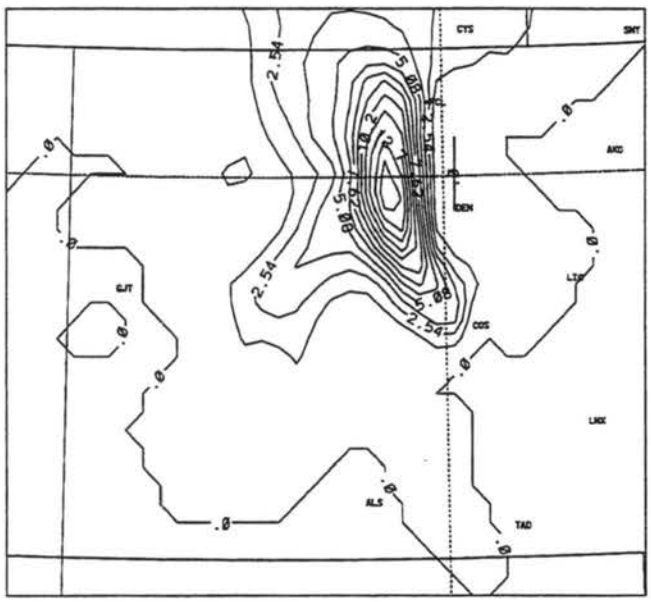

Figure 5.9: Accumulated aggregate precipitation, April 19 24-hr forecast, microphysics model.

It seems that aggregate hydrometeors have difficulty reaching the ground. More specifically, significant aggregate concentrations often appear above the ground, but the aggregates almost always disappear before they reach the ground in large quantities. An example is shown in Figure 5.11, which is a cross-section through the fine grid at the latitude of Fort Collins. Typical is the distribution of aggregates closer to the surface on the upwind side of the ridge than on the downwind side, where the species is advected in a tail over the crest. The fact that the aggregates are well above the surface on the lee slopes would explain the extreme rain-shadow effect mentioned in the previous section, if sublimation were in fact

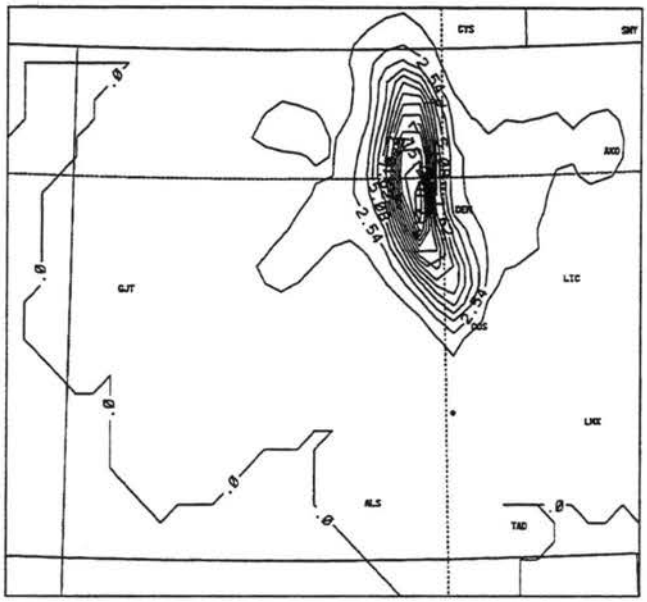

Figure 5.10: Accumulated graupel precipitation, April 19 24-hr forecast, microphysics model.

removing too much aggregate precipitation. Even on the windward side, though, aggregates often don't reach the ground. In the case of Figure 5.11, no measurable precipitation was produced by the model near the Front Range crest during the April 25 microphysics simulation. The only cases where significant aggregate precipitation occurs seem to be, as in the April 26 case, when the aggregates travel only through saturated or nearly-saturated levels on the way to the ground (see Figures 5.12 and 5.13). This does not mean that all aggregate precipitation must rime and become graupel or hail in order to reach the ground, as cases exist where aggregate precipitation exists with little or no graupel or hail precipitation. However, the existence of cloud liquid water does seem to be a prerequisite for aggregate accumulations at the surface, which implies that the degree of vapor saturation is an important factor to their survival.

Another factor which could be accounting for the underprediction of SNOTEL precipitation could be convective snowfall. As noted in Chapter 4, on April 25 thunderstorms were reported in advance of the winter storm of April 26. The SNOTEL sites actually reported more snow in the period from midnight, April 25 to midnight, April 26 (MDT) than in

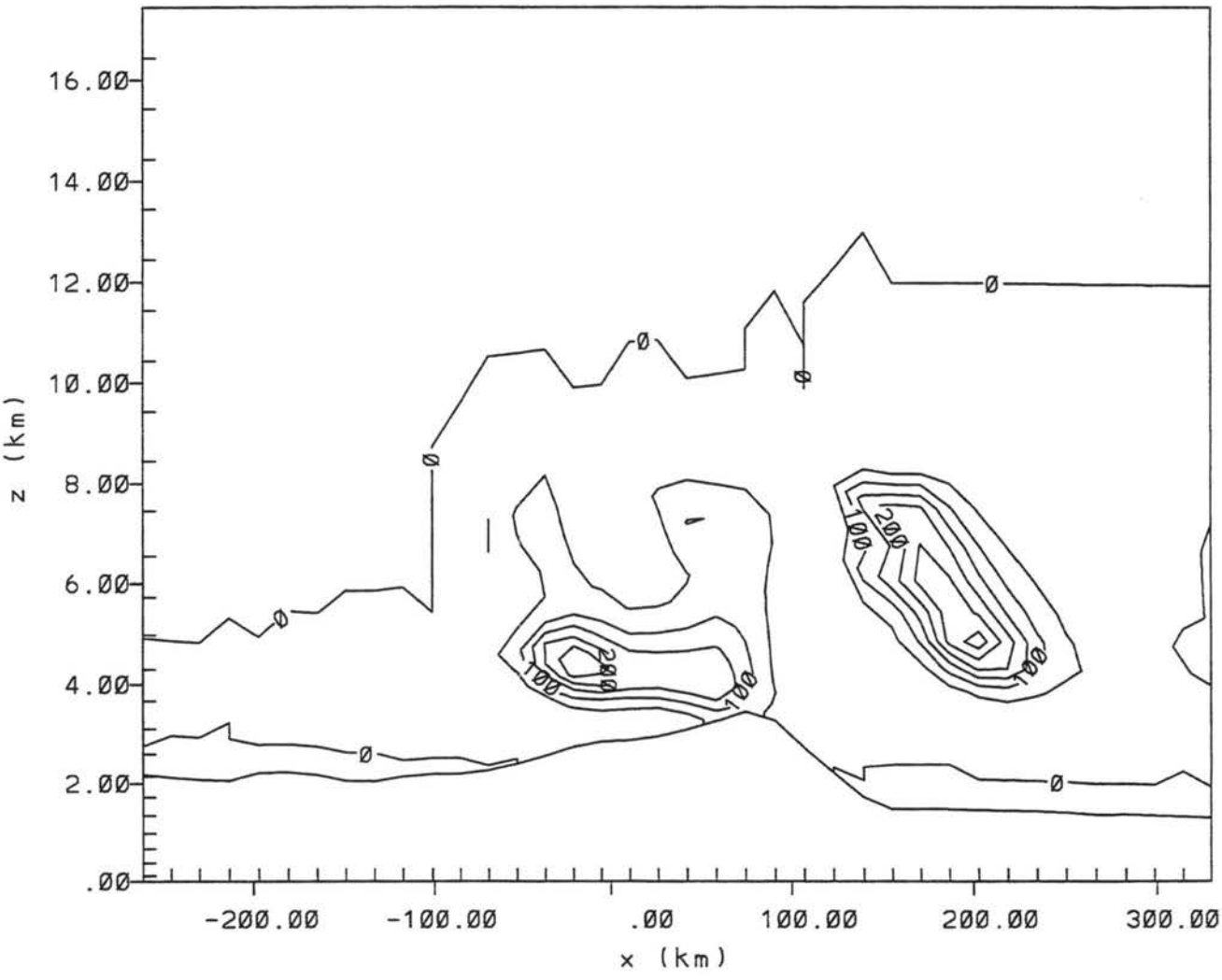

Figure 5.11: Cross section of aggregate mixing ratio through Grid 2, April 25 24-hr forecast, for microphysics model. Latitude is that of Fort Collins. East is at right. Maximum value is 0.30 g kg^{-1}.

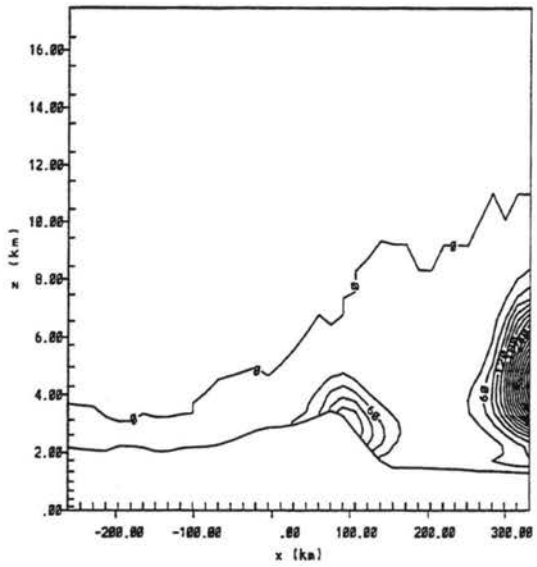

Figure 5.12: Same as Figure 5.11, but for April 26 12-hr forecast. Maximum value is 0.48 g kg^{-1}.

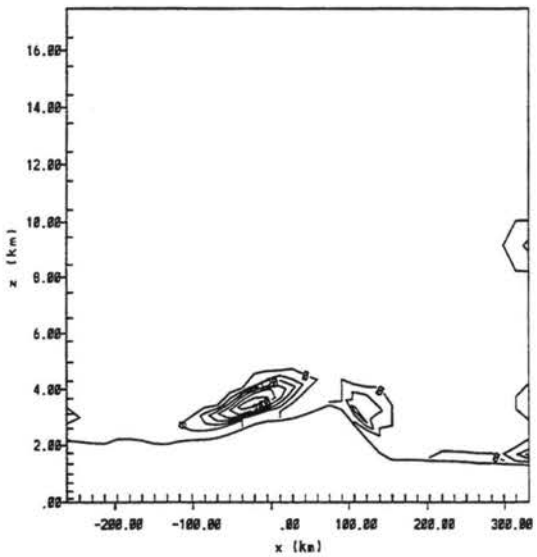

Figure 5.13: Cross section of cloud water mixing ratio through Grid 2, April 26 12-hr forecast, for microphysics model. Maximum value is 0.32 g kg^{-1}.

the following 24-hour period. In fact, some sites recorded some of the largest precipitation totals observed in the study (see Table 5.11). This, coupled with the large lapse rates seen in the Denver sounding from 0000 GMT April 26, which drops from 16 to -22°C in the four kilometers from the surface to 500 mb (Figure 5.14), strongly implies that much of the snow was convective. The convective parameterization used with the model actually showed, correctly, some convective precipitation on the eastern plains (Figure 5.15), though the amount of precipitation (up to 20.8 mm at DIA) could not be replicated. However, no convective precipitation was produced by the model in the mountains. Probably any effectiveness of a convective scheme at the quite coarse 16-km scale would be completely negated in the mountains, where terrain features on the roughly 2-km scale of the convective elements would not be available for cloud-forcing. Clearly this would be a problem with any forecast model, regardless of precipitation scheme, without kilometer-scale resolution or a cumulus parameterization appropriate to the grid-spacing used.

To see if convection might be an important factor, Table 5.12 was made, where the 700 mb and 500 mb temperatures at Denver were taken of the 0000 GMT model initialization files. These were differenced to provide an indication of atmospheric instability; a standard atmospheric lapse rate of 6.5 K km^{-1} would provide a difference of about 16° C between the two levels, whereas a difference of 25° C would be a dry adiabatic lapse rate. Also in the table is the ratio of observed to microphysics-predicted precipitation for the SNOTEL verification period which includes the analysis time (e.g., the April 9 SNOTEL period, from midnight April 9 to midnight April 10, MDT, includes the 0000 GMT April 10 initialization). A definite correlation is found in the table between steep lapse rates and underprediction of precipitation. All the days in which microphysics predicted better than about 46% of the observed precipitation featured temperature differences less than 20° C, and most of the poor performance days possessed the greater temperature differences. It would appear, then, that prediction of total storm precipitation for the current forecast model is most favorable during non-convective events.

The underprediction of mountain snowfall on low stability days could be due to one of two factors: either the convective parameterization tends to underforecast in the moun-

ID	Name	Precipitation (4/25/95)
41	APISHAPA SNOTEL	0
49	BUTTE SNOTEL	10
51	COPELAND LAKE SNOTEL	20
55	CULEBRA #2 SNOTEL	3
57	DEADMAN SNOTEL	25
58	DRY LAKE SNOTEL	10
60	ELK RIVER SNOTEL	3
61	SNOTEL	15
63	HOOSIER PASS SNOTEL	13
64	INDEPENDENCE PASS SNOTEL	10
65	IDARADO SNOTEL	5
66	JOE WRIGHT SNOTEL	28
67	KILN SNOTEL	10
68	LAKE ELDORA SNOTEL	18
69	LIZARD HEAD PASS SNOTEL	0
79	OVERLAND RSVR SNOTEL	5
80	PHANTOM VALLEY SNOTEL	13
81	PARK CONE SNOTEL	0
82	PORPHYRY CREEK SNOTEL	13
83	PARK RSVR SNOTEL	5
86	RED MOUNTAIN PASS SNOTEL	5
87	ROACH SNOTEL	28
90	SLUMGULLION PASS SNOTEL	0
94	SUMMIT RANCH SNOTEL	10
97	TOWER SNOTEL	18
98	UPPER RIO GRANDE SNOTEL	3
99	UPPER SAN JUAN SNOTEL	0
100	UNIVERSITY CAMP SNOTEL	18
101	VALLECITO SNOTEL	3
102	VAIL MTN SNOTEL	15
104	WILLOW CREEK PASS SNOTEL	18
106	WHISKEY CREEK SNOTEL	0

Table 5.11: Observed precipitation at SNOTEL sites, from midnight April 25 to midnight April 26, MDT. Values are in mm of precipitated water. Uncertainty in measurements is about 3 mm (0.1 in.).

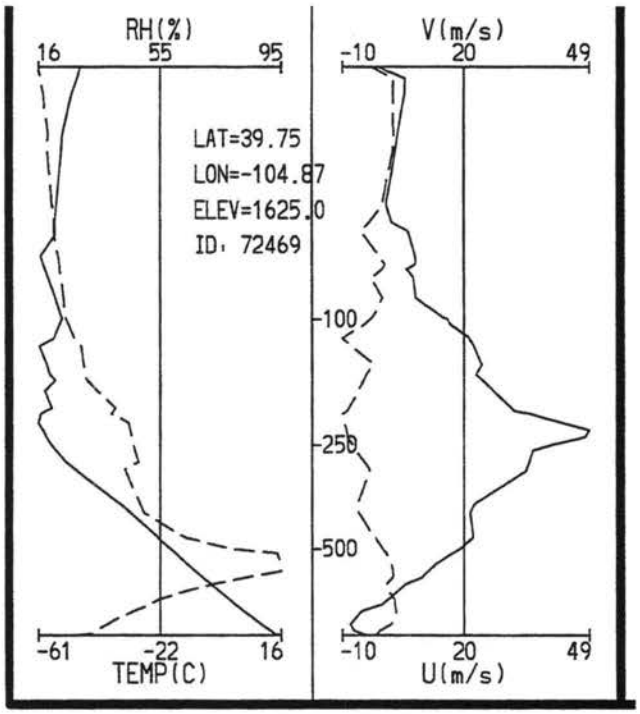

Figure 5.14: Lapse rate at Denver International Airport for 0000 GMT 1995 April 26. Vertical axis is pressure in millibars. Left plot is for temperature (solid line) and relative humidity (dashed line) while right plot is for u (solid line) and v (dashed line) velocity components.

Analysis Time	$T_{700} - T_{500}$	p_{obs}/p_{micro}
0000 GMT April 27	15	0.93
0000 GMT April 22	16	1.02
0000 GMT April 18	17	1.08
0000 GMT April 23	18	1.49
0000 GMT April 17	17	1.54
0000 GMT April 11	16	1.59
0000 GMT April 10	17	2.17
0000 GMT April 16	21	3.14
0000 GMT April 24	21	3.66
0000 GMT April 30	16	4.00
0000 GMT April 19	18	4.00
0000 GMT April 26	21	4.08
0000 GMT April 25	23	9.00
0000 GMT April 12	15	9.67
0000 GMT April 9	24	10.45

Table 5.12: Difference between 700 mb temperatures and 500 mb temperatures at Denver from model initialization, in Celsius. Third column is ratio of observed SNOTEL precipitation for major events to microphysics-predicted precipitation for the daily period including the initialization time shown.

tains, or the activation of the parameterization elsewhere in the fine grid is having a negative impact on mountain precipitation, either by removing water or inducing subsidence. The comparison of a convective versus non-convective model run done in Chapter 4 for the April 23 would suggest that at least the second is happening. An additional re-simulation was performed on the April 25 day without the convective scheme, since the atmosphere was rather unstable at both the starting and finishing times of the simulation. In this case it appears that the convective activity along the urban corridor completely inhibits microphysics precipitation over the mountains (compare Figures 5.15 and 5.16), which is correlated to a shift in vertical velocity from largely upwards to downwards over the mountain ridge (Figures 5.17 and 5.18). So it can be concluded that mountain accumulations are generally suppressed by the convective scheme when upper-level instability occurs. However, Figure 5.16 implies that even when the scheme is turned off, precipitation is still underestimated in the mountains.

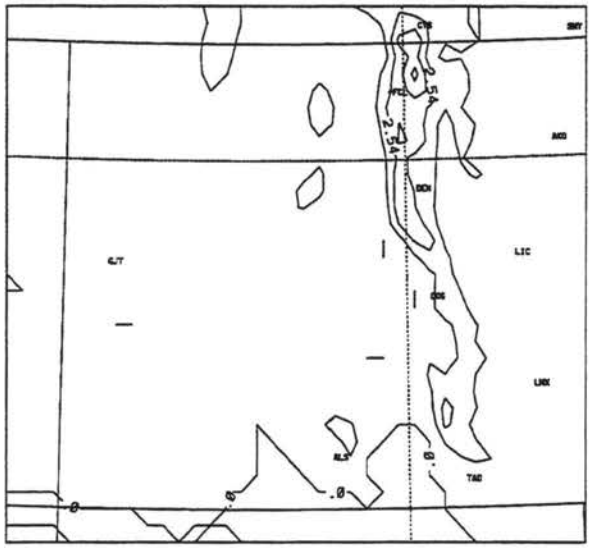

Figure 5.15: Accumulated precipitation, April 25 forecast, microphysics model.

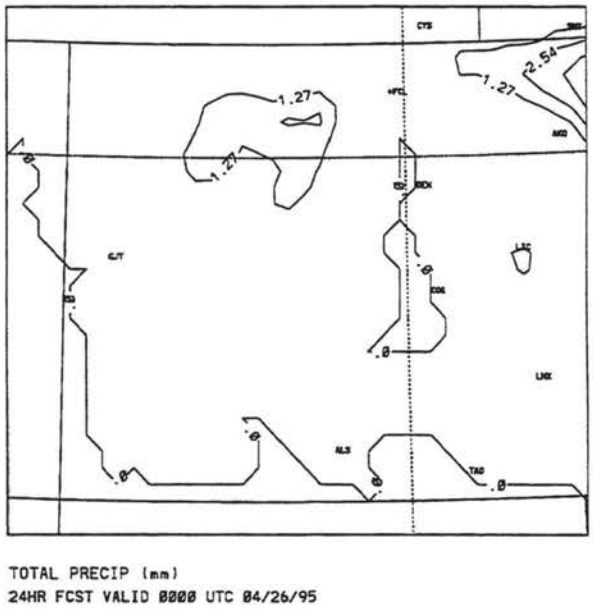

Figure 5.16: Same as 5.15, but without convective scheme.

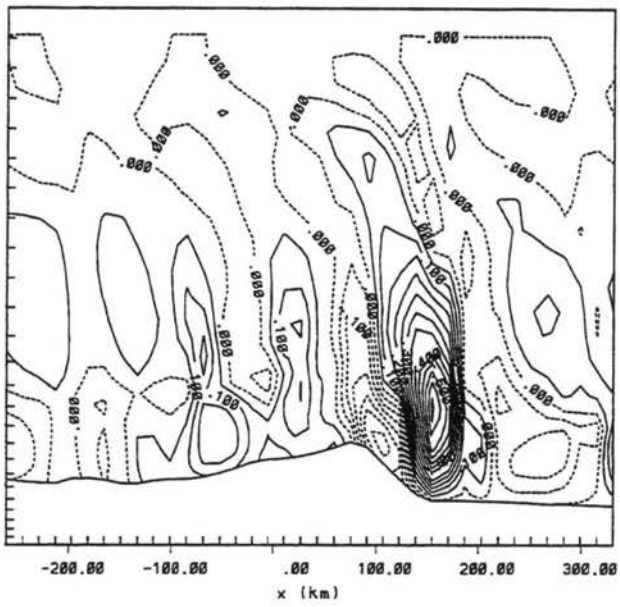

Figure 5.17: Cross section of vertical velocity on fine grid, April 25, with convective scheme. Latitude is that of Fort Collins. Contour interval is 5 cm s^{-1}. Maximum value is 0.65 m s^{-1}

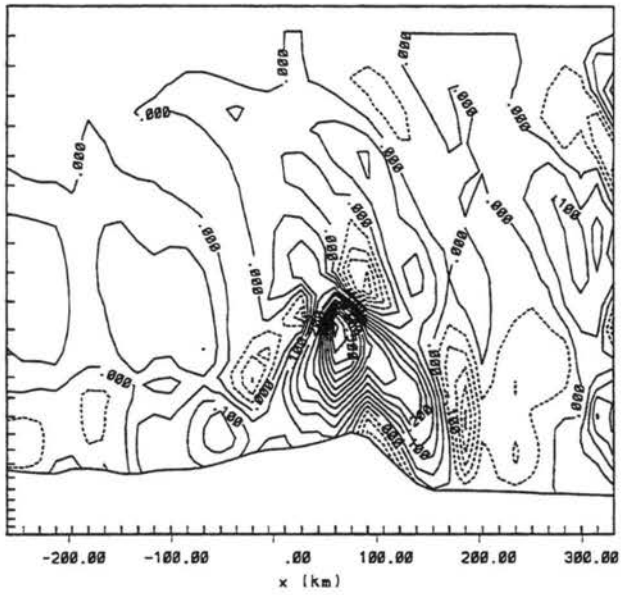

Figure 5.18: Same as Figure 5.17, except without convective scheme. Maximum value is 0.65 m s^{-1}

Some hope for improving the snow forecasting ability at the SNOTEL sites was found late in this study when an error was found in the sedimentation scheme of the model. The error had the effect of decreasing the amount of surface precipitation from the higher vertical levels when the grid is stretched vertically. When a fixed version of the forecast model was used to re-simulate the April 25 case (with convection turned off), the forecast precipitation field (Figure 5.19) showed a marked improvement. Clearly this error could help explain the previously noted difficulties with hydrometeors reaching the ground. It is not clear yet why or even if the mountains would be more heavily influenced by this phenomenon, though it could be that over the long fall trajectories over the plains, where additionally there is more of a chance for the aggregates to reach a height below the lifting condensation level, the hydrometeors often would be sublimated by the model anyway before they reach the ground. So only over the mountains would a numerical depletion of this category be noticed.

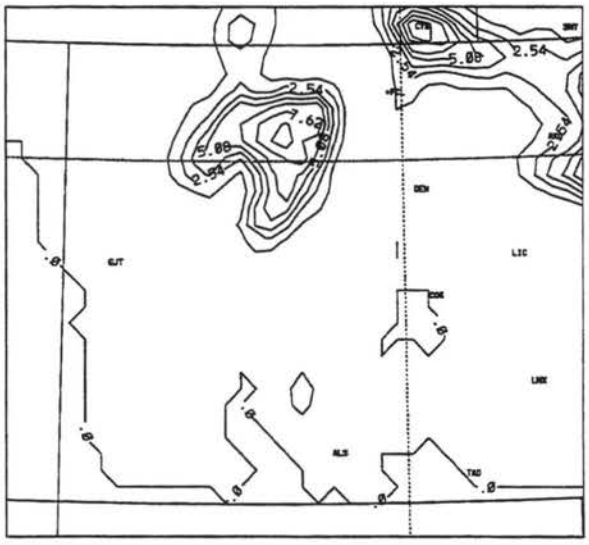

Figure 5.19: Same as 5.16, but with new sedimentation.

5.9 Finer Resolution Runs – Statistics

For April 19, a statistical analysis can be performed on the 8-km model run with bulk microphysics (performed prior to the sedimentation modification) using the climatological

station data. The finer-scale model run precipitation totals replaced the values for the corresponding coarser-scale model run, and as before a daily precipitation record was formed taking into account the verification time of each station. The statistics for April 19 at each station were combined, and the results are shown in Table 5.13, along with the results from the 16-km run. Much of what is shown in the table was alluded to earlier. The finer-scale model does a better job at forecasting the total amount of precipitation, and has a variability (σ_{model}) closer to the natural variability. However, the rms becomes worse. The bias scores all increase, which is an improvement for all except the lowest threshold. The Heidke skill scores all become worse. In general, though, for all skill scores the relative performance of the finer-scale model increases as the threshold increases. This implies that the main improvement introduced by the finer grid is forecasting the size and degree of the most extreme events for a given case, which can alleviate underprediction of precipitation but still does not produce any noticeable improvement in the rms score. However, it should be noted that the convective parameterization was used for this run, and the influence of this scheme was discussed in previous section. It is possible that the effect of finer-resolved topography is to increase the possible moisture convergence possible, which would induce greater vertical velocities, and since the cumulus scheme seems to produce narrow, well-defined regions of vertical velocity, the result would probably be increased precipitated water for the regions receiving the most precipitation.

For the three-grid run on April 23, a similar analysis between the standard microphysics run, the convection-free microphysics run, and the three grid (10-km and 2-km fine grids) run was performed (Table 5.14), only this time the SNOTEL stations were used. The nearest Grid 3 grid point was used to compute the precipitation at each station, unless the station was not located on the finest grid, in which case the nearest Grid 2 grid point was used. Comparing the two runs which differ only in grid spacing (the last two columns) reveals that the three-grid run only improves the statistical scores for the lower thresholds, opposite to the tendency noted for the April 23 case, and the finer-grid run actually produces less total SNOTEL precipitation than the coarser-grid run. However, the consequence of turning off the convective scheme is a significant improvement in the precipitation forecasts for the

Statistic	16-km	8-km
p_{obs}/p_{model}	1.86	1.33
$\mathrm{rms}/\sigma_{obs}$	0.96	1.07
$\sigma_{model}/\sigma_{obs}$	0.48	0.67
Bias, 0.254 mm	1.06	1.25
Threat, 0.254 mm	0.82	0.75
Heidke, 0.254 mm	0.57	0.11
Bias, 2.54 mm	0.81	0.90
Threat, 2.54 mm	0.47	0.39
Heidke, 2.54 mm	0.32	0.13
Bias, 6.35 mm	0.57	0.84
Threat, 6.35 mm	0.28	0.30
Heidke, 6.35 mm	0.29	0.27
Bias, 12.7 mm	0.04	0.48
Threat, 12.7 mm	0.04	0.06
Heidke, 12.7 mm	0.07	-0.05

Table 5.13: Comparative statistics, 16-km and 8-km microphysics models, for April 19.

mountains. Table 5.15 applies to the same set of model simulations, but data for the stations that are located within Grid 3 of the three-grid simulation are combined, and are compared with the data for the stations not located on Grid 3. The table shows that stations in the 2-km grid spacing region did show better statistics than the stations located only on the 10-km grid, though still not as good statistically as the corresponding 16-km run without convective parameterization. Since the nesting ratio from Grid 1 to Grid 2 in the three grid run was relatively large the possibility exists that numerical noise in the three-grid run could be responsible for producing subsidence which hinders precipitation development on the finer grids. Future studies of increased model resolution on precipitation forecasting should contain enough grids to ensure that excessive reflection does not occur at model boundaries. Some artificial features in the map-view plots of the vertical velocity field could be seen, but they did not clearly correspond to details in the precipitation field (see Figure 4.29). Instead 'statistical noise' seems to be the main cause of the poor model results – when both model and observational data exhibit fine scale structure, their combined variability can produce larger quantitative model errors than those of models with smaller spatial variability, even if both model versions show a similar spatial displacement of features from the 'true' location.

It also could be that the important scale for the orographic events described in this thesis is on the order of a kilometer and that a reduction of scale to even 10 km adds little to the performance of a model. Additional studies on the bulk microphysics performance in this intermediate range, based from this study, should not include a cumulus parameterization designed for larger-scale models because the scheme can interfere with the bulk resolved microphysics, even when convection is expected to occur over the mountains on the particular day. The impact of the error in the sedimentation algorithm also needs to be examined.

Statistic	16-km	no conv.	three-grid
p_{obs}/p_{model}	3.66	2.19	3.61
rms/σ_{obs}	1.26	1.24	1.26
$\sigma_{model}/\sigma_{obs}$	0.26	0.68	0.38
Bias, 0.254 mm	1.07	1.07	1.03
Threat, 0.254 mm	0.94	0.94	0.97
Heidke, 0.254 mm	0.00	0.00	0.65
Bias, 2.54 mm	0.33	0.33	0.30
Threat, 2.54 mm	0.00	0.29	0.26
Heidke, 2.54 mm	-0.03	-0.04	-0.04
Bias, 6.35 mm	0.12	0.35	0.24
Threat, 6.35 mm	0.06	0.28	0.11
Heidke, 6.35 mm	-0.01	0.22	-0.01
Bias, 12.7 mm	0.00	0.50	0.12
Threat, 12.7 mm	0.00	0.20	0.00
Heidke, 12.7 mm	0.00	0.20	-0.06

Table 5.14: Comparative statistics, 16-km, 16-km without convection, and three-grid microphysics models, for April 23.

	On Grid 3			Not on Grid 3		
Statistic	16-km	no conv.	three-grid	16-km	no conv.	three-grid
p_{obs}/p_{model}	2.73	1.25	1.97	4.67	4.20	7.63
rms/σ_{obs}	1.14	1.16	1.10	1.50	1.45	1.59
$\sigma_{model}/\sigma_{obs}$	0.14	0.49	0.31	0.36	0.64	0.18

Table 5.15: Same as 5.14, but comparing stations located on Grid 3 of the three grid run to stations not on Grid 3.

5.10 Summary

In summary, we can conclude:

1) In terms of rms error, neither model shows a significant advantage over the other, nor much forecasting skill, except for the April 10 case.

2) Both models predict about 85% of observed precipitation amounts when averaged over all the climatological stations, though the actual amount varies from case to case. For the SNOTEL stations, located in regions susceptible to heavy snowfall, the percentage decreases to 50% for the microphysics run and 38% for the dump-bucket model.

3) In terms of skill scores, the microphysics model generally shows superior bias and Heidke skill scores, implying a greater skill at quantifying areas of precipitation.

4) In terms of the MRBP correlation coefficient ρ, the dump-bucket model is superior for the climatological stations while the microphysics model does better for the SNOTEL stations. Overall, though, both models show better statistics for the climatological stations. Microphysics seems to show the best results in mountainous regions and immediately adjacent sloping terrain. It does least well on high plateaus or lowlands far from mountainous regions.

5) Microphysics underprediction at the SNOTEL sites and in the lee of mountain crests could be due to a combination of several factors: the loss of the aggregate category due to sublimation, the presence of strong convective snow events at the SNOTELs, and the error in the sedimentation scheme. These explanations could be interconnected: there is some evidence that finer-resolution model runs increase mountain precipitation by increasing uplift speeds, which increases the extent of cloud water, which allows more riming and more aggregates to reach the ground.

6) The Kuo cumulus parameterization scheme may have some qualitative value in forecasting convection on the eastern plains of Colorado, but generally is not even qualitatively correct over the mountains, where in fact there is evidence that the convective scheme hinders the formation of precipitation by the bulk microphysics.

7) The finer-resolution simulations performed for this study do not show statistical improvement over the coarser-scale forecasts. It is possible that this is due to the grid spacing differential between Grid 1 and Grid 2, since stations located within Grid 3 did show improvements in forecasting skill over stations located only within Grid 2. It is also possible, though that in this range of grid spacing (about 10 km), decreasing model resolution does not significantly increase forecasting skill and in fact statistical noise decreases it. Though the maximum precipitation amounts were increased with finer resolution (see Chapter 4), their areal coverage was so small that the model-produced precipitation for the network of SNOTEL stations actually decreased from the two-grid to the three-grid model run.

Chapter 6

SUMMARY AND CONCLUSIONS

6.1 Summary

The purpose of this study was to produce daily forecasts in real-time using RAMS with full bulk microphysics, and to assess the effectiveness of the microphysics in QPF during the winter season by comparing it to observations. Because of increased computing speed and optimizations made in the microphysics algorithms of Version 3b of RAMS, real-time forecasts using microphysics have been produced since the fall of 1995. The microphysics forecasts have demonstrated an ability to predict realistic areas and amounts of precipitation.

To assess the performance of the microphysics option, forecasts were produced for the month of April 1995 using both a dump-bucket precipitation scheme and bulk microphysics. A set of 167 climatological stations and 32 SNOTEL stations were used as an observational verification. Qualitative examination of the forecast precipitation amounts suggest that the microphysics is usually the better model at forecasting the areal extent of smaller amounts of precipitation and the maximum amount of precipitation that can be expected from a given storm. However, the microphysics model has more trouble at locating the precise geographical locations of these features.

Quantitatively, a combination of case-by-case root-mean-square errors, skill scores, and MRBP statistics were used to analyze model performance against observations. It was found that both microphysics and the dump-bucket scheme showed similar skill and that the most important factor in model performance is the particular case being examined. According to MRBP analysis, both models show precipitation forecast skill comparable to that of other model studies for the climate stations, but less performance for the SNOTEL

stations. The dump-bucket model is slightly better at forecasting for the climate station network overall, whereas the microphysics performs slightly better for the SNOTEL stations. The microphysics also improves forecasting skill for much of the upper Platte River valley, southeastern Colorado, and regions near the Continental Divide, while skill is decreased in the Rio Grande valley, the lower Platte River Valley, and the Palmer Divide region. Neither model does well in high mountain valleys and the western plateau region. Terrain slope seems to be positively correlated to the relative skill of the microphysics model.

In terms of total precipitation produced by a given storm, both models did comparably well at the climatological stations, underpredicting on average by about 15%; at the SNOTEL stations, however, the microphysics performs substantially better. Both schemes still underpredict total accumulations at the SNOTEL sites, however. The dump-bucket scheme predicts 38% of the total precipitation at these stations; the microphysics predicts 50% of the total.

The existing tendency of the microphysics scheme to underpredict precipitation in the mountains was in part attributed to the failure of the forecast model to properly represent convective winter precipitation events caused by high instabilities aloft. Specifically, the model does not seem to be able to duplicate the rapid snow accumulations that can characterize these events. Furthermore, the convective scheme that is used in the forecast model tends to induce generally subsident wind fields over the SNOTEL regions, which can hinder the bulk microphysics' ability to produce precipitation there. Another factor in the underprediction of mountainous precipitation could be the depletion of aggregate category mass to sublimation, since the contribution of aggregates to the total precipitation tends to increase with proximity to a mountain crest. A recently found coding error in the forecast model's sedimentation scheme is also probably a quite important factor in the model's statistical scores.

Tests of the influence of finer-resolution models were inconclusive because of the nature of the simulations. Qualitatively, many if not most precipitation features were better resolved when finer grid spacing was used, but because the spatial variability of these features

is so much greater than the coverage of the domain with SNOTEL sites, a quantitative demonstration of enhanced model performance is very difficult to achieve.

6.2 Conclusion

Because of the similarities of performance between the two models, and the increased computational cost of the microphysics option of RAMS, if the duration of the forecast model run is severely restrained, then the dump-bucket scheme may be considered for such forecasts. Some account should be made of the fact that the precipitation efficiency needs to be increased at the higher elevations. One the other hand, use of the microphysics option can provide better estimates of yes/no forecasts of measurable precipitation and the maximum amount of precipitation expected in mountainous regions. The microphysics also allows the specific type of hydrometeor to be identified, as well as the concentration and amounts of hydrometeors at the levels above ground, options which are not available in a dump-bucket parameterization.

6.3 Future Work

The use of a forecast version of RAMS which can operate on a parallel cluster of workstations appears to be imminent. Such a model would allow much faster computational speeds. If such speeds are used to decrease the model grid spacing, a better assessment of model's forecasting ability at higher resolutions could be performed. At this point, though, it appear that grid spacings might have to be less than 2 km, unless the precipitation is predominately stratiform.

Certainly simulations using the new sedimentation scheme need to be performed. Further increases in the mean sizes of the snow and aggregate categories could be performed, although the model does not seem to be very sensitive to this parameter. However, the use of a two-moment microphysics scheme (one which predicts both the mixing ratio and number concentrations of water species; see Meyers (1995)) would allow a more accurate representation of the sizes of all the hydrometeors (since both their bulk mass and total

concentration would be known) and hence should provide a better prediction of their growth and dissipation.

A lot of the problems encountered in this study could be traced to the use of a convective parameterization at a scale smaller than the scheme was designed for. If a cumulus parameterization could be found appropriate to scales from approximately one to twenty kilometers, such a scheme could be tested in the forecast model to determine if it can better capture the more unstable mountain precipitation events. A cumulus scheme developed by Rafkin (1996) will be tested in the forecast model in the near future.

Finally, it should be noted here that ultimately precipitation forecasts are dependent on the forecasts of other meteorological variables such as wind and moisture, and so a precipitation forecast model is (at best!) only as good as the wind and moisture forecasting schemes. The inclusion of a more sophisticated radiation scheme (both shortwave and longwave) in the forecast model would help improve the temperature forecasts. The inclusion of variable soil moisture and snow coverage would affect the soil heat capacity and albedo, respectively; these influence the temperature and moisture fields, which influence the location of precipitation, which in turn changes the previous soil moisture and albedo. Thus another daily data assimilation system would have to be produced. Even with the current data assimilation system, improvements could be made by using a finer-scale initialization dataset such as the Meso-Eta model; and by using a more continuous data ingest cycle, instead of requiring that all the data for the entire forecast be present at the time of initialization.

References

Anthes, R.A., 1983: Regional models of the atmosphere in middle latitudes. *Mon. Wea. Rev.*, **111**, 1306-1335.

Anthes, R.A., and T.T. Warner, 1978: Development of hydrodynamic models suitable for air pollution and other mesometeorological studies. *Mon. Wea. Rev.*, **196**, 1045-1078.

Anthes, R.A., E.-Y. Hsie, and Y.-H. Kuo, 1987: Description of the Penn State/NCAR Mesoscale Model Version 4 (MM4). NCAR tech. note NCAR/TN-282+STR, 66 pp.

Anthes, R.A., Y.-H. Kuo, E.-Y. Hsie, S. Low-Nam, and T.W. Bettge, 1989: Estimation of skill and uncertainty in regional numerical models. *Q. J. R. Meteorol. Soc.*, **115**, 763-806.

Arakawa, A. and V.R. Lamb, 1981: A potential enstrophy and energy conserving scheme for the shallow water equations. *Mon. Wea. Rev.*, **109**, 18-36.

Barros, A.P. and D.P. Lettenmaier, 1994: Dynamic Modeling of Orographically Induced Precipitation. *Rev. Geophys.*, **32**(3), 265-284.

Beitler, B.A., 1994: Mesoscale numerical prediction of Colorado snowfall and winds. M.S. Thesis, Atmos. Sci. Paper No. 556, Colorado State University, Dept. of Atmospheric Science, Fort Collins, CO 80523, 84 pp.

Benjamin, S.G., T.L. Smith, P.A. Miller, D. Kim, T.W. Schlatter, and R. Bleck, 1991: Recent improvements in the MAPS isentropic-sigma data assimilation system. Preprints, *Ninth Conf. on Numerical Weather Prediction*, Denver, CO, Amer. Meteor. Soc., 118-121.

Bergeron, T., 1965: On the low-level redistribution of atmospheric water caused by orography. *Suppl., Proc. Int. Conf. Cloud Phys.*, Tokyo, Japan, IAMAP/IUGG and WMO, 96-100.

Bleck, R. and S.G. Benjamin, 1993: Regional weather prediction with a model combining terrain-following and isentropic coordinates. Part I: Model Description. *Mon. Wea. Rev.*, **121**, 1770-1785.

Browning, K.A., 1983: Air motion and precipitation growth in a major snowstorm. *Q. J. R. Meteorol. Soc.*, **109**, 225-242.

Chen, C. and W.R. Cotton, 1983: A one-dimensional simulation of the stratocumulus-capped mixed layer. *Boundary-Layer Meteor.*, **25**, 289-321.

Choularton, T.W., and S.J. Perry, 1986: A model of the orographic enhancement of snowfall by the seeder-feeder mechanism. *Q. J. R. Meteorol. Soc.*, **112**, 335-345.

Clark, T.L, 1979: Numerical simulations with a three-dimensional model cloud model: Lateral boundary condition experiments and multicellular severe storm simulations. *J. Atmos. Sci.*, **36**, 2191-2215.

Clark, T.L., and R.D. Farley, 1984: Severe downslope windstorm calculations in two and three spatial dimensions using anelastic interactive grid nesting: A possible mechanism for gustiness. *J. Atmos. Sci.*, **41**, 329-350.

Cotton, W.R. and R.A. Anthes, 1989: *Storm and cloud dynamics.* Academic Press, 883 pp.

Cotton, W.R., G. Thompson, and P.W. Mielke, 1994: Real-time mesoscale prediction on workstations. *Bull. Amer. Meteor. Soc.*, **75**(3), 349-362.

Cotton, W.R., J.F. Weaver, and B.A. Beitler, 1995: An unusual summertime downslope wind event in Fort Collins, Colorado, on 3 July 1993. *Wea. Forecasting*, **10**(4), 786-797.

Cullen, M.J.P., 1993: The Unified Forecast/Climate Model. *Meteorol. Mag.*, **122**, 81-94.

Dickinson, R.E., A. Henderson-Sellers, P.J. Kennedy, and M.F. Wilson, 1986: Biosphere-atmosphere transfer scheme for the NCAR community climate model. Technical Report NCAR/TN-275+STR, NCAR, Boulder, 69 pp.

Doesken, N. and G. Schaefer, 1987: The contribution of SNOTEL precipitation measurements to climate analysis, monitoring, and research in Colorado. *Proc. Western Snow Conference, 55th annual meeting*, Vancouver, B.C., Canada, 20-30.

Doswell, C.A., III, R. Davies-Jones, and D.K. Leller, 1990: On summary measures of skill in rare event forecasting based on contingency tables. *Wea. Forecasting*, **5**, 576-585.

Dudhia, J.,1989: Numerical study of convection observed during the Winter Monsoon Experiment using a mesoscale two-dimensional model. *J. Atmos. Sci.*, **46**, 3077-3107.

Dudhia, J.,1993: A nonhydrostatic version of the Penn State/NCAR mesoscale model. *Mon. Wea. Rev.*, **121**, 1493-1513.

Flatau, P.J., G.J. Tripoli, J. Verlinde, W.R. Cotton, 1989: The CSU-RAMS cloud microphysical module: General theory and code documentation. Atmos. Sci. Paper No. 451, Colorado State University, Dept. of Atmospheric Science, Fort Collins, CO 80523, 88 pp.

Gal-Chen, T. and R.C.J. Somerville, 1975: On the use of a coordinate transformation for the solution of the Navier-Stokes equations. *J. Comput. Phys.*, **17**, 209-228.

Gayno, G.A., N.L. Seaman, A.M. Lario, and D.R. Stauffer, 1994: Forecasting visibility using a 1.5-order closure boundary layer scheme in a 12-km non-hydrostatic model. Preprints, *Tenth Conf. on Numerical Weather Prediction*, Portland, OR, Amer. Meteor. Soc., 18-23.

Glahn, H.R., 1985: Yes, precipitation forecasts have improved. *Bull. Amer. Meteor. Soc.*, **66**, 820-830.

Golding, B.W., 1987: The U.K. Meteorological Office mesoscale model. *Boundary-Layer Meteor.*, **41**, 97-107.

Golding, B.W., 1992: An efficient non-hydrostatic forecast model. *Meteorol. Atmos. Phys.*, **50**, 89-103.

Harrington, J.Y., M.P. Meyers, R.L. Walko, and W.R. Cotton, 1995: Parameterization of ice crystal conversion processes due to vapor deposition for mesoscale models using double-moment basis functions. Part I: Basic formulation and parcel model results. *J. Atmos. Sci.*, **52**, 4344-4366.

Hill, F.F., K.A. Browning, and M.J. Bader, 1981: Radar and raingauge observations of orographic rain over south Wales. *Q. J. R. Meteorol. Soc.*, **107**, 643-670.

Hobbs, P.V., E.C. Easter, and A.B. Fraser: A theoretical study of the flow of air and fallout of solid precipitation over mountainous terrain, Part II: Microphysics, 1973. *J. Atmos. Sci.*, **30**, 813-823.

Hoke, J.E., N.A. Phillips, G.J. DiMego, J.T. Tuccillo, and J.G. Sela, 1989: The Regional Analysis and Forecast System of the National Meteorological Center. *Wea. Forecasting*, **4**, 323-334.

Hsie, E.-Y., R.A. Anthes, and D. Keyser, 1984: Numerical simulation of frontogenesis in a moist atmosphere. *J. Atmos. Sci.*, **41**, 2581-2594.

Imbard, M., R. Juvanon du Vachat, A. Joly, Y. Durand, A. Craplet, J.- F. Geleyn, J.M. Audoin, N. Marie, and J.M. Pairin, 1987: The PERIDOT fine-mesh numerical weather prediction system. Description, evaluation, and experiments. Preprints, *NWP Symp.*, Tokyo, Japan, WMO/IUGG, 455-465.

Junker, N.W., J.E. Hoke, and R. H. Grumm, 1989: Performance of NMC's regional models. *Wea. Forecasting*, **4**, 368-390.

Kalb, M.W., 1985: Results from a limited area mesoscale numerical simulation for 10 April 1979. *Mon. Wea. Rev.*, **113**, 1644-1662.

Kaplan, M.L., J.W. Zack, V.C. Wong, and J.J. Tuccillo, 1982: Initial results from a mesoscale atmospheric simulation system and comparisons with the AVE-SESAME I data set. *Mon. Wea. Rev.*, **110**, 1564-1590.

Keyser, D., and R.A. Anthes, 1977: The applicability of a mixed-layer model of the planetary boundary layer to real-data forecasting. *Mon. Wea. Rev.*, **105**, 1351-1371.

Klemp, J.B. and R.B. Wilhelmson, 1978: Simulations of right- and left-moving storms produced through storm-splitting. *J. Atmos. Sci.*, **35**, 1097-1110.

Koch, S.E., 1985: Ability of a regional-scale model to predict the genesis of intense mesoscale convective systems. *Mon. Wea. Rev.*, **113**, 1693-1713.

Lee, T.J., 1992: The impact of vegetation on the atmospheric boundary layer and convective storms. Ph.D. dissertation, Atmos. Sci. Paper No. 509, Colorado State University, Dept. of Atmospheric Science, Fort Collins, CO 80523, 137 pp.

Mahrer, Y., and R.A. Pielke, 1977: A numerical study of the airflow over irregular terrain. *Beitr. Phys. Atmos.*, **50**, 98-113.

Marshall, J.S., and W.M. Palmer, 1948: The distribution of raindrops with size. *J. Meteorol.*, **5**, 165-166.

McMillan, G.D., 1981: SNOTEL: A management tool for the future. *Proc. Western Snow Conference, 49th annual meeting*, St. George, UT, 116-119.

Mellor, G.L., and T. Yamada, 1974: A hierarchy of turbulence closure models for the planetary boudnary layer. *J. Atmos. Sci.*, **31**, 1791-1806.

Mesinger, F., and R.E. Treadon, 1995: "Horizontal" reduction of pressure to sea level: Comparison against the NMC's Shuell method. *Mon. Wea. Rev.*, **123**, 59-68.

Mesinger, F., Z.I. Janjić, S. Ničković, D. Gavrilov, and D. Deaven, 1988: The step mountain coordinate: Model description and performance for cases of Alpine lee cyclogenesis and for a case of an Appalachian redevelopment. *Mon. Wea. Rev.*, **116**, 1493-1518.

Meyers, M.P., 1995: The impact of a two-moment cloud model on the microphysical structure of two precipitation events. Ph.D. dissertation, Atmos. Sci. Paper No. 575, Colorado State University, Dept. of Atmospheric Science, Fort Collins, CO 80523, 165 pp.

Meyers, M.P. and W.R. Cotton, 1992: A wintertime orographic quantitative precipitation forecast with an explicit cloud model. Part I: Two-dimensional sensitivity experiments. *J. Appl. Met.*, **31**, 26-50.

Mielke, P.W., 1984: Meteorological applications of permutation techniques based on distance functions. *Handbook of statistics, vol. 4*, P.R. Krishnaiah and P.K. Sen, Eds., Elsevier, 813-830.

Mielke, P.W., 1985: Geometric concerns pertaining to application of statistical tests in the atmospheric sciences. *J. Atmos. Sci.*, 42, 1209-1212.

Mielke, P.W., 1991: The application of multivariate permutation methods based on distance functions in the earth sciences. *Earth-Sci. Rev.*, **31**, 55-71.

National Oceanographic and Atmospheric Administration (NOAA): *Climatological Data*, **100**(4), available from: National Climatic Data Center (NCDC), Asheville, North Carolina 28801.

Neiburger, M., 1949: Reflection, absorption, and transmission of insolation by stratus cloud. *J. Appl. Meteor.*, **6**, 98-104.

Nicholls, M.E., R.A. Pielke, and W.R. Cotton, 1991: A two-dimensional numerical investigation of the interaction between sea breezes and deep convection over the Florida peninsula. *Mon. Wea. Rev.*, **119**, 298-323.

Orlanski, I., 1975: A rational subdivision of scales for atmospheric process. *Bull. Amer. Meteor. Soc.*, 56, 527-530.

Perkey, D.J., and C.W. Kreitzberg, 1976: A time-dependent lateral boundary scheme for limited-area primitive equation models. *Mon. Wea. Rev.*, **104**, 744-755.

Pielke, R.A., 1984: *Mesoscale meteorological modeling.* Academic Press, 612 pp.

Pielke, R.A., 1994: The status of mesoscale meteorological models. Chapter 3.3 in *Planning and managing regional air quality modeling and measurement studies: a perspective*

through the San Joaquin Valley air quality study and AUSPEX. Lewis Publishers, Chelsea, Michigan, 435-463.

Pielke, R.A., W.R. Cotton, R.L. Walko, C.J. Tremback, W.A. Lyons, L.D. Grasso, M.E. Nicholls, M.D. Moran, D.A. Wesley, T.J. Lee, and J.H. Copeland, 1992: A comprehensive meteorological modeling system – RAMS. *Meteorol. Atmos. Phys.*, **49**, 69-91.

Pruppacher, H.R. and J.D. Klett, 1978: *Microphysics of clouds and precipitation.* D. Reidel, 714 pp.

Rafkin, S.C.R., 1996: Development of a cumulus parameterization suitable for mesoscale to large-scale models. Ph.D. dissertation, in preparation, Colorado State University, Dept. of Atmospheric Science, Fort Collins, CO 80523.

Rauber, R.M., 1992: Microphysical structure and evolution of a central Sierra Nevada orographic cloud system. *J. Appl. Meteorol.*, **31**, 3-24.

Reinking, R.F., and J.F. Boatman, 1986: Upslope precipitation events. *Mesoscale meteorology and forecasting*, P.S. Ray, Ed., Amer. Meteorol. Soc., 437-471.

Rhea, J.O., 1978: Orographic precipitation model for hydrometeorological use. Ph.D. dissertation, Atmos. Sci. Paper No. 287, Colorado State University, Dept. of Atmospheric Science, Fort Collins, CO 80523, 199 pp.

Schultz, P., 1995: An explicit cloud physics parameterization for operational numerical weather prediction. *Mon. Wea. Rev.*, 123, 3331-3343.

Segami, A., K. Kurihara, H. Nakamura, M. Ueno, I. Takano, and Y. Tatsumi, 1989: Operational mesoscale weather prediction with Japan Spectral Model. *J. Met. Soc. Japan*, **67**, 907-924.

Smagorinsky, J., 1963: General circulation experiments with the primitive equations. Part 1: The basic experiment. *Mon. Wea. Rev.*, **91**, 99-164.

Snook, J.S., 1993: An investigation of Colorado Front Range winter storms using a nonhydrostatic mesoscale numerical model designed for operational use. Ph.D. dissertation, Atmos. Sci. Paper No. 541, Colorado State University, Dept. of Atmospheric Science, Fort Collins, CO 80523, 373 pp.

Stoelinga, M.T., T.T. Warner, and W.C. Lambert, 1994: Numerical simulation of an East Coast snow storm with emphasis on very-short-range aviation forecasting of cloud ceiling, precipitation, and visibility. Preprints, *Tenth Conf. on Numerical Weather Prediction*, Portland, OR, Amer. Meteor. Soc., 24-26.

Tanguay, M., A. Robert, and R. Laprise, 1990: A semi-implicit semi-Lagrangian fully compressible regional forecast model. *Mon. Wea. Rev.*, **118**, 1970-1980.

Thompson, G., 1993: Prototype real-time mesoscale prediction during 1991-1992 winter season and statistical verification of model data. Masters thesis, Atmos. Sci. Paper No. 521, Colorado State University, Dept. of Atmospheric Science, Fort Collins, CO 80523, 105 pp.

Tremback, C.J., 1990: Numerical simulation of a mesoscale convective complex: Model development and numerical results. Ph.D. dissertation, Atmos. Sci. Paper No. 465, Colorado State University, Dept. of Atmospheric Science, Fort Collins, CO 80523, 247 pp.

Tripoli, G.J., 1992: A nonhydrostatic numerical model designed to simulate scale interaction. *Mon. Wea. Rev.*, **120**, 1342-1359.

Tripoli, G.J. and W.R. Cotton, 1981: The use of ice-liquid water potential temperature as a thermodynamic variable in deep atmospheric models. *Mon. Wea. Rev.*, 109, 1094-1102.

Tripoli, G.J. and W.R. Cotton, 1982: The Colorado State University three-dimensional cloud/mesoscale model – 1982. Part I: General theoretical framework and sensitivity experiments. *J. Rech. Atmos.*, **16**, 185-220.

Tucker, D.F., P.W. Mielke, and E.R. Reiter, 1989: The verification of numerical models with multivariate randomized block permutation procedures. *Meteor. Atmos. Phys.*, **40**, 181-188.

Tucker, D.F., and E.R. Reiter, 1988: Modeling heavy precipitation in complex terrain. Internal paper. Available from the Center for Cybernetic Communication Research, Colorado State University, Fort Collins, CO 80523.

Walko, R.L., W.R. Cotton, M.P. Meyers, and J.Y. Harrington, 1995: New RAMS cloud microphysics parameterization. Part I: The single-moment scheme. *J. Atmos. Res.*, **38**, 29-62.

Warner, T.T. and N.L. Seaman, 1990: A real-time mesoscale numerical weather-prediction system for research, teaching, and public service at Pennsylvania State University. *Bull. Amer. Meteor. Soc.*, **71**, 792-805.

Wesley, D.A., 1991: An investigation of the effects of topography on Colorado Front Range winter storms. Ph.D. dissertation, Atmos. Sci. Paper No. 489, Colorado State University, Dept. of Atmospheric Science, Fort Collins, CO 80523, 197 pp.